University of Iceland
Faculty of Natural Sciences
Department of Physics

RH-18-2002

Magnetization of interacting confined two-dimensional electron systems

by

Gabriel Vasile

A thesis submitted in partial satisfaction of the
requirements for the degree of
Master of Science in Physics at the University of Iceland

Committee in charge:
Viðar Guðmundsson, Chair
Andrei Manolescu

Reykjavík
July 2002

Contents

1 Introduction **4**

2 Methods of fabricating quantum dots **6**

2.1 Two-dimensional electron gas (2DEG) 6

2.2 Nanostructure fabrication 8

2.2.1 Field-effect-induced quantum dots 9

2.2.2 Etched quantum dots 10

2.2.3 Quantum dots for FIR measurements 11

3 The quantum dot Hydrogen **13**

3.1 An isotropic harmonic quantum dot in a perpendicular magnetic field . . . 13

3.2 Quantum dots with various shapes 15

4 Many-electron quantum dots **24**

4.1 The Hartree-Fock approximation 24

4.2 The iteration process 27

5 Magnetization of quantum dots and rings **30**

5.1 Magnetization of quantum dots 30

5.2 Magnetization of quantum rings 35

6 Summary and conclusions **77**

7 Acknowledgments **79**

A Matrix elements **80**

A.1 The matrix elements of the confinement $\langle \Phi_j | V_\varphi | \Phi_i \rangle$ 80

A.2 The Hartree matrix elements $\langle \Phi_k | V_H | \Phi_l \rangle$ 83

A.3 The Fock matrix elements $\langle \Phi_k | V_F | \Phi_l \rangle$ 87

A.4 The matrix elements of the confinement potential for a ring 88

A.5 The matrix elements of position x, $\langle \Phi_j | x | \Phi_i \rangle$ 90

A.6 The matrix elements of position y, $\langle \Phi_j | y | \Phi_i \rangle$ 91

B Magnetization **93**

B.1 The orbital magnetization $\mathscr{M}_o$ 93

B.2 The Hartree-Fock orbital magnetization $\mathscr{M}_o$ 96

Chapter 1

Introduction

In this thesis we investigate the ground state and the magnetization of quantum dots and rings of various shapes by model calculations. A quantum dot is a small electron system, a few tens of nanometers in diameter, which can be made by modern fabrication techniques. The motion of the electrons is confined in all three dimensions leading to a discrete energy spectrum. The discrete energy spectrum and man-made confining potential characterize a quantum dot as an *artificial atom*. The usual energy level spacing of a quantum dot lies in the range of a few meV, that is, within the far-infrared range of the electromagnetic spectrum.

Properties of quantum dots have been studied intensively in the last 20 years. The far-infrared absorption of large arrays of regular dots has been measured [1, 2] and calculated by several groups [3, 4, 5, 6, 7, 8]. At the same time the transport or tunneling through individual large dots was measured and information about the ground state of the system has been obtained [9, 10, 11].

In the last two years the group of Detlef Heitmann at the University of Hamburg has succeeded to measure the magnetization of the electron system inside an array of quantum dots. In response two groups have calculated the magnetization of quantum dots with few electrons [12, 13]. The magnetic field applied perpendicular to the plane of the electrons, has important effects on their energy spectra and magnetization. The measurement of the magnetization may be one of the most direct probes into the ground state electronic structure of a quantum dot.

The thesis is structured in several chapters, as follows:

- The methods of fabricating quantum dots are sketched in the **Chapter 2**.
- **Chapter 3** describes the calculations of the ground state of a single electron quantum dot and ring for a parabolic confinement potential, with circular, elliptic or square symmetry in the (x,y) plane. The effects of the confinement on energy spec-

tra, as a function of the magnetic field, will be discussed.

- The next step is to consider more than one electron in the system (**Chapter 4**). In this case, like in a many-electron atom the electron-electron Coulomb interaction has important effects, for example on the electron density. The electron-electron Coulomb interaction is taken into account within the Hartree-Fock approximation.

- The effects of the Coulomb interaction on the magnetization and electron density of quantum dots and rings is presented in **Chapter 5** for circular, elliptic and square symmetric cases.

Chapter 2

Methods of fabricating quantum dots

In this chapter the methods of making quantum dots are briefly described. These systems are man-made structures formed in semiconductor heterostructures by self-organized growth, etching, or defined by structured metal gates on top of the semiconductor.

The preparation of large arrays of identical quantum dots is difficult and several methods have been tried and developed. An alternative method has lead to so-called *self-organized quantum dots* that form irregular arrays of similar dots on the surface of certain semiconductors like water droplets on a polished metal surface.

2.1 Two-dimensional electron gas (2DEG)

The starting point of making arrays of quantum dots is the two-dimensional electron gas (2DEG) formed at the interface of an AlGaAs-GaAs heterojunction. The reason why these semiconductors are chosen is that both have nearly the same lattice constant (GaAs - 5.653Å and AlGaAs - 5.660Å), while the energy gaps between the conduction and valence band differ considerably (GaAs has 1.51 eV and $Al_xGa_{1-x}As$ has $(1.5+0.7x)$ eV, where x is the Al concentration) leading to a band discontinuity at their interface (see Fig. 2.2).

With the technique of molecular beam epitaxy (MBE) growth, see Fig. 2.1, they are grown on top of each other, with atomic monolayer precision with quasi perfect GaAs/AlGaAs interface. The general scheme for growing the heterostructures is as follows: First a layer of GaAs is grown on a substrate, usually made of GaAs. On top of it a layer of *undoped* AlGaAs is grown, so-called *spacer layer*. Because all the samples are at liquid helium temperature during experiment, the semiconductors are insulating. Therefore doping the AlGaAs-layer with Si atoms, free carriers are introduced. Only three of the four electrons in the outer shell of the Si atom, that replace the Al or As atoms in

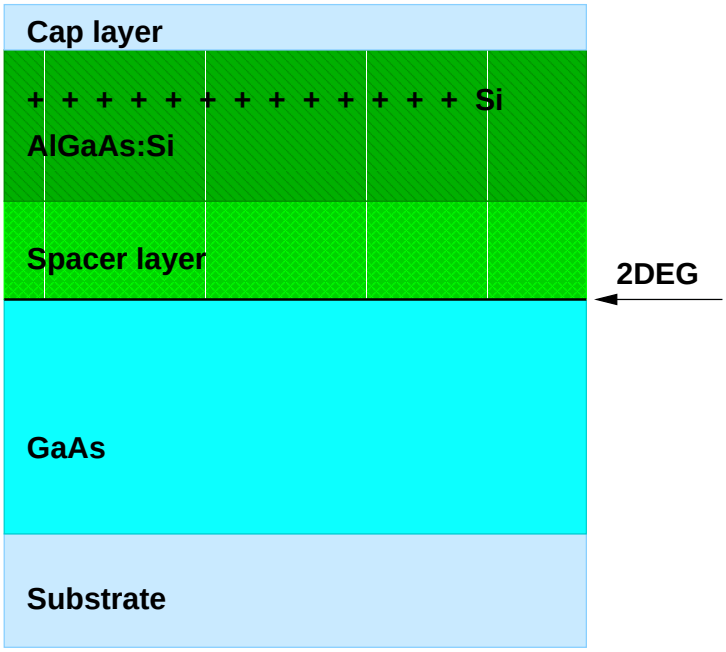

Figure 2.1: MBE growth sketch for a heterostructure.

the lattice, contribute to the crystal binding, while the extra electrons can move to the interface and drop into the energetically more preferable GaAs material. When the GaAs, which is p-doped, comes in contact with the AlGaAs, which is n-doped, electrons flow across the interface. The flow from the n-doped region in the GaAs occurs until the charge distribution is in equilibrium, characterized by a continuous chemical potential across the interface. At the interface, at the conduction band discontinuity, a triangular potential-well is formed and the conduction electrons are confined by this potential to a layer of a few nanometers thickness, leading to a quantization of the electron motion perpendicular to the interface and a free motion in the $x-y$ plane parallel to the AlGaAs/GaAs interface [14]. The energy spectrum is thus

$$E_i = E_i^z + \frac{\hbar^2}{2m^*}(k_x^2 + k_y^2)\,, \tag{2.1}$$

where $i = 0, 1, 2, \ldots$, m^* is the electron effective mass ($m^* = 0.067 m_e$ for GaAs, m_e is the free-electron mass), k_x and k_y are the wave vectors in the plane of 2DEG, E_i^z is the level spacing of the 2D sub-bands. The effective Bohr radius in GaAs is $a_0^* = 9.79$ nm, much larger than the lattice constant (5.653Å for GaAs).

The reason for using the spacer layer is to avoid scattering of the electrons in the 2DEG by the ionized donors (the Si atoms act as donors for the 2DEG and the spacer layer acts as a barrier between electrons and donors). At a distance of approximately

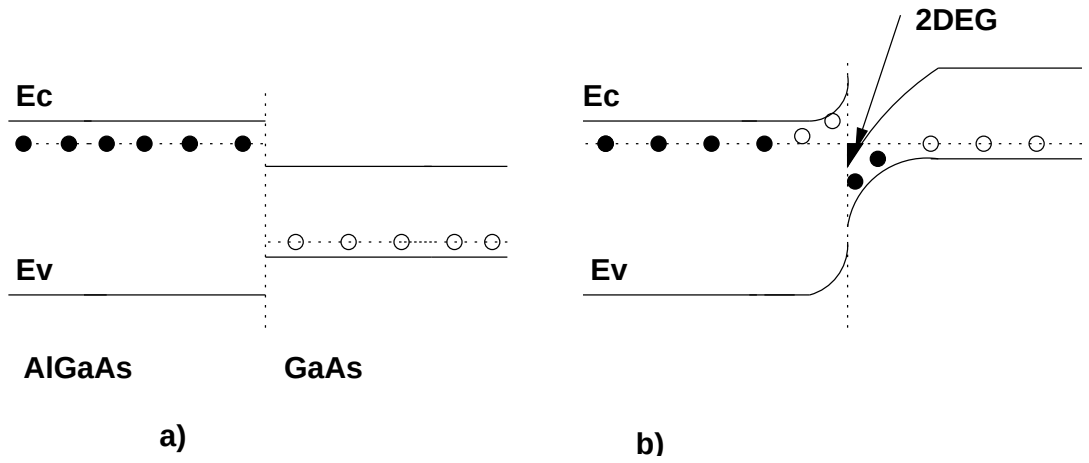

Figure 2.2: A schematic figure of the bandstructure at the heterostructure interface (Fig. a) and of the conduction bandedge of the heterostructure (Fig. b).

300 nm underneath the 2DEG, a Si-layer is integrated which serves as a backgate in the sample design. The distance to the backgate is chosen in such a way that the 2DEG can be treated as independent from the Si-layer. To avoid diffusion of the Si atoms into the AlGaAs and an oxidation of Al atoms, one monolayer of GaAs is grown directly on top of the AlGaAs:Si with the purpose of sealing it, called *cap layer*.

2.2 Nanostructure fabrication

There are several ways of making quantum dots from the 2DEG and we discuss only two types of quantum dots: *The field-effect-induced quantum dots* and *etched quantum dots*.

In order to grow or etch structures on the sample, it is necessary to deposit on it some kind of a resist, a polymer solution. The resist is selectively radiated according to the desired pattern [15]. The radiation breaks the chemical bonds where the resist is exposed to radiation. After the resist is removed by immersing it in a solution which acts preferentially, it does not affect the unradiated part (see Fig. 2.3). The resolution of the pattern in the resist depends on the wavelength of the radiation used. For UV-radiation, the highest resolution is approximately $0.1\ \mu m$, for mass production, but for obtaining a higher resolution for smaller patterns other radiation sources must be used. For example, for a resolution below 10 nm, an electron beam is used to develop the resist.

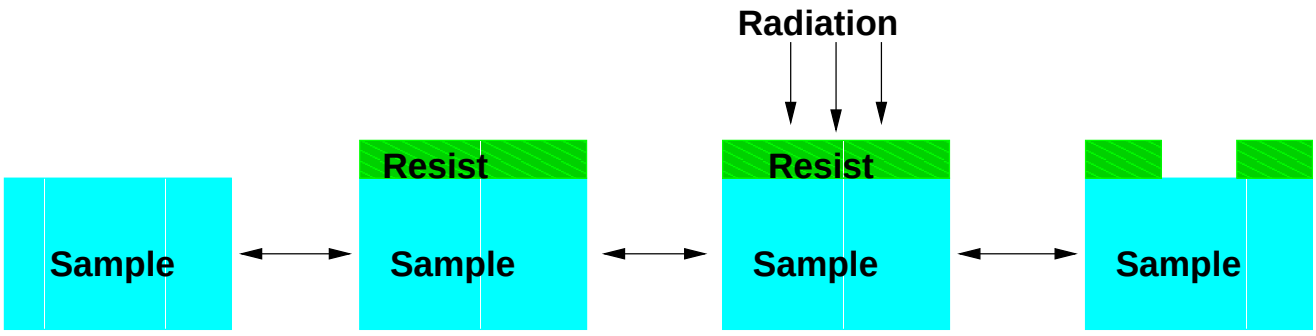

Figure 2.3: A schematic figure of nanostructure fabrication.

2.2.1 Field-effect-induced quantum dots

After the pattern on the resist is set, a thin film of Ti (thickness about 5 nm) is deposited by evaporation on top of the structure (see Fig. 2.4), serving as a contact. Field-effect-

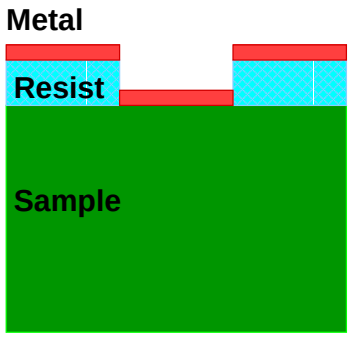

Figure 2.4: A thin metal film is evaporated on the structure.

induced quantum dots can be accomplished by applying a negative voltage between a Ti topgate on the sample surface, through AuGe/Ni bonding pad, and a Si backgate, integrated in the structure during the MBE growth. Applying a negative voltage, under the metal contact, the electrons can be driven off by increasing their potential energy. Depending on the strength of the voltage, the density is lowered or the 2DEG is totally depleted under the contact, but underneath the resist electrons will be gathered forming an island of electrons, so-called a quantum dot space (see Fig. 2.5). The advantage of this technique is the ability to adjust the voltage to control the strength of the confining potential at the AlGaAs/GaAs interface, and at the same time the electron density. In such samples the electron density can be tuned from a high density 2DEG into a system of iso-

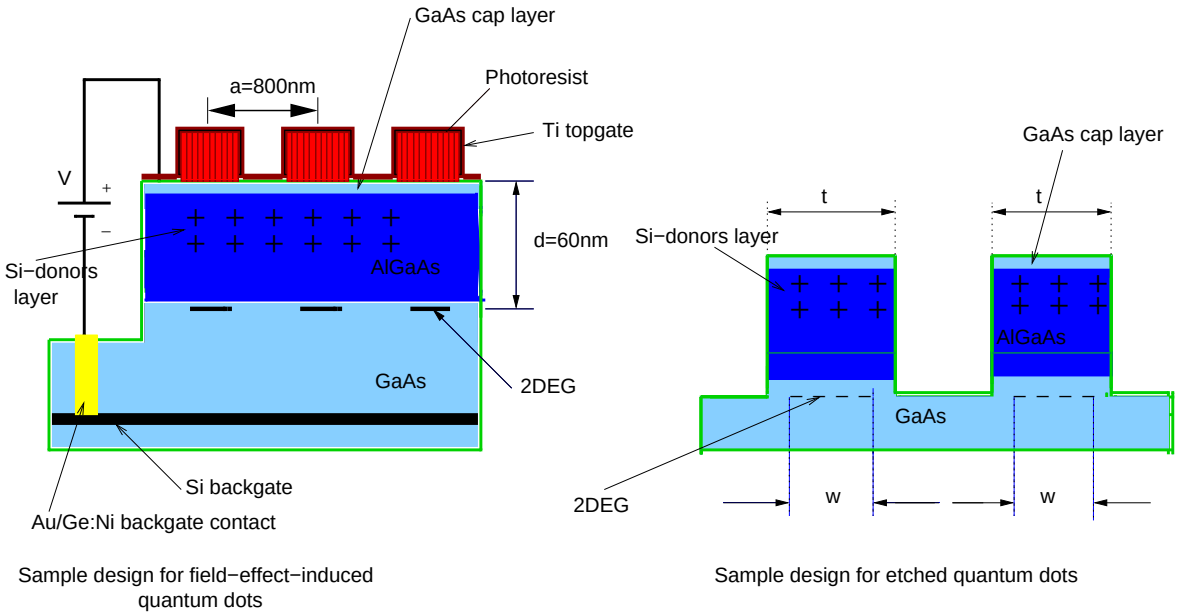

Figure 2.5: A schematic figure of the field-effect-induced quantum dots and etched quantum dots.

lated quantum dots, that can even be homogeneously charged with single electrons. These quantum dots may be understood as artificial atoms in the sense that a certain number of electrons (1, 2, 3, . . .) occupies discrete energy levels of the confining potential.

2.2.2 Etched quantum dots

The main difference between this method and the field-effect-induced quantum dots is that, instead of using metal gates to confine electrons, the sample is simply etched down below the 2DEG system.

A structure in the sample can be made using either dry or wet etching. In the first method, dry etching, reactive gases or plasma are used while in the second method, wet etching, a selective solvent which leaves the resist unaffected, or at least deteriorates it much more slowly than the sample, is used (see Fig. 2.5).

For example, see [16], a possible solvent consists in a mixture of: 1 part H_2SO_4 (96 %), 8 parts H_2O_2 (30 %), 1200 parts H_2O. The sample is etched for 200 s, which removes 100 nm of material. If the sample (see Fig. 2.5) is etched into the donor layer, fewer donors will contribute to the 2DEG in that region, causing a lower density in the 2DEG under the etched area.

2.2.3 Quantum dots for FIR measurements

Because of the fact that the signals, in FIR absorption measurements, are usually very weak it is necessary to produce an array of many identical dots, in order to get the signal as strong as possible. This is achieved with holografic lithography and etching processes.

Essentially, this method is based on placing, on top of the AlGaAs/GaAs structure a layer of a sensitive material to an incident light beam, called *photoresist*. The light beam from a laser, is focused on a pinhole and then expanded and parallelized by a lens. To control the exposure time, an electronic shutter is placed behind the expansion optics (see Fig. 2.6)

The beam is then directed in two directions with a beam-splitter and the two beams are reflected by two adjustable mirrors (on each side of the sample) on the sample surface. Then, the photo-resist is developed, where the two beams interfered constructively, that is where the light shines on the resist. The period of this array is determined by the angle of incidence α and the laser wavelength. A dot structure can be fabricated by a double exposure with a rotation of 90° in between of the exposures.

- Circular quantum dots: are formed by exposing the sample to light for equally long times in each direction of the sample
- Elliptic quantum dots: are formed by exposing the sample to light for different times in the two directions. The proportion of times gives the proportion between the major and minor axes of the dots.
- Square symmetric quantum dots: are formed by an anisotropic plasma-etching.

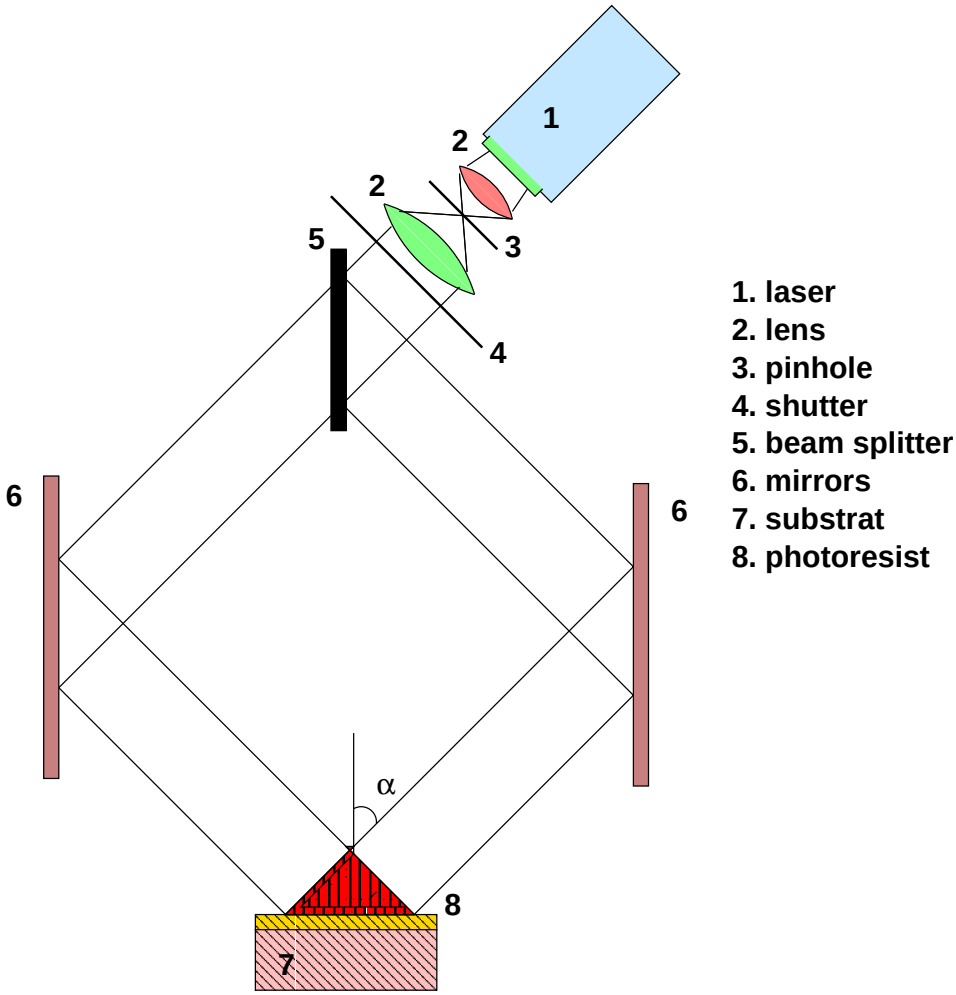

Figure 2.6: Holografic lithography scheme.

Chapter 3

The quantum dot Hydrogen

A quantum dot containing a single electron may be called a quantum dot Hydrogen. For a single electron in a perpendicular magnetic field, the energy spectrum and wave functions of the associated Hamiltonian were found by Fock and Darwin [17, 18].

3.1 An isotropic harmonic quantum dot in a perpendicular magnetic field

The Hamiltonian of a single electron of mass m^* moving freely in an external magnetic field is given by:

$$H_0 = \frac{\hbar^2}{2m^*}\left(-i\nabla + \frac{e}{\hbar}A\right)^2 + g^*\mu_B BS\,. \tag{3.1}$$

Using the vector potential in the symmetric gauge, $A = \frac{1}{2}B(-y,x,0)$, the Hamiltonian H_0, in polar coordinates, is:

$$H_0(r,\varphi) = \frac{\hbar^2}{2m^*}\left(\partial_r^2 + \frac{1}{r}\partial_r + \frac{1}{r^2}\partial_\varphi^2 + \frac{i}{l^2}\right) + \frac{m^*\omega_c^2}{8}r^2 + g^*\mu_B BS\,, \tag{3.2}$$

where:

$$l = \sqrt{\frac{\hbar}{eB}} \longrightarrow \text{magnetic length}\,, \tag{3.3}$$

$$\omega_c = \frac{eB}{m^*} \longrightarrow \text{cyclotron frequency}\,, \tag{3.4}$$

with: g^* the effective gyromagnetic factor in GaAs, μ_B the Bohr magneton, B the magnetic field, and S the z component of the spin. For a quantum dot with parabolic confinement potential and circular symmetry in the plane of the 2DEG,

$$V_{\text{conf}}(r,\varphi) = \frac{1}{2}m^*\omega_0^2 r^2\,. \tag{3.5}$$

In a perpendicular magnetic field the single-electron Hamiltonian is:

$$H(r,\varphi) = H_0(r,\varphi) + V_{\text{conf}}(r,\varphi)\,. \tag{3.6}$$

Solving the corresponding Schrödinger equation

$$(H_0 + V_{\text{conf}})|\Phi\rangle = E|\Phi\rangle \tag{3.7}$$

we find:

- The eigenvalues (energy spectrum):

$$E_{M,n_r} = \left[n_r + \frac{|M|}{2} + \frac{1}{2}\right]\hbar\Omega - \frac{1}{2}M\hbar\omega_c^2 + g^*\mu_B BS\,, \tag{3.8}$$

  where:

$$\Omega = \sqrt{\omega_c^2 + 4\omega_0^2} \tag{3.9}$$

  is a characteristic confinement frequency, a combination of the cyclotron frequency and the parabolic confinement frequency.

- The single-particle eigenfunctions (noninteracting wave functions):

$$\Phi_{M,n_r}(r,\varphi) = A_{M,n_r}\left(\frac{r}{a}\right)^{|M|} e^{\frac{-r^2}{4a^2}} L_{n_r}^{|M|}\left(\frac{r^2}{2a^2}\right) e^{-iM\varphi}\,, \tag{3.10}$$

  where:

$$A_{M,n_r} = \frac{1}{2^{\frac{|M|+1}{2}}a}\left(\frac{n_r!}{\pi(|M|+n_r)!}\right)^{\frac{1}{2}}, \tag{3.11}$$

$$a^2 = \frac{l^2}{\sqrt{1+4\left(\frac{\omega_0}{\omega_c}\right)^2}} \longrightarrow \text{characteristic length scale} \tag{3.12}$$

  formed by the magnetic length l, the parabolic confinement frequency ω_0 and the cyclotron frequency ω_c.

  $L_{n_r}^{|M|}$ – Laguerre polynomial (see [19]).

  n_r – radial quantum number ($n_r = 0,1,2,\ldots,n_r^{max}$).

  M – angular momentum quantum number ($M = -n_r^{max}, -n_r^{max}+1,\ldots,n_r^{max}$), which describes rotation around the z-axis. The relationship between the quantum numbers is sketched in the Fig. 3.1.

At zero magnetic field the eigenvalue formula (see Eq. (3.8)) simplifies into:

$$E_{M,n_r} = (2n_r + |M| + 1)\hbar\omega_0 \tag{3.13}$$

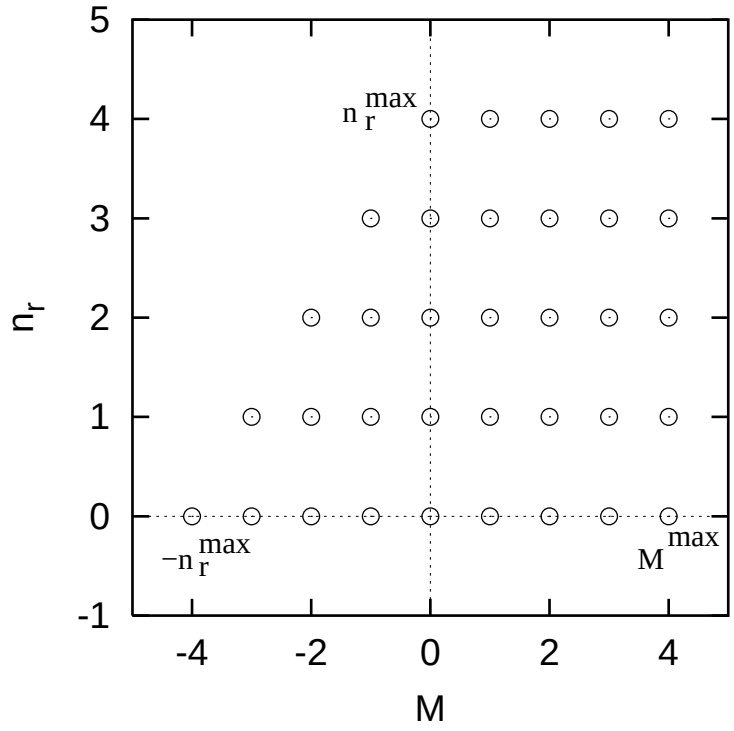

Figure 3.1: The relationship between M and n_r in a truncated subspace with $n_r^{max} = 4$ and $M^{max} = 4$. For a given n_r, the minimum value of M is $-n_r^{max}$ and the lowest value of n_r is 0.

To see the degeneracy more explicitly, the energy is plotted as a function of the angular quantum number M, in Fig. 3.2.

For a given radial quantum number the energy levels can be interpolated with lines of slope $\pm\hbar\omega_0$. Increasing the external magnetic field, for negative M the slope increases and for positive M the slope decreases. This lifts the degeneracy for higher magnetic fields. Using the general formula of eigenvalues, we can plot the energy spectrum versus the external magnetic field, this is known as Fock-Darwin diagram (see Fig. 3.3).

3.2 Quantum dots with various shapes

In order to describe dots with more complex shape we introduce a multi-pole expansion in two dimensions to the circular parabolic confinement potential. The circular symmetry

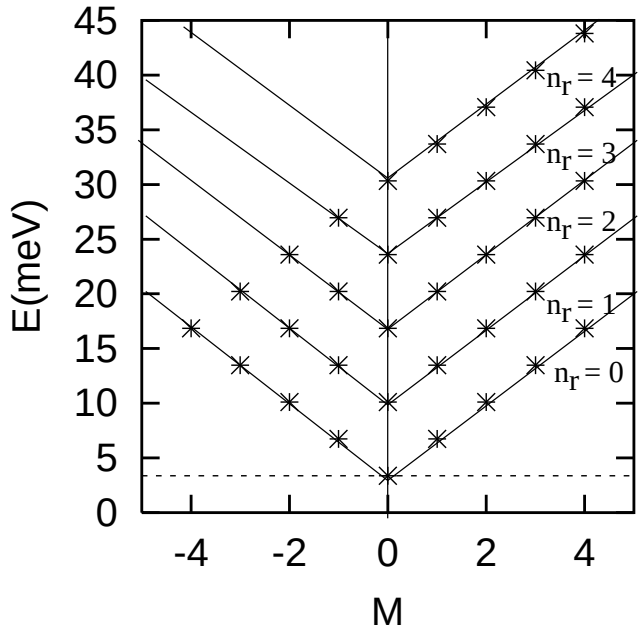

Figure 3.2: The energy levels at $B = 0$ T, $n_r^{max} = 4$, $M^{max} = 4$.

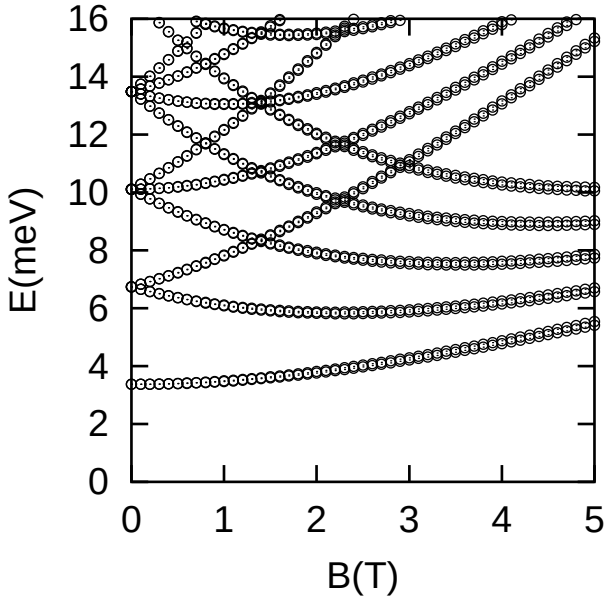

Figure 3.3: The Fock-Darwin diagram of an isotropic harmonic quantum dot.

can thus be broken [13, 20, 21]

$$V_{\text{conf}}(r,\varphi) = \frac{1}{2}m^*\omega_0^2 r^2\left[1+\sum_{p=1}^{p_{max}}\alpha_p\cos(2p\varphi)\right]. \tag{3.14}$$

This is a multi-pole expansion in 2 dimensions with high symmetry. The dipole contribution, $p = 1$, produces an elliptical shape, while the quadrupole term, $p = 2$, produces a square symmetric shape. Therefore the potential remains symmetric at reflections along the x and y-axis. Thus, varying the coefficients α_p, we can change the shape of the confinement potential, as follows:

1. Circular confinement: $\alpha_p = 0$ for all p.
2. Elliptic confinement: $\alpha_1 \neq 0$ and $\alpha_p = 0$ for all $p \neq 1$. In this special case the total potential becomes:

$$V_{\text{conf}}(r,\varphi) = \frac{1}{2}m^*\omega_0^2 r^2[1+\alpha_1\cos(2\varphi)], \tag{3.15}$$

which can be written in Cartesian coordinates as:

$$V_{\text{conf}}(x,y) = \frac{1}{2}m^*\omega_0^2 r^2[(1+\alpha_1)x^2+(1-\alpha_1)y^2]. \tag{3.16}$$

The equipotential lines of this confinement potential are ellipses. The ratio between the minor and major axis of an equipotential curve is seen from Eq. (3.16), to be:

$$\frac{a_x}{a_y} = \sqrt{\frac{1-\alpha_1}{1+\alpha_1}}\,, \tag{3.17}$$

where a_x and a_y are the minor and major axis lengths respectively. Fig. 3.4 shows a comparison between equipotential lines of an elliptic confinement and equipotential lines of a circular confinement. The deviation increases with increasing α_1.

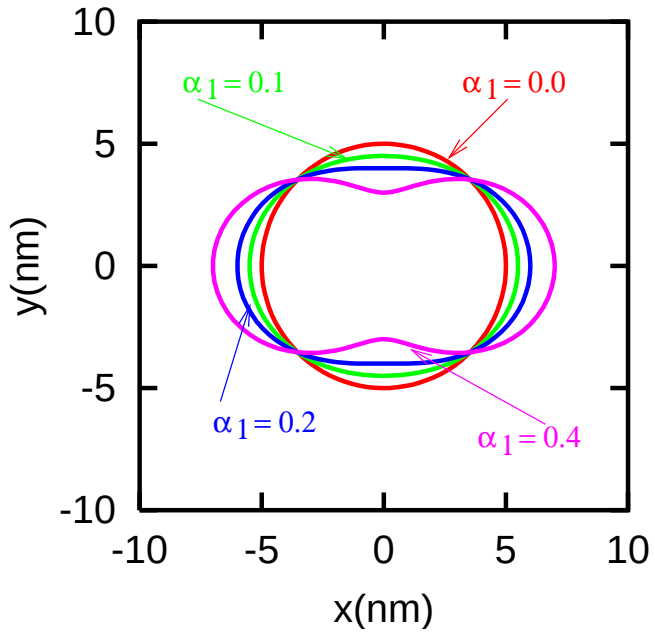

Figure 3.4: Deviation from circular shape in the cases $\alpha_1 = 0.1,\ \alpha_1 = 0.2,\ \alpha_1 = 0.4$.

The energy spectra for different values of α_1 are shown in Fig. 3.5. Unlike Fig. 3.3 for zero magnetic field we see that some degeneracy is lifted because the off-diagonal matrix elements for which $\Delta M = \pm 2$ are non-zero (see Appendix).

$$\langle N, m_r | V_\varphi | M, n_r \rangle \approx \int_0^{2\pi} d\varphi e^{-i\Delta M\varphi} \cos(2\varphi) = \pi[\delta_{\Delta M,2} + \delta_{\Delta M,-2}] \tag{3.18}$$

where $\Delta M = M - N$. Therefore, the corresponding states are coupled and the corresponding degeneracy is lifted, as is seen very well for $\alpha_1 = 0.1$. For $\alpha_1 = 0.2$ there occurs an accidental degeneracy at $E \approx 11.24$ meV while for the same states in the case $\alpha_1 = 0.4$ there is an anti-crossing lifting the accidental degeneracy at $E \approx 12.15$ meV.

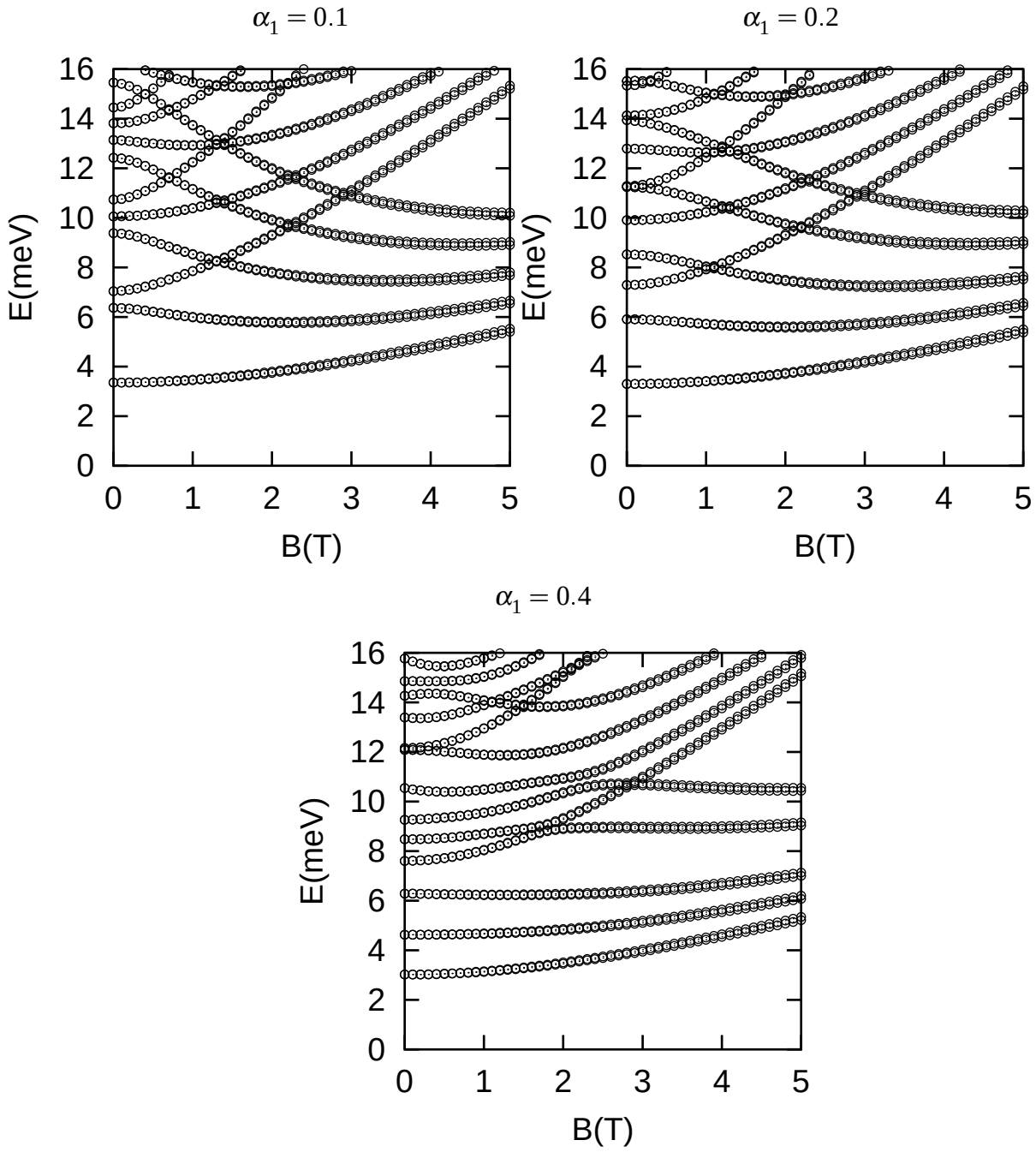

Figure 3.5: Fock-Darwin energy spectra of an elliptic quantum dot, for different values of α_1.

3. Square symmetric deviation from a circular parabolic confinement: $\alpha_2 \neq 0$ and $\alpha_p = 0$ for all $p \neq 2$. In this special case the total potential becomes:

$$V_{\text{conf}}(r,\varphi) = \frac{1}{2} m^* \omega_0^2 r^2 [1 + \alpha_2 \cos(4\varphi)] \,, \tag{3.19}$$

Trying to write it in Cartesian coordinates leads to a more complicated formula because of the complicated expansion of $\cos(4\varphi)$. Fig. 3.6 shows a comparison between equipotential lines of a square symmetric confinement and equipotential lines of a parabolic confinement. Fig. 3.7 shows a picture of a possible square symmetric confinement potential for $\alpha_2 = 0.4$.

The energy spectra for different values of α_2 are shown in Fig. 3.8. Unlike Fig. 3.3 for zero magnetic field degeneracy is lifted because the off-diagonal matrix elements for which $\Delta M = \pm 4$ are non-zero (see Appendix).

$$\langle N, m_r | V_\varphi | M, n_r \rangle \approx \int_0^{2\pi} d\varphi e^{-i\Delta M \varphi} \cos(4\varphi) = \pi [\delta_{\Delta M,4} + \delta_{\Delta M,-4}] \,, \tag{3.20}$$

where $\Delta M = M - N$. Fig. 3.8 reveals an anti-crossing at $B \approx 2.3$ T corresponding to states $|1,0\rangle$ and $|-3,0\rangle$, which are coupled according to Eq. (3.20).

In order to model a ring from a quantum dot we can also add a circular symmetric hill in the center of the dot [22, 23].

$$V_{\text{conf}}(r,\varphi) = \frac{1}{2} m^* \omega_0^2 r^2 \left[1 + \sum_{p=1}^{p_{max}} \alpha_p \cos(2p\varphi) \right] + V_0 exp(-\gamma r^2) \,, \tag{3.21}$$

where V_0 controls the high of the hill and γ the width. Changing the values of α_p we obtain an elliptic or square symmetric quantum dot with a circular potential barrier in the center.

The single-electron energy spectra for a circular, elliptic and square symmetric quantum ring shows an interesting phenomenon (see Fig. 3.10, 3.11, 3.12). We know the energy spectrum of an ideal ring is a periodic function of the magnetic flux [24]. If the ring has a finite thickness then this periodicity is lost as soon as the magnetic length becomes smaller than the thickness of the ring. Therefore we see the periodicity for low values of the magnetic field B and the energy. At higher magnetic field a complex Landau-band structure emerges.

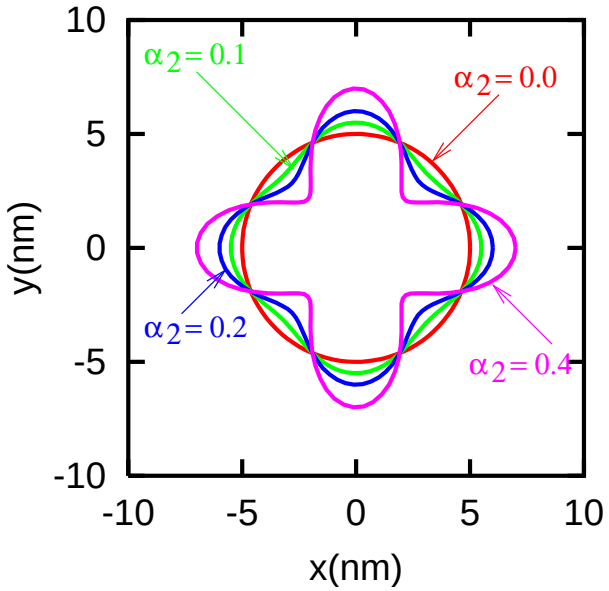

Figure 3.6: Deviation from circular shape in the cases $\alpha_2 = 0.1$, $\alpha_2 = 0.2$, $\alpha_2 = 0.4$.

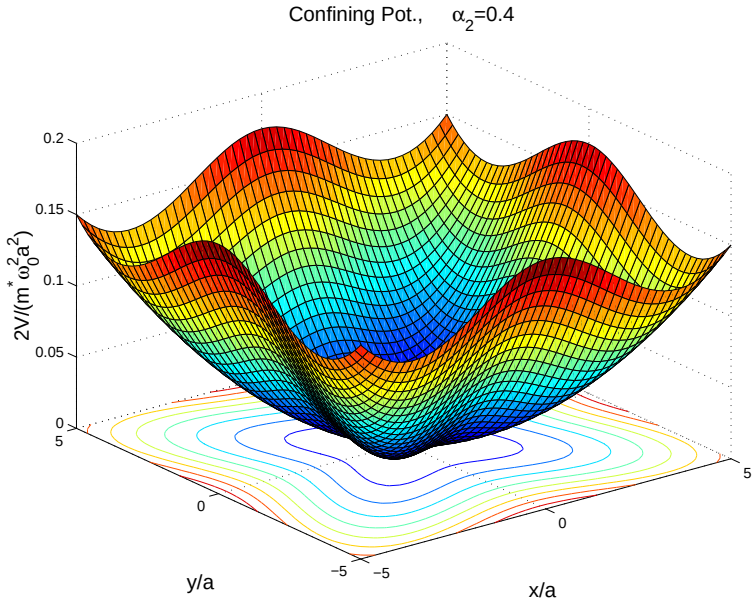

Figure 3.7: Square symmetric confinement potential.

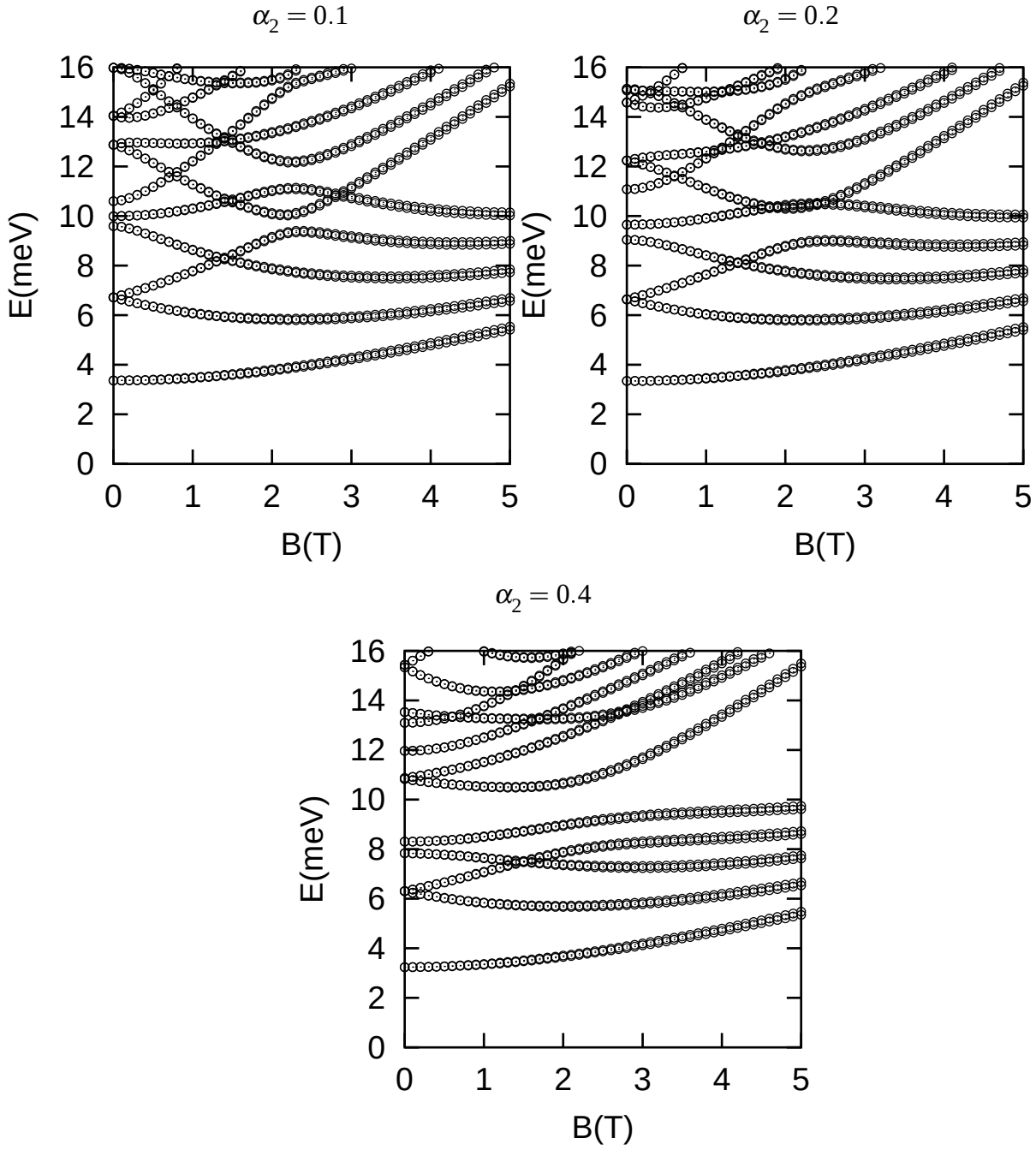

Figure 3.8: Fock-Darwin energy spectra of an square symmetric quantum dot, for different values of α_2.

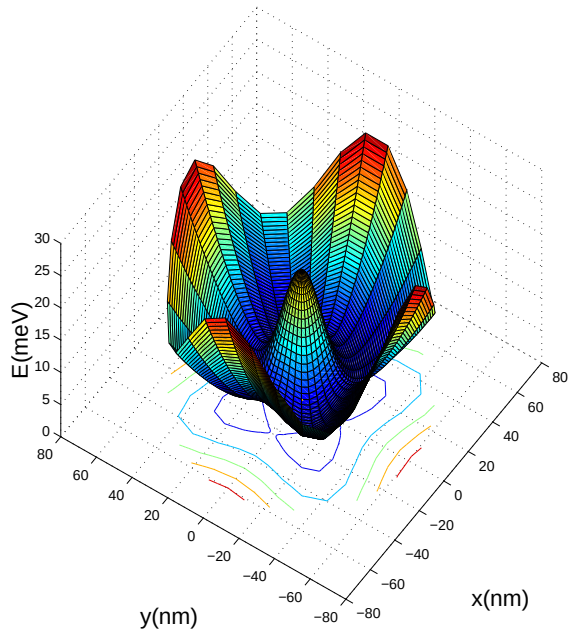

Figure 3.9: Square symmetric confinement potential with a hill at the center.

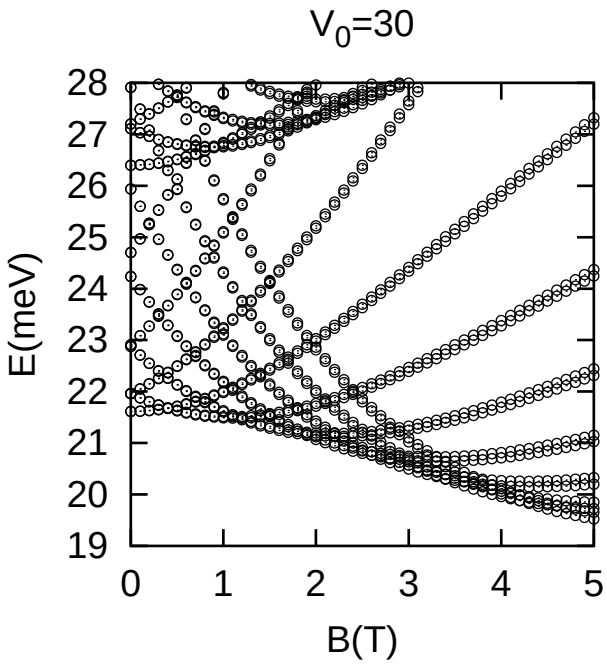

Figure 3.10: Energy spectrum of a circular quantum ring.

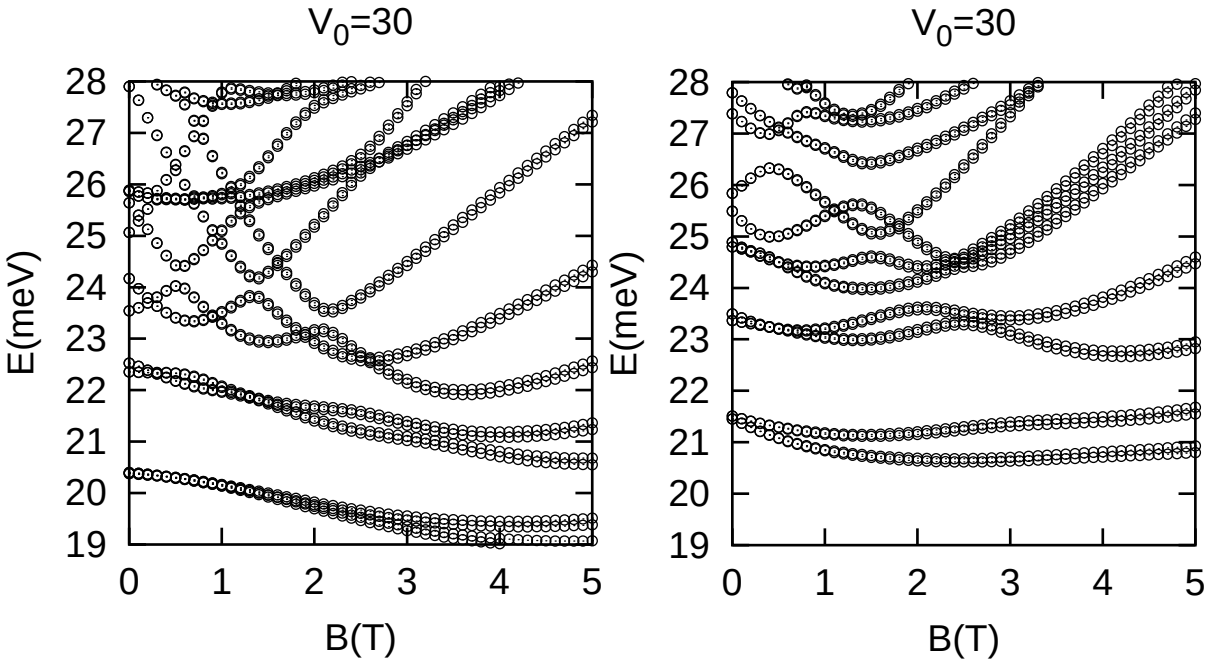

Figure 3.11: Energy spectra of an elliptic quantum ring ($\alpha_1 = 0.1,\ \alpha_1 = 0.2$).

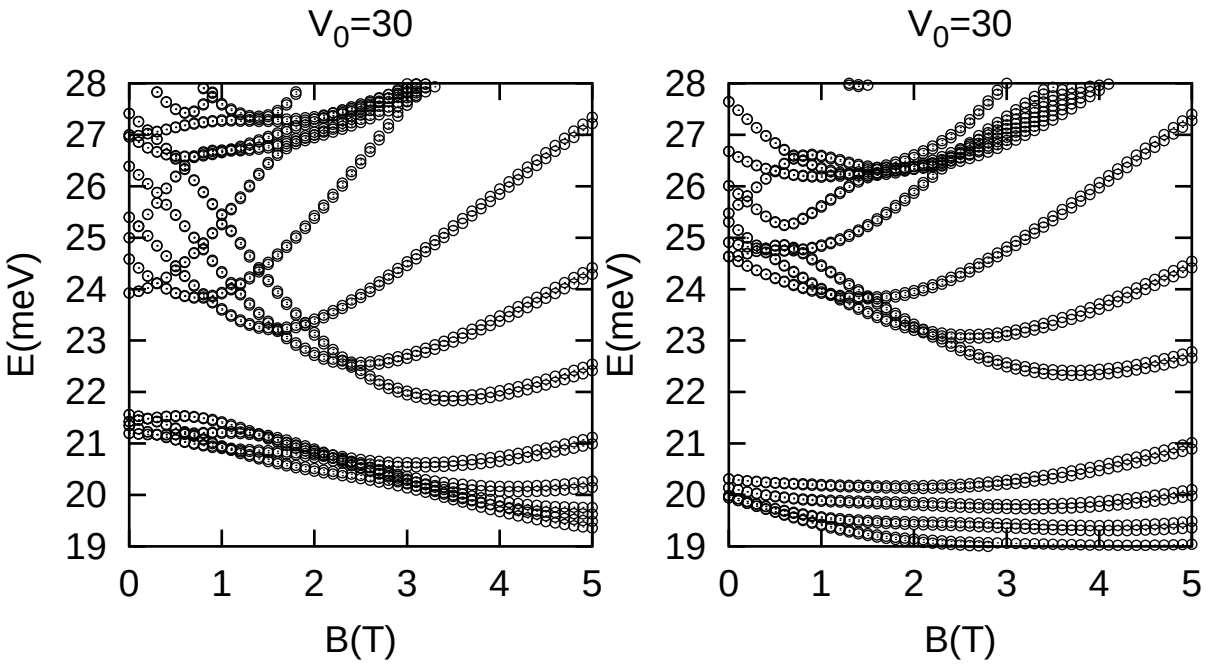

Figure 3.12: Energy spectra of a square symmetric quantum ring ($\alpha_2 = 0.1,\ \alpha_2 = 0.2$).

Chapter 4

Many-electron quantum dots

In the previous chapter we discussed the single-electron quantum dot, the so called quantum dot Hydrogen. The next step is to consider more than one electron in the system. In this case, like in a many-electron atom the electron-electron Coulomb interaction has important effects. But in an atom the confinement, i. e. the nuclear potential, is fixed and to a good approximation it is spherical symmetric. In a quantum dot the confinement potential is experimentally designed, it is two-dimensional, and it can have many shapes. The Coulomb repulsion of electrons may act differently for different confinement potentials. The Coulomb interaction will be included within the Hartree-Fock approximation [25, 26].

4.1 The Hartree-Fock approximation

The Hartree-Fock approximation is based on the idea that we can approximately describe an interacting system in terms of effective single-particle perturbed states. It is known that a single-particle description forms a surprisingly good approximation in many different systems, for example, metals, atoms or nuclei.

The starting point is the idea that each particle moves in a mean-field potential, which is produced by all the particles, and by an external potential, if present. In the non-interacting case each of the N particles occupies a single-particle state, such that its motion is independent of the presence of the other particles. However, this situation will be clearly changed by turning on the interaction between particles, then the particles move in an average potential resulting from the presence of all the particles. Therefore, the single-particle energy should then be the unperturbed (non-interacting) energy plus the potential energy of interaction averaged over the states occupied by all the other particles.

The Hartree-Fock approximation is a mean-field approximation. It consists of an ef-

fective equation of motion for each electron, containing the single-electron wave functions corresponding to *all* electrons. The problem is reduced to solving a nonlinear Schrödinger equation. Because of the nonlinearity of the resulting Schrödinger equation, the self-consistent equations can be solved only numerically. In this work we use an iterative method.

The Hartree-Fock many-particle wavefunction of the system is written as a Slater determinant due to its antisymmetry:

$$\Psi_{HF}(x_1,\ldots,x_N) = \frac{1}{\sqrt{N!}} \begin{vmatrix} \varphi_{\alpha_1}(x_1)\ldots\varphi_{\alpha_N}(x_1) \\ \vdots \\ \varphi_{\alpha_1}(x_N)\ldots\varphi_{\alpha_N}(x_N) \end{vmatrix}, \tag{4.1}$$

where $\alpha_1,\ldots,\alpha_N$ label the single-particle states and $\varphi_{\alpha_i}(x_j)$ are the single-particle wave functions. This is precisely the content of the Pauli principle, according to which two fermions with equal spin $s_i = s_j$ cannot be in the same quantum state $\alpha_i = \alpha_j$ (the exclusion principle prevents two particles of the same spin from occupying the same single-particle state).

The effective equation of motion for one electron is written as:

$$\{H + V_H(\vec{r})\}\Psi_\alpha(\vec{r}) - \int_{R^2} d^2\vec{r}\,'\Delta(\vec{r},\vec{r}\,')\Psi_\alpha(\vec{r}\,') = \varepsilon_\alpha\Psi_\alpha(\vec{r}), \tag{4.2}$$

where $V_H(\vec{r})$ is the Hartree potential,

$$V_H(\vec{r}) = \frac{e^2}{4\pi\varepsilon_r\varepsilon_0}\int_{R^2} d^2\vec{r}\,'\frac{n(\vec{r}\,')}{|\vec{r}-\vec{r}\,'|}, \tag{4.3}$$

and $\Delta(\vec{r},\vec{r}\,')$ is the Fock exchange kernel,

$$\Delta(\vec{r},\vec{r}\,') = \frac{e^2}{4\pi\varepsilon_r\varepsilon_0}\sum_{\beta,s'} f(\varepsilon_\beta-\mu)\frac{\Psi^*_\beta(\vec{r}\,')\,\Psi_\beta(\vec{r})}{|\vec{r}-\vec{r}\,'|}, \tag{4.4}$$

with ε_0 the permittivity of the vacuum, ε_r the relative dielectric constant of the semiconductor material of the quantum dot, μ the chemical potential and $f(\varepsilon_\beta-\mu)$ the Fermi distribution. The Hartree potential, Eq. (4.3), describes the electrostatic interaction energy of one electron with the whole electron density. The Fock exchange kernel (exchange potential), Eq. (4.4), has its root in the antisymmetry of many-body wave function. The Hartree potential depends directly on the density and is spin-independent while the Fock potential cannot be described in terms of density and, unlike the Hartree potential, is spin-dependent even if the Hamiltonian of the system does not explicitly depend on spin. Therefore, we have set in Eq. (4.3): $n(\vec{r}) = \sum_s n(\vec{r},s)$.

The non-physical self-interaction present in the Hartree approximation, where each electron "sees" itself is canceled by the exchange term. For a short-range interparticle

potential (as in the nuclear physics), the Hartree and exchange potential are comparable in magnitude; for a long-range interparticle potential (as in the atomic physics), the exchange contribution is usually much smaller than the Hartree potential. Indeed, the exchange term is occasionally entirely neglected in determining the self-consistent energy levels of atoms, and the corresponding approximation is known as the Hartree approximation.

When the external potential varies on a larger scale than the mean distance between electrons, the contribution of the exchange effects reduces increasing the importance of the Hartree interaction while when the potential scale is comparable with the average distance, than the opposite is true.

The electron density is calculated in terms of the Fermi distribution and interacting wave functions:

$$n(\vec{r}) = \sum_{\alpha} f(\varepsilon_\alpha) |\Psi_\alpha(\vec{r})|^2 , \tag{4.5}$$

where:

1. for thermal equilibrium

$$f(\varepsilon_\alpha) = \left[exp\left(-\frac{\varepsilon_\alpha - \mu}{k_B T} \right) + 1 \right]^{-1} \longrightarrow \text{Fermi distribution} \tag{4.6}$$

2.

$$|\Psi_\alpha\rangle = \sum_i c_{\alpha i} |\Phi_i\rangle \longrightarrow \text{interacting states} \tag{4.7}$$

By fixing the number of electrons in the dot the chemical potential, μ, is determined by:

$$N = \sum_{\alpha} f(\varepsilon_\alpha) . \tag{4.8}$$

The self-consistent equations are:

$$H|\Psi_\alpha\rangle = \varepsilon_\alpha |\Psi_\alpha\rangle , \tag{4.9}$$

$$n(\vec{r}) = \sum_{\alpha} f(\varepsilon_\alpha) |\Psi_\alpha(\vec{r})|^2 , \tag{4.10}$$

$$V_{HF}(\vec{r}) = \frac{e^2}{4\pi\varepsilon_r\varepsilon_0} \int_{R^2} d^2\vec{r}\,' \frac{n(\vec{r}\,')}{|\vec{r} - \vec{r}\,'|} - \frac{e^2}{4\pi\varepsilon_r\varepsilon_0} \sum_{\alpha,s} \int_{R^2} d^2\vec{r}\,' \frac{\Psi^*_\alpha(\vec{r}\,')\,\Psi_\alpha(\vec{r})}{|\vec{r} - \vec{r}\,'|} . \tag{4.11}$$

We see that the effective potential contains the wave functions that we want to calculate, and the Schrödinger equation is nonlinear in Ψ_α.The numerical solution of this system can be found iteratively until the self-consistency is achieved, that is, the convergence is reached such that the new wave functions and new energies are the same as the ones found in previous steps.

4.2 The iteration process

The Schrödinger equation is:

$$(H_0 + V_{\text{conf}} + V_{HF})|\Psi_\alpha\rangle = \varepsilon_\alpha |\Psi_\alpha\rangle \,. \tag{4.12}$$

Mathematically, we expand the interacting single-particle states in the mathematical basis formed by noninteracting single-particle states

$$|\Psi_\alpha\rangle = \sum_i c_{\alpha i} |\Phi_i\rangle \,, \tag{4.13}$$

where $i : (M, n_r)$ and Φ_i are the noninteracting single-particle wave functions previously defined by Eq. (3.10). After few algebraic steps the initial Schrödinger equation takes the matrix form:

$$\sum_i \{E_i \delta_{ij} + \langle \Phi_j | V_{\text{conf}} | \Phi_i \rangle + \langle \Phi_j | V_H | \Phi_i \rangle \; + \langle \Phi_j | V_F | \Phi_i \rangle \} c_{\alpha i} = \varepsilon_\alpha c_{\alpha j} \,. \tag{4.14}$$

The eigenvalues ε_α are calculated iteratively, as follows: An initial set of single-particle wave functions and energies is assumed known, the Hartree-Fock potential is calculated, see Eq. (4.11). Then the Schrödinger equation, seen as an one-body eigenvalue equation, determines a new set of eigenfunctions and eigenvalues which are used to recompute the Hartree-Fock potential energy. This process is continued until a self-consistent solution is obtained for *both* Φ_j and ε_j.

To reach the convergence it is necessary to mix the matrix elements and stepwise increase the interaction. We have found the scheme designed by Magnúsdóttir [21] for the Hartree approximation to be quite effective also for the Hartree-Fock approximation and use it here. The new matrix elements are mixed with the last previous matrix elements calculated in iteration $(n-1)$ and respectively in iteration $(n-2)$. Therefore in the n-th iteration, the matrix elements are mixed according to:

$$H_{ij} = (H_0 + V_{\text{conf}})_{ij} + \lambda(\alpha V_{HF,ij} + (1-\alpha)(\beta V^{\text{old1}}_{HF,ij} + (1-\beta) V^{\text{old2}}_{HF,ij})) \,, \tag{4.15}$$

with: $V^{\text{old1}}_{HF,ij}$ – matrix elements calculated in iteration $(n-1)$, $V^{\text{old2}}_{HF,ij}$ – matrix elements calculated in iteration $(n-2)$, $\alpha = 0.5$, $\beta = 0.7$, and $\lambda \in (0,1]$ is a coefficient determining the strength of the interaction. The choice of the values for α and β was made because they gave faster results. The procedure for the Hartree-Fock iteration is shown schematically in Fig. 4.1.

The convergence is measured by:

$$conv = \frac{1}{i_{\max}} \sum_{i,j}^{i_{\max}} \sqrt{\frac{(V_{HF,ij} - V^{\text{old1}}_{HF,ij})^2}{V^2_{HF,ij} + \varepsilon}} \,, \tag{4.16}$$

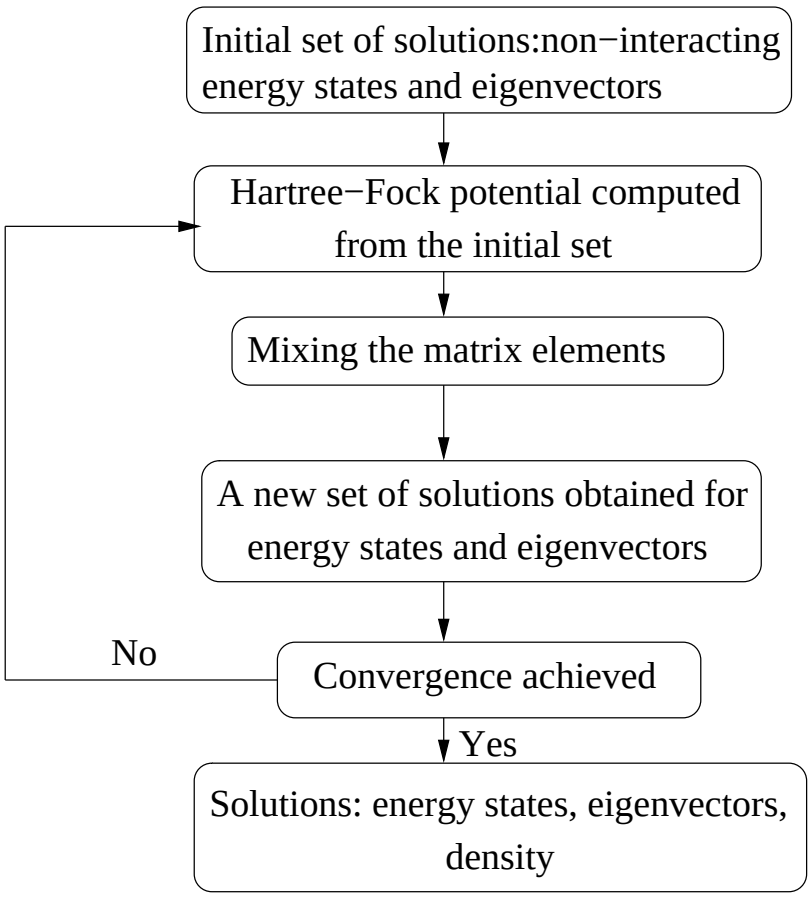

Figure 4.1: The Hartree-Fock iteration sketch.

with $\varepsilon = 10^{-3}$, which was added in the denominator to avoid division by zero. When the criterion

$$conv < 10^{-2} \tag{4.17}$$

was reached, λ was increased

$$\lambda \to \lambda + 0.2\,, \tag{4.18}$$

and the system experiences more interaction. When the system experiences the full interaction, corresponding to $\lambda = 1$ and the criterion

$$conv < 10^{-3} \tag{4.19}$$

was reached, then the changes in results are negligible and the density has stabilized.

In Fig. 4.2 and 4.3 the convergence is shown for four and six electrons. The large oscillations correspond to the stepwise increment of the interaction while the small ones correspond to internal changes in the configuration of the electron structure.

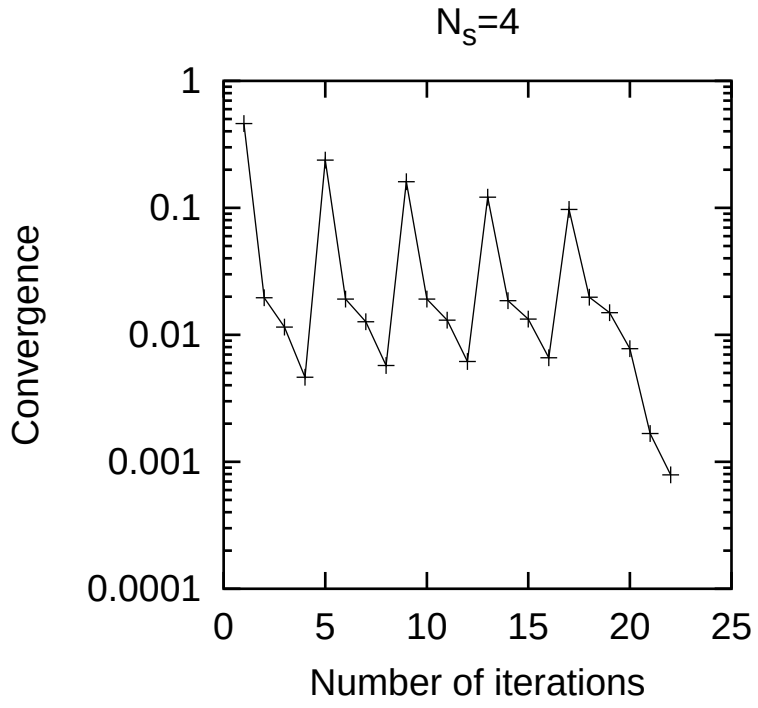

Figure 4.2: Convergence for a circular quantum ring with 4 electrons, $M^{max} = 6$, ${n_r}^{max} = 4$, $B = 0.2$ T.

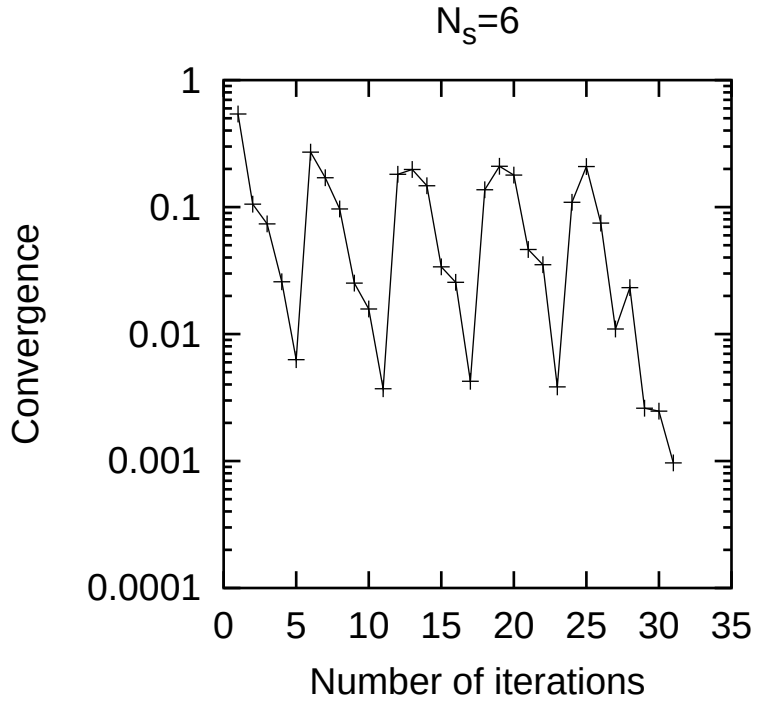

Figure 4.3: Convergence for a circular quantum dot with 6 electrons, $M^{max} = 4$, ${n_r}^{max} = 4$, $B = 0.2$ T.

Chapter 5

Magnetization of quantum dots and rings

Earlier, it has been observed that in the case of noninteracting or Hartree interacting electrons confined in a quantum dot the magnetization depends strongly on the number of electrons and to a lesser extent on the shape of the dot [13]. We expect the exchange interaction and the spin configuration of the ground state to be important. Therefore within this chapter the magnetization of quantum dots deviating from circular symmetry is calculated for noninteracting electrons and electrons interacting according to the Hartree-Fock approximation (HFA). Recently, new [27, 28] or improved methods [29] to measure the magnetization of a two-dimensional electron gas (2DEG) have been applied to give important information about the structure of the many-electron ground state in dots with few hundred electrons each. The experimentalist are eager to develop their methods further in order to be able to access the magnetization of quantum dots with few electrons, where more drastic transformations occur in the electron and the spin structure with changing magnetic field. In anticipation, we concentrate here on systems with few electrons. In principle, our methods and models are applicable to dots with up to several tens of electrons.

5.1 Magnetization of quantum dots

The total magnetization with an orbital contribution $\mathscr{M}_o$ defined in terms of the quantum thermal average of the current density, and a spin contribution $\mathscr{M}_s$, derived from the average value of the spin density, is defined as:

$$\vec{\mathscr{M}}_o + \vec{\mathscr{M}}_s = \frac{1}{2}\int_{R^2} d\vec{r}\left[\vec{r}\times\langle\vec{J}(\vec{r})\rangle\right]\cdot\hat{n} - g\mu_B\int_{R^2} d\vec{r}\langle\sigma_z(\vec{r})\rangle \tag{5.1}$$

where μ_B is the Bohr magneton. In the HFA we have a nonlocal equation of motion and no explicit single-electron Hamiltonian. The charge current density does not have the same simple local expression as in the Hartree approximation. By defining the current density as

$$\vec{J} = -e\dot{\vec{r}} = \frac{ie}{\hbar}[\hat{H}, \hat{r}], \tag{5.2}$$

we construct the matrix elements of the contribution of each Hartree-Fock state $|\alpha)$ of the magnetization operator $\vec{M} = \vec{r} \times \vec{J}$ and sum up the total magnetization of the system

$$\vec{\mathscr{M}} = \sum_{\alpha} f_\alpha (\alpha|\vec{M}|\alpha), \tag{5.3}$$

where f_α is the occupation of the state $|\alpha)$ according to the equilibrium Fermi distribution. An extended derivation of the Hartree-Fock magnetization is found in the appendix B.2.

We calculate the magnetization of quantum dots with four, five and six electrons and with various shapes, like circular, elliptic and square symmetric. In this calculation we use GaAs parameters $m^* = 0.067m_0$, $\kappa = 12.4$, $g^* = -0.44$, and we select the confinement frequency $\hbar\omega_0 = 3.37$ meV in order to study quantum dots with few electrons in the regime where the energy scale of the Coulomb interaction is of the same order of magnitude as or larger than the quantization energy due to the geometry and the magnetic field. For the GaAs parameters the spin contribution to the magnetization is generally very small, but the exchange effects can have a large influence on the orbital contribution.

To see clearly the information about the structure of the ground state discernible in the curves of the magnetization versus the magnetic field B we start by investigating a dot with noninteracting electrons. As a guiding principle we use the fact that the total magnetization of a large electron system can be expressed via the thermodynamic formula:

$$\mathscr{M}_o + \mathscr{M}_s = -\frac{\partial F}{\partial B} = -\frac{\partial}{\partial B}(E_{\text{total}} - TS), \tag{5.4}$$

where S and E_{total} are the entropy and the total energy of the system, respectively. Because of the fact that our calculations are performed at a low temperature regime ($T = 1$ K), the free energy F can in some cases be approximated by the total energy E_{total},

$$\mathscr{M}_o + \mathscr{M}_s \approx -\frac{\partial E_{\text{total}}}{\partial B}, \tag{5.5}$$

if the thermal energy, $k_B T \approx 0.09$ meV, is much smaller than the typical energy level spacing, often in the range of few or several meV in the dot. This is not true in all cases as we shall see later.

The noninteracting orbital magnetization shows jumps, that can be explained with the discontinuities in the derivative of E_{total} with respect to the magnetic field B, reflecting crossing of single-electron states, or equivalently, changes in the many-electron structure of the ground state. In a circular dot, each single-electron state can be assigned a definite

quantum number M for the angular momentum. As the magnetic field is increased the occupation of a state with a higher angular momentum is energetically favorable.

In an elliptic dot at low magnetic field increasing the deviation from circular symmetry results in a change of the curvature of some of the initially degenerate single-electron energy levels as a function of the magnetic field B. Looking at the magnetization for $N_s = 4$ (see Fig. 5.2 and 5.5), we see it differs only at low magnetic field for different strength of deviation α_1, reflecting that the lowest occupied single-electron state has almost unchanged curvature for low magnetic field (see Fig. 3.5), but the curvature of the second state changes slightly for low B as the degeneration of the $M = \pm 1$ states is lifted. In the case of $N_s = 5$ the magnetization differs at low magnetic field and also around $B \approx 1$ T, where the third and the fourth single-electron states cross (see Fig. 5.15 and 5.16). This is to a large extent an effect of the lifting of the degeneracy of the $M = 0, \pm 2$ states at $B \approx 0$ T.

Increasing the number of electrons in the dot to $N_s = 6$, the changes in the curvature for low magnetic field of the second and the third states cancel, leaving the magnetization unaffected by the changes in the shape of the dot. Instead, the magnetization changes increasing α_1 around $B \approx 1$ T (see Fig. 5.22 and 5.24), where the third and the fourth single-electron state crosses. According to the Darwin-Fock diagram (see Fig. 3.5), the crossing point varies with α_1, shifting the location of the jump in the magnetization.

By changing the deviation from ellipticity to square symmetry, the square deviation doesn't lift the degeneracy of the second and third single-energy levels (the $M = \pm 1$ states) at zero magnetic field and at the same time it doesn't move too much the crossing point between the third and the fourth energy levels (see Fig. 3.8). Therefore the magnetization for $N_s = 4, 5, 6$ electrons is not strongly affected by the increased square shape of the quantum dot (see Fig. 5.8, 5.11, 5.17, 5.18, 5.26, 5.28).

The main difference in the magnetization of a quantum dot with an elliptical or a square shape comes from the fact the elliptical deviation has nonzero matrix elements between single-electron states with a dominant contribution of basis states of a circular dot satisfying $|\Delta M| = 2$, whereas the square shape can connect only states with a dominant contribution satisfying $|\Delta M| = 4$. For weak deviation the square dot needs the occupation of more states than the elliptical dot to show effects in the magnetization different from the magnetization of a circular quantum dot [13].

By turning on the Coulomb interaction between the electrons in the system, we notice important effects on the electron density, energy spectrum and magnetization. One reason is that the interaction enhances the deviation and the size of the anticrossing energy gap in the effective single-electron spectrum. However this behavior is observed only in dots with few electrons; in larger dots the interaction generally smoothes the shape of the electron density. Another reason is the magnetic field; it is very well known that, in the presence of a magnetic field the electrons become spin-polarized. In the ground state the Zeeman energy competes with the kinetic energy and favors the spin alignment along the

field. The larger the magnetic field, the more electron spins flip over and at sufficiently strong B the whole system appears to be in the fully spin-polarized state. This alignment of spins is further enhanced by the exchange force.

One problem with the HFA is the possibility that the system gets trapped in a certain spin configuration that may not correspond to the real ground state. We try to overcome this by starting the iterations for the same parameters with different initial conditions, usually by varying the spin polarization of the initial system by an abnormally large g factor that is then relaxed to its normal value in subsequent iterations. We can never map out all possible end states in a reasonable time but commonly we manage to find the states with highest spin polarization by artificial initial factor in the range $g_i = -40$ to $g_i = -100$.

The Coulomb interaction in a circular dot cannot change the angular symmetry of the dot, but as soon as the symmetry is broken by the confinement potential, the interaction modifies the angular shape of the dot. Comparing the magnetization of interacting electron system with the magnetization corresponding to the noninteracting electron system we noticed some differences, that can only be explained by the Coulomb repulsion. In the range of a low magnetic field the Coulomb repulsion between electrons causes changes in the electron structure to happen earlier as B is increased. It is energetically favorable for electrons to occupy states associated with higher angular momentum when B increases. Therefore the jumps in the magnetization are shifted towards lower B. The distance between the monotonic high magnetic field tails of interacting magnetization and noninteracting magnetization increases. This occurs because for higher magnetic fields the magnetic length l decreases (it is proportional with $1/\sqrt{B}$) and thus the interaction is stronger with increasing magnetic field. This fact is also observed in the structure of electron density that becomes flatter with increasing magnetic field B, as the typical inter-electron distance, that is proportional with l for a noninteracting system, is expanded by the Coulomb interaction.

For $B = 0$ T we expect the magnetization to vanish as no asymmetry in the occupation of $\pm M$ states can be justified. This condition is not always fulfilled by the final states that the HFA delivers at a very low magnetic field. Our computational method does not work at $B = 0$ T.

Increasing the number of electrons in the system, the Coulomb repulsion obviously increases leading to changes in the electron structure observable in the magnetization, the total energy curves and in the electron density as well. By breaking the circular symmetry with elliptic or square symmetric deviation of the confinement, we notice that the magnetization doesn't suffer major changes but we observe a kind of a "screening effect" enhanced with increasing deviation. The deviation from the circular symmetry always weakens the confinement potential somewhere. In the case of the square symmetric deviation the electrons find more space in the corners. In the case of dots with few electrons the Coulomb interaction enhances the deviation, and the electrons can more effectively

screen out the weaker parts of the confinement. This enhanced deviation also spreads out the electronic density of a dot and thus lowers the total energy. We can in our calculation see the total energy decreasing with increasing deviation. In the case of dots with circular and square symmetry with four and five electrons (see Fig. 5.1, 5.8, 5.11, 5.14, 5.17, 5.18), we see that the electron system is trapped in a certain spin configuration that doesn't correspond to the real ground state leading to a nonzero magnetization at $B = 0$ T, while the elliptic symmetry helps the system to achieve an appropriate spin configuration that corresponds to the real ground state and therefore to a zero magnetization (see Fig. 5.2, 5.5, 5.15, 5.16). When the number of electrons rises to six, for any studied configuration, circular, elliptic and square symmetric, the magnetization becomes zero at $B = 0$ T (see Fig. 5.19, 5.22, 5.24, 5.26, 5.28). The reason is that having either four and five electrons in the system, the $(0,0)$ is doubly occupied but the $(\pm 1,0)$ are not symmetrically occupied (see Fig. 3.2). Having six electrons, the occupation of the $(\pm 1,0)$ is always symmetric (see Fig. 3.2).

As previously noted, the elliptic symmetry is more favorable in getting the right ground state, with a zero magnetization at any degree of deviation. The magnetization suffers major changes as the number of particles increases, but it is not very sensitive to slight changes in shape of the quantum dot. The magnetic field itself can induce structural changes; At a low magnetic field four electrons in a quantum dot with elliptical shape are not spin polarized, and the elliptic density has two humps. At $B = 3$ T, the system experiences changes in its structure, observed in a jump of the orbital magnetization, the total energy, and also in the electron density that develops four humps (see Fig. 5.3, 5.6). At first one would expect the four electrons all to have parallel spin, but the total z component of the spin is zero. Instead, a spin wave state has been found; the spin density in each direction has two humps connected through the center of the dot and they are perpendicular to each other. Here is very clear that the spin-density state is not the ground state [30, 31].

If we start with four spin polarized electrons in the elliptic dot the density evolves differently with increasing magnetic field. We start with a elliptical density with a dimple in the center (see Fig. 5.4, 5.7). This "circle" or dimple fades away with increasing magnetic field and for the range of magnetic field we use we do not find a structure with four humps representing the four electrons. With increasing number of particles, the elliptic density has a more obvious "circle" in the middle and with increasing magnetic field it develops further interesting shapes (see Fig. 5.23, 5.25). The presence of this circle will be much better understood below. The circular structure in the electron density with six electrons is explained with aid of Fig. 3.2. The occupied states are among others $(0,0)$ and $(\pm 1,0)$ and the corresponding squared moduli of the wavefunctions are:

$$|\Phi_{0,0}|^2 \approx e^{-\frac{r^2}{2a^2}} \tag{5.6}$$

$$|\Phi_{\pm 1,0}|^2 \approx \frac{1}{2}\left(\frac{r}{a}\right)^2 e^{-\frac{r^2}{2a^2}}, \tag{5.7}$$

with similar proportionality factors. Therefore, we have equivalent contributions to the density structure from the $(\pm 1,0)$ states resulting in more weight in the density. With

increasing magnetic field higher $+M$ states are occupied and $-M$ states emptied and the circle structure fades away (see Fig. 5.20) for the spin unpolarized electrons. In case of the polarized case, the density undergoes some changes but the circle does not fade away (see Fig. 5.21). This explains why the elliptic electron density resembles somewhat the density of a circular quantum dot, one difference is the fact that for elliptic confinement, the surface within a given equipotential line is larger than if $\alpha_1 = 0.0$ (see Fig. 3.4).

By changing the deviation from circular symmetry to square symmetry the orbital and the spin magnetization and the total energy change with increasing number of electrons but not strongly with increasing deviation (see Fig. 5.8, 5.11, 5.17, 5.18, 5.26, 5.28). The square symmetric density with four electrons evolves for different degrees of deviation from flatter four peaks density structures corresponding to nonpolarized spin states (see Fig. 5.9, 5.12) to a very emphasized four peaks density structure corresponding to polarized spin states (see Fig. 5.10, 5.13), showing the fact that the four electrons are localized in the corners of the square symmetric dot. An interesting phenomenon occurs at $B = 0$ T for $\alpha_2 = 0.2$ when the system reaches close to the real ground state evidenced by a magnetization close to zero. Here we have only been able to reach a spin polarized final state in our HFA iterations for a magnetic field very close to 0 T, but for higher magnetic fields we find both spin polarized and unpolarized states (see Fig. 5.11, 5.12, and 5.13). Increasing the number of electrons to six, the square is more pronounced and we sometimes achieve spin polarization for a normal g factor, present also as a jump in the total energy (see Fig. 5.26, 5.28). At $B = 1$ T we notice that the square symmetric density shows clearly how the six electrons are distributed in the density (see Fig. 5.27, 5.29) and that with increasing magnetic field the density shows more screening of the interaction leading to a flatter square shape.

In order to illustrate how the density can reflect the number of particles in the system when we replace the circular symmetry with elliptic and square symmetry we collect some representative figures of the electron density (see Fig. 5.30, 5.31). The four electrons are seen as four peaks in the elliptic symmetry, while in the case of square symmetric confinement the electrons are distributed in the corners. The five electrons form five peak structures for both the elliptic and square symmetric density while the six electrons form an elliptic density with three parallel peaks and a kind of an X-dot for the square symmetric density.

5.2 Magnetization of quantum rings

By adding a circular symmetric hill to the center of the confinement potential (see Fig. 3.9) we get a dot with a hole in the middle, or a quantum ring of finite thickness. The dimensions of the center are adjusted by V_0 (controls the height of the hill) and γ (controls the width of the hill) in Eq. (3.21). We know that in the case of an infinitely thin ring the energy spectrum is a periodic function of the magnetic flux [32]. The relation between

the magnetization and the persistent currents has been studied in a model of ring with finite width but no Coulomb interaction between the electrons [33, 34]. In a ring of finite width the energy spectrum for the lowest states is quasi periodic, observable in Fig. 3.10, 3.11 and 3.12, and the periodicity is lost as soon as the magnetic length becomes smaller than the thickness of the ring. The same behavior is seen in the magnetization curves. The magnetization has many oscillations at low magnetic field while at the high magnetic field they are blurred behaving like a dot in a high magnetic field. We see by increasing the parameter V_0 the hole increasing (see Fig. 5.40) and the oscillations in the magnetization becoming clearer as the ring gets thinner (see Fig. 5.32, 5.33, 5.36). It is interesting to notice that the total energy for the electrons in a ring with our selection of parameters does not increase with increasing B, it can even decrease. This is due to the fact that as the magnetic length decreases the system fits better into the narrows confinement potential. Despite of this behavior the magnetization has similar over all negative slope with increasing B as in the case of quantum dots. Here we cannot approximate the free energy F with E_{total} since the single-electron levels are very close and the entropy S cannot be neglected.

When we deviate the shape of the ring away from the circular symmetry on the outer rim we decrease fast the quasi periodic oscillations of the magnetization. This is independent of whether we use an elliptic or square symmetric deviation of the outer confinement. With a combination of the center hole and the square or elliptical symmetry we get easily into a range of parameters where the electronic density forms two or more almost separate islands (see Fig. 5.35, 5.39), and within our range of the magnetic field (0-3 T) the magnetization becomes almost linear (see Fig. 5.34, 5.37, 5.38).

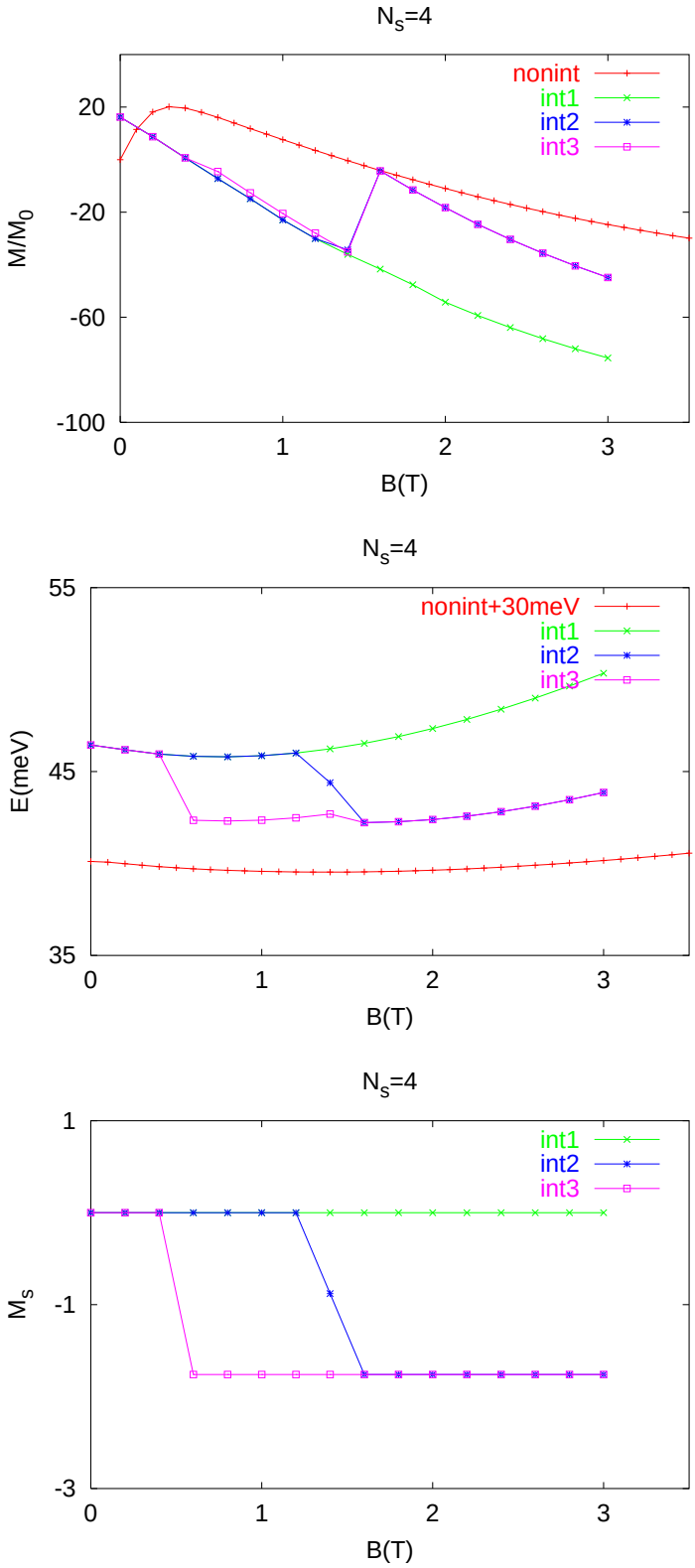

Figure 5.1: The orbital M_o and spin magnetization M_s and the total energy of a four-electron quantum dot in the case of circular confinement ($\alpha_1 = 0.0,\ \alpha_2 = 0.0$) for both noninteracting ("nonint") and interacting electrons ("int1", "int2" and "int3" corresponding to $g = -0.44,\ g_i =$

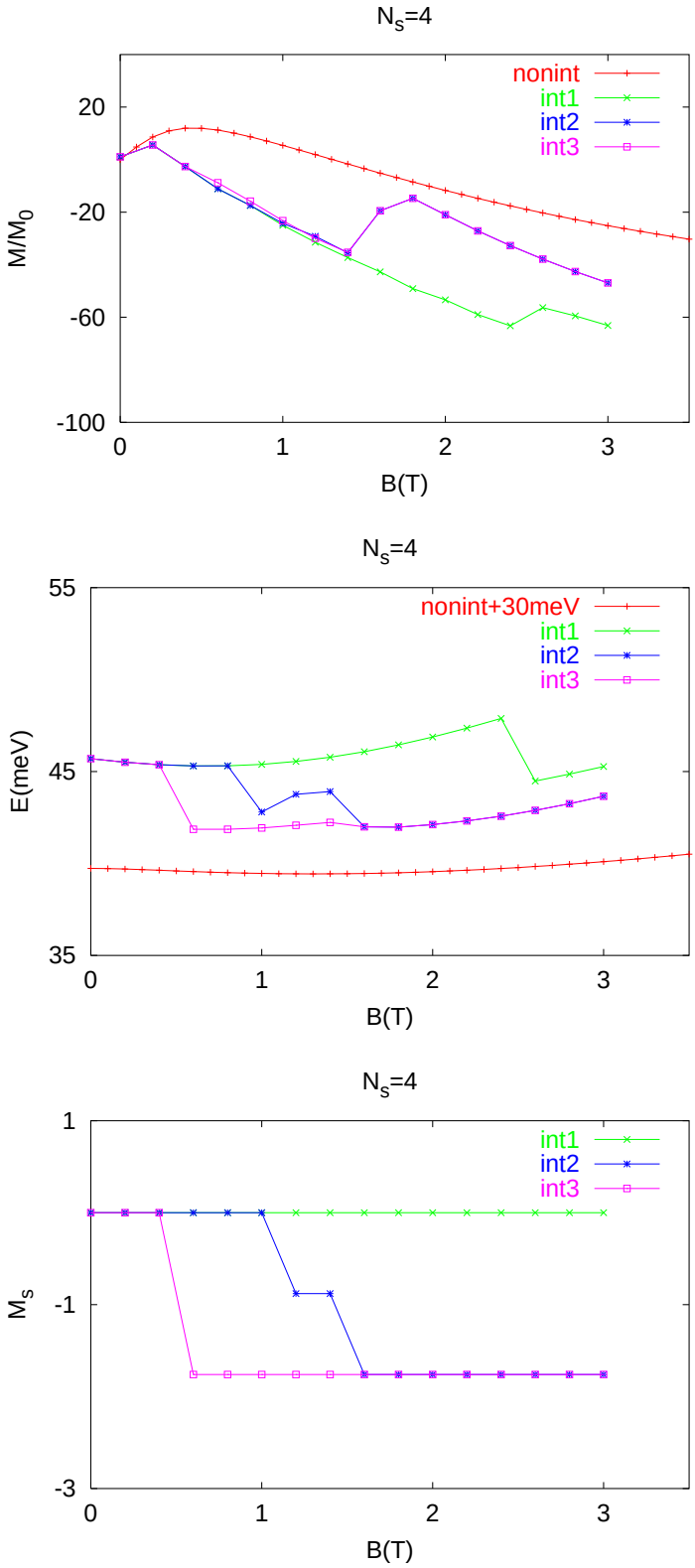

Figure 5.2: The orbital M_o and spin magnetization M_s and the total energy of a four-electron quantum dot in the case of elliptic confinement ($\alpha_1 = 0.1,\ \alpha_2 = 0.0$) for both noninteracting ("nonint") and interacting electrons ("int1", "int2" and "int3" corresponding to $g = -0.44,\ g_i =$

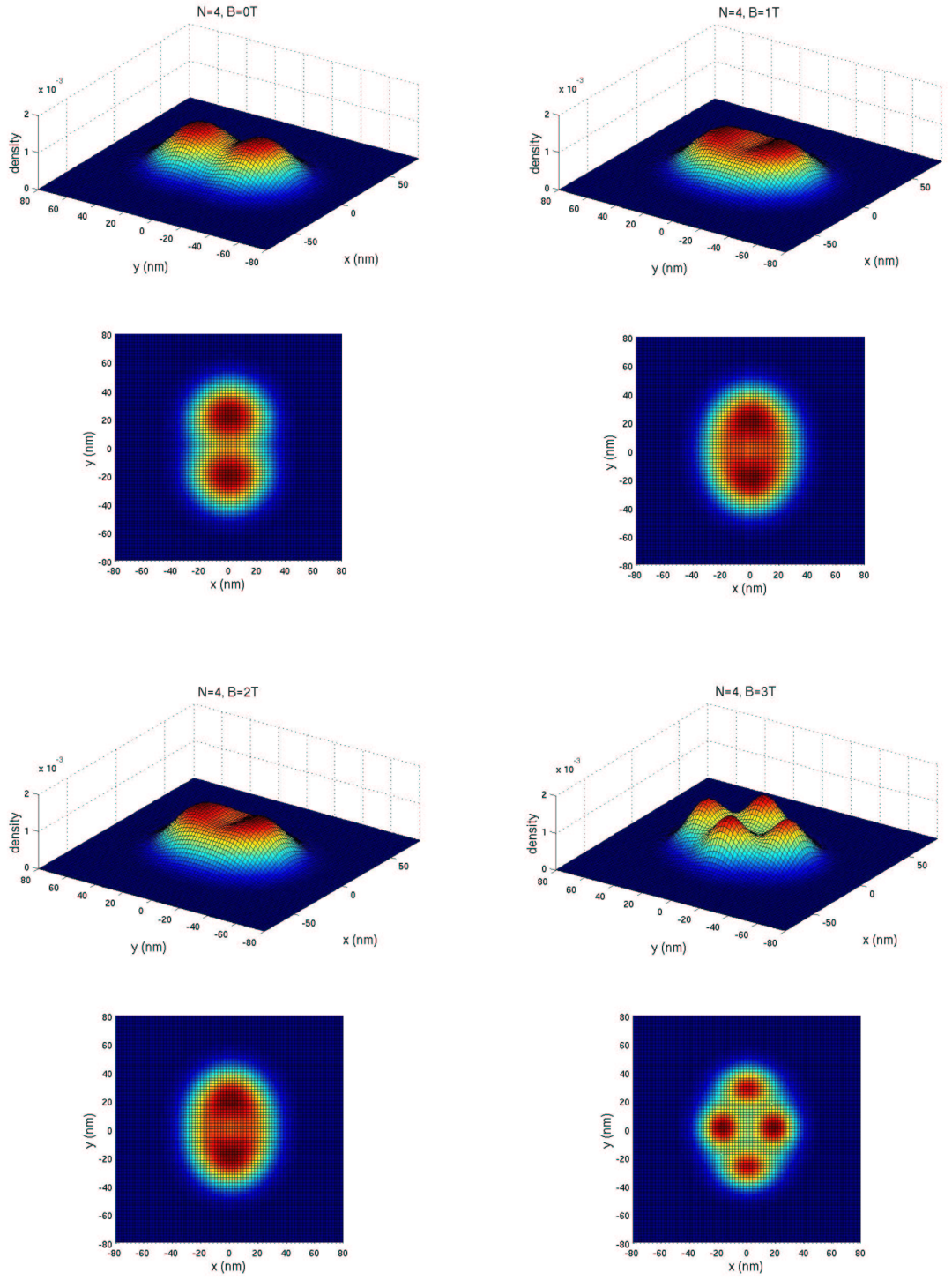

Figure 5.3: The electron densities of a four-electron quantum dot in the case of elliptic confinement ($\alpha_1 = 0.1,\ \alpha_2 = 0.0$) for nonpolarized ($g = -0.44$) interacting electrons at different values of magnetic field $B = 0$ T, $B = 1$ T, $B = 2$ T and $B = 3$ T.

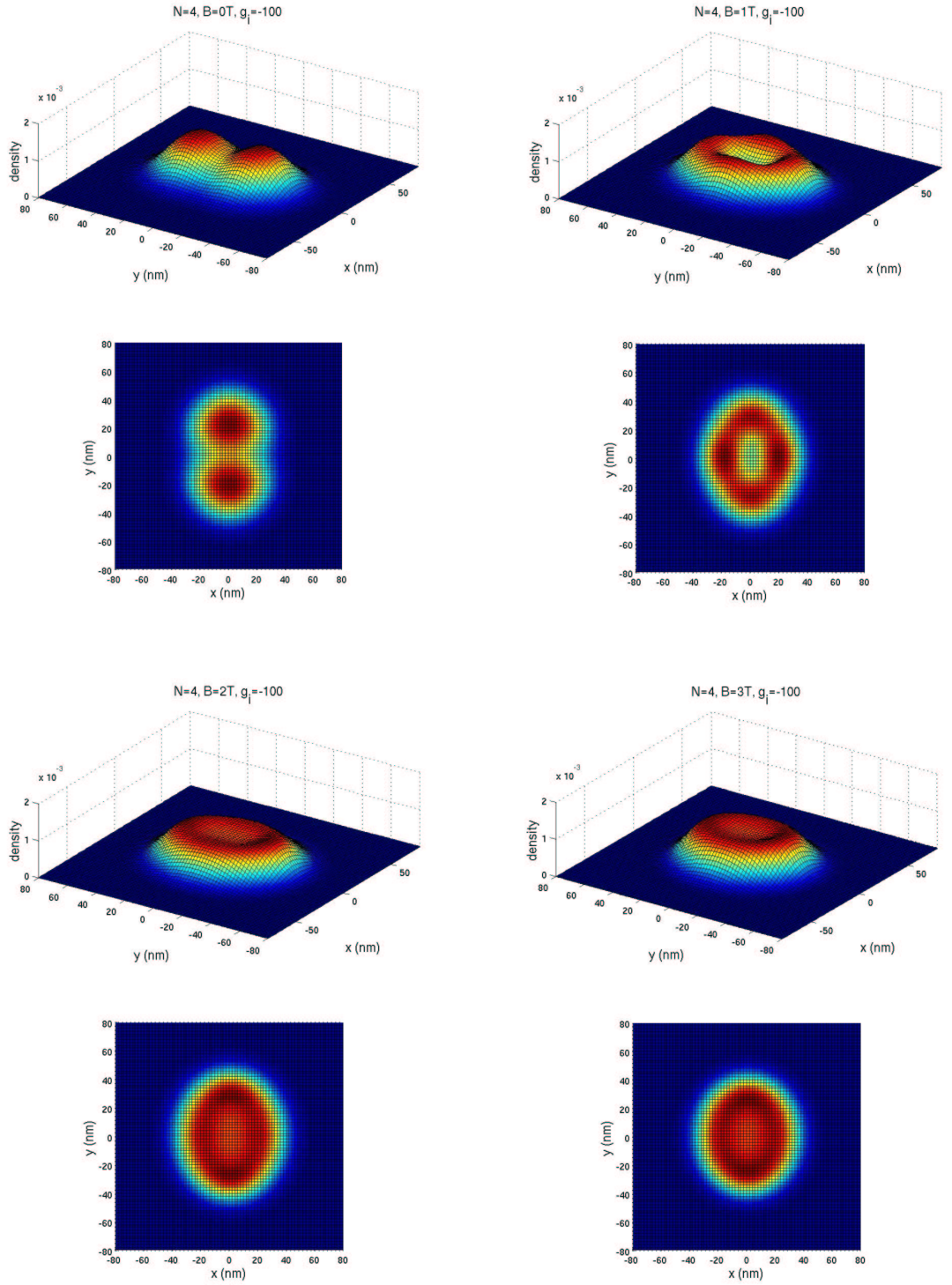

Figure 5.4: The electron densities of a four-electron quantum dot in the case of elliptic confinement ($\alpha_1 = 0.1,\ \alpha_2 = 0.0$) for polarized ($g_i = -100$) interacting electrons at different values of magnetic field $B = 0$ T, $B = 1$ T, $B = 2$ T and $B = 3$ T.

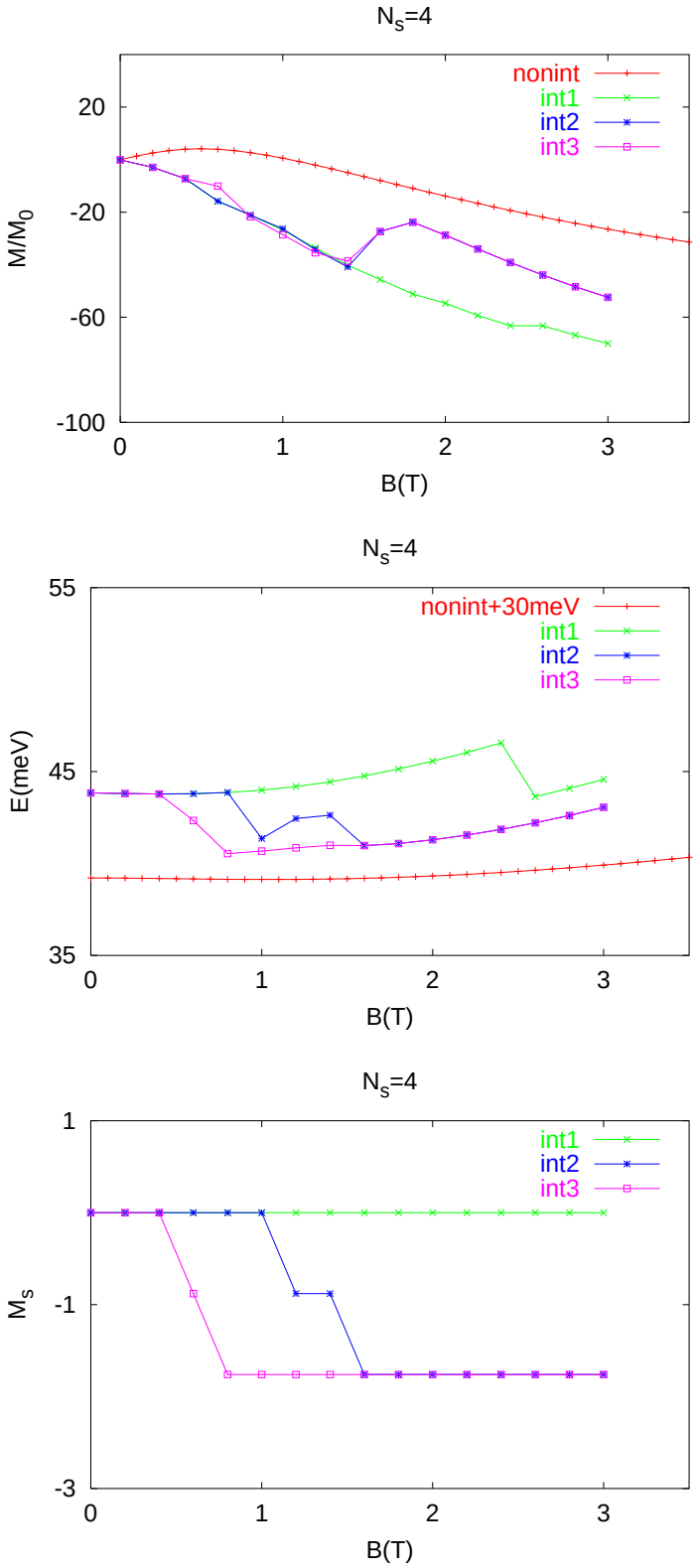

Figure 5.5: The orbital M_o and spin magnetization M_s and the total energy of a four-electron quantum dot in the case of elliptic confinement ($\alpha_1 = 0.2,\ \alpha_2 = 0.0$) for both noninteracting ("nonint") and interacting electrons ("int1", "int2" and "int3" corresponding to $g = -0.44,\ g_i =$

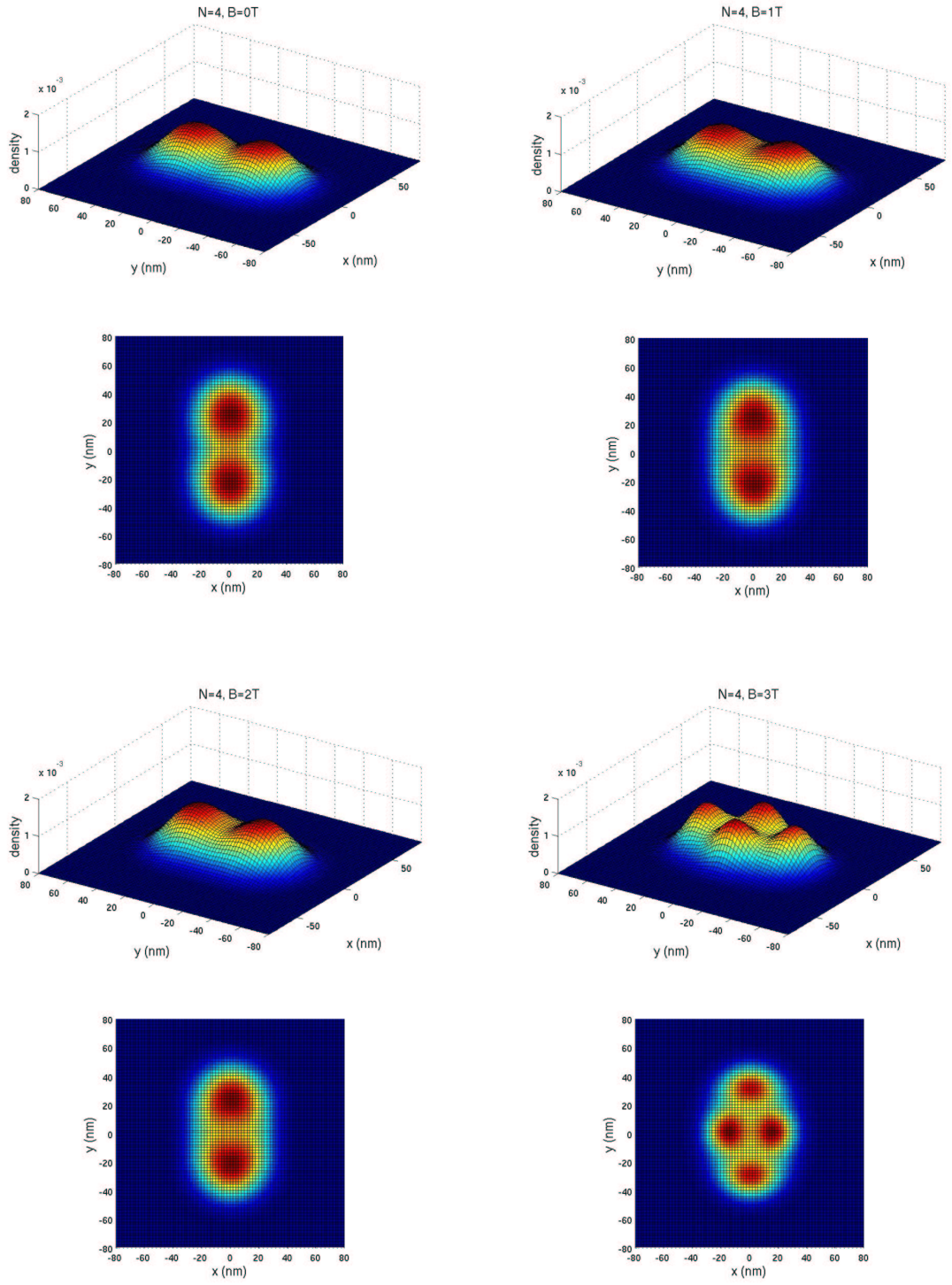

Figure 5.6: The electron densities of a four-electron quantum dot in the case of elliptic confinement ($\alpha_1 = 0.2,\ \alpha_2 = 0.0$) for polarized ($g = -0.44$) interacting electrons at different values of magnetic field $B = 0$ T, $B = 1$ T, $B = 2$ T and $B = 3$ T.

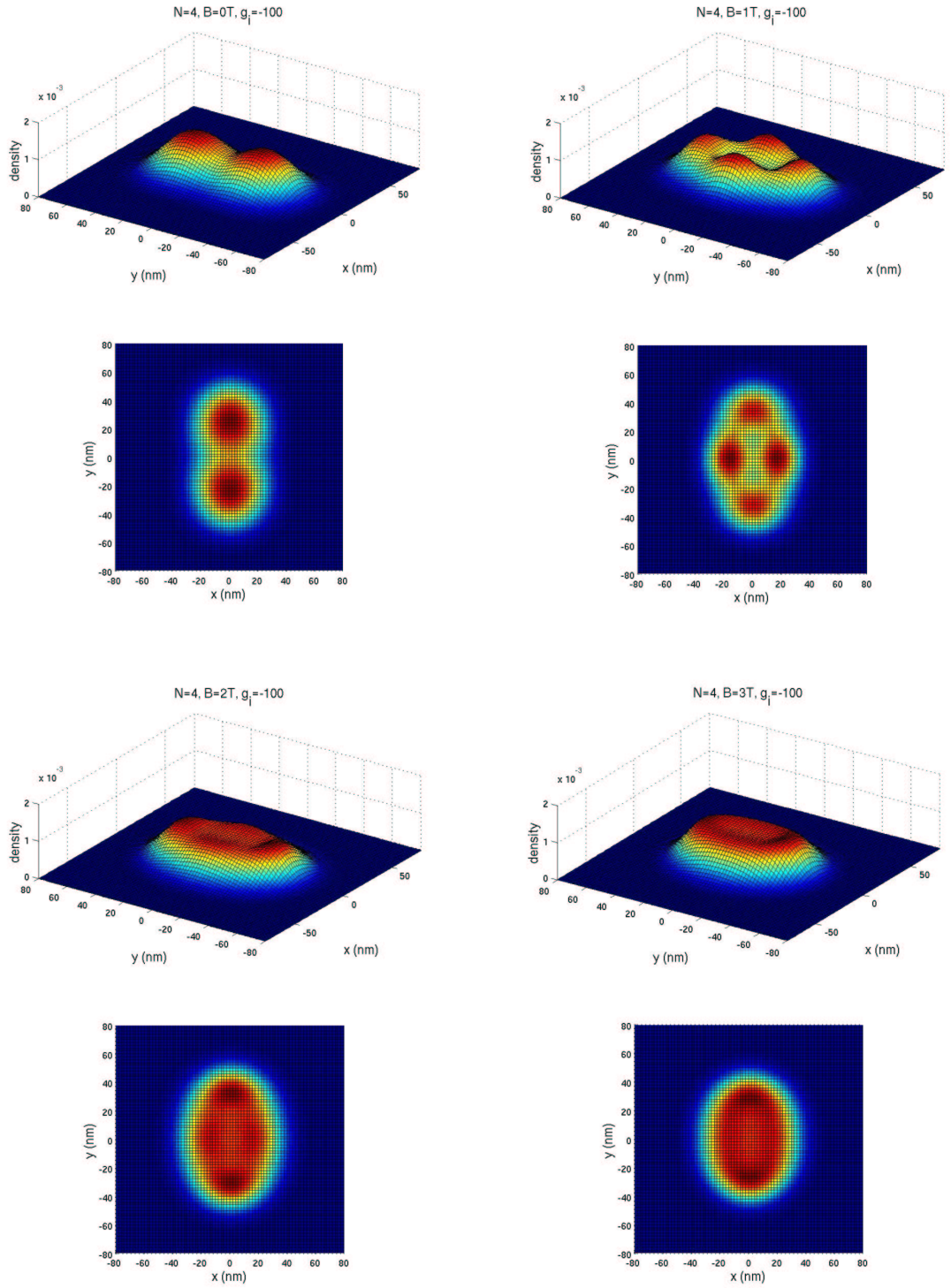

Figure 5.7: The electron densities of a four-electron quantum dot in the case of elliptic confinement ($\alpha_1 = 0.2,\ \alpha_2 = 0.0$) for polarized ($g_i = -100$) interacting electrons at different values of magnetic field $B = 0$ T, $B = 1$ T, $B = 2$ T and $B = 3$ T.

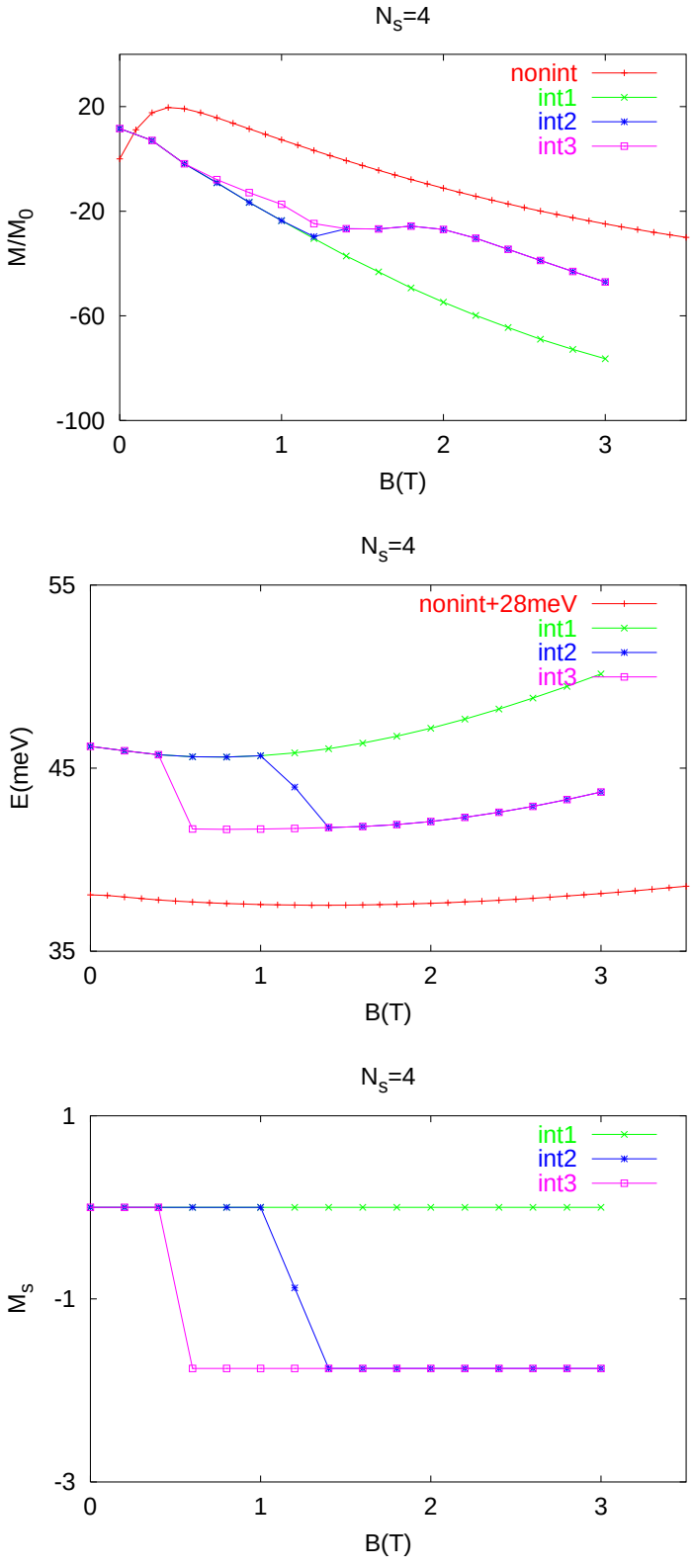

Figure 5.8: The orbital M_o and spin magnetization M_s and the total energy of a four-electron quantum dot in the case of square symmetric confinement ($\alpha_1 = 0.0,\ \alpha_2 = 0.1$) for both noninteracting ("nonint") and interacting electrons ("int1", "int2" and "int3" corresponding to $g = -0.44$,

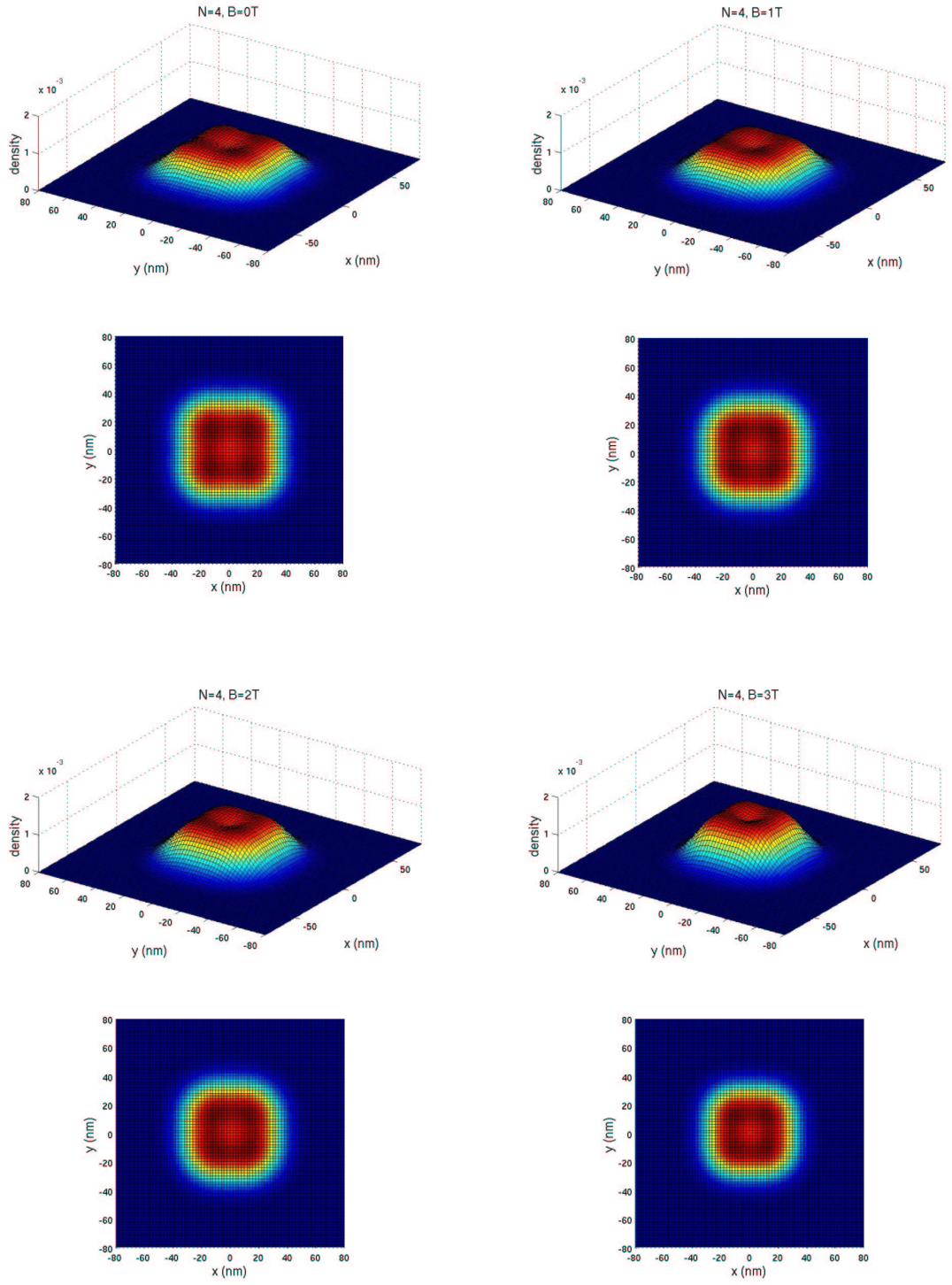

Figure 5.9: The electron densities of a four-electron quantum dot in the case of square symmetric confinement ($\alpha_1 = 0.0,\ \alpha_2 = 0.1$) for unpolarized ($g = -0.44$) interacting electrons at different values of magnetic field $B = 0$ T, $B = 1$ T, $B = 2$ T and $B = 3$ T.

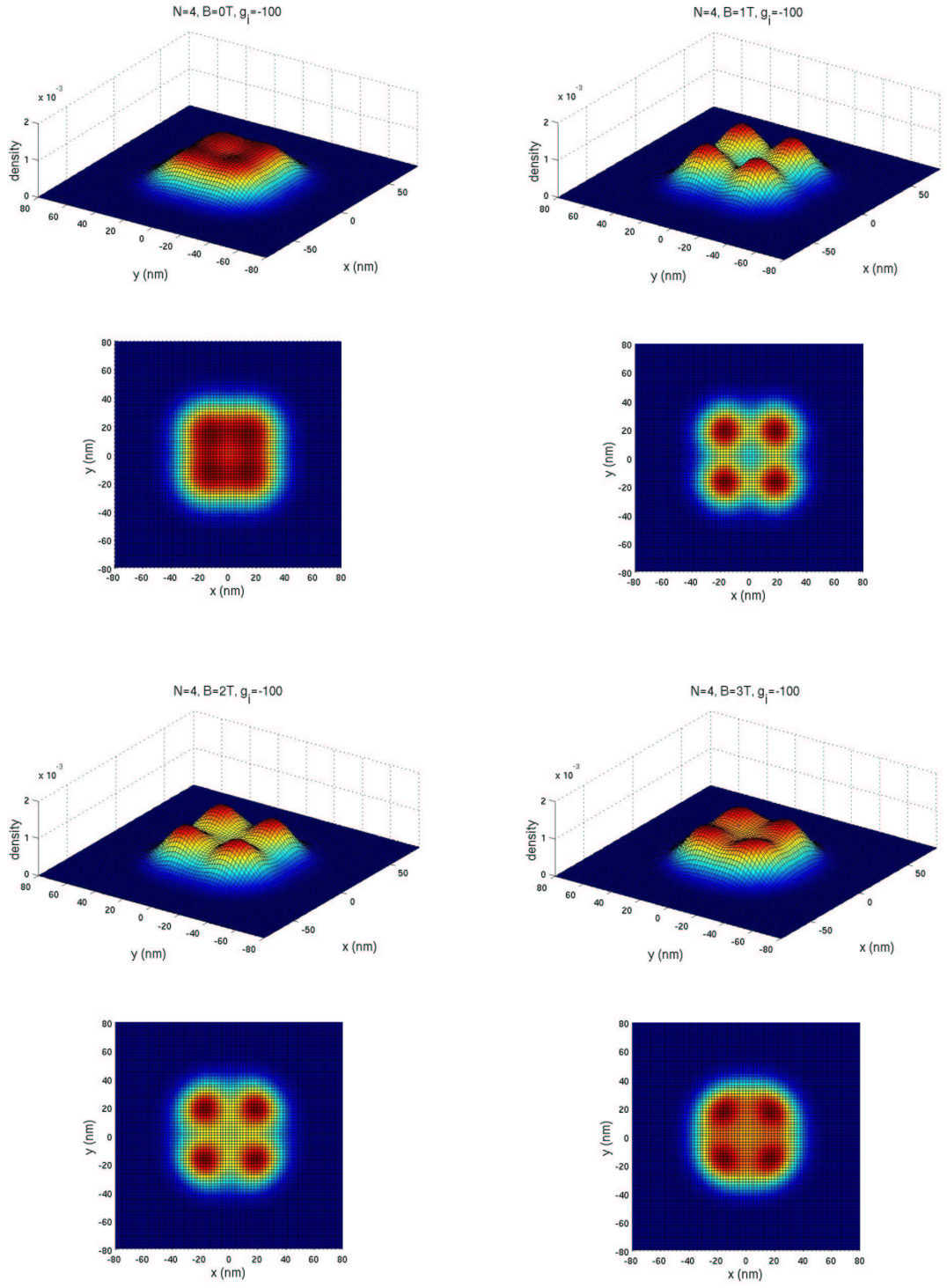

Figure 5.10: The electron densities of a four-electron quantum dot in the case of square symmetric confinement ($\alpha_1 = 0.0,\ \alpha_2 = 0.1$) for polarized ($g_i = -100$) interacting electrons at different values of magnetic field $B = 0$ T, $B = 1$ T, $B = 2$ T and $B = 3$ T.

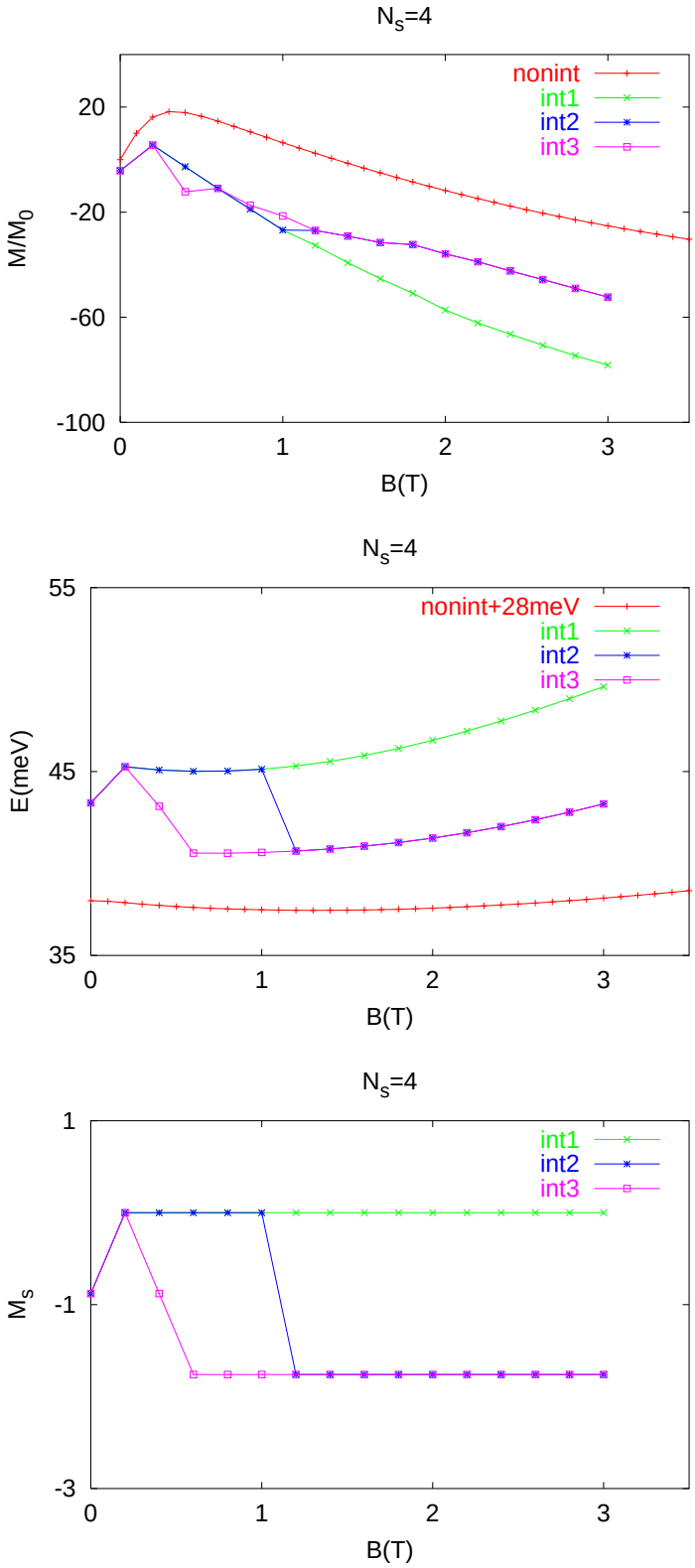

Figure 5.11: The orbital M_o and spin magnetization M_s and the total energy of a four-electron quantum dot in the case of square symmetric confinement ($\alpha_1 = 0.0,\ \alpha_2 = 0.2$) for both noninteracting ("nonint") and interacting electrons ("int1", "int2" and "int3" corresponding to $g = -0.44$,

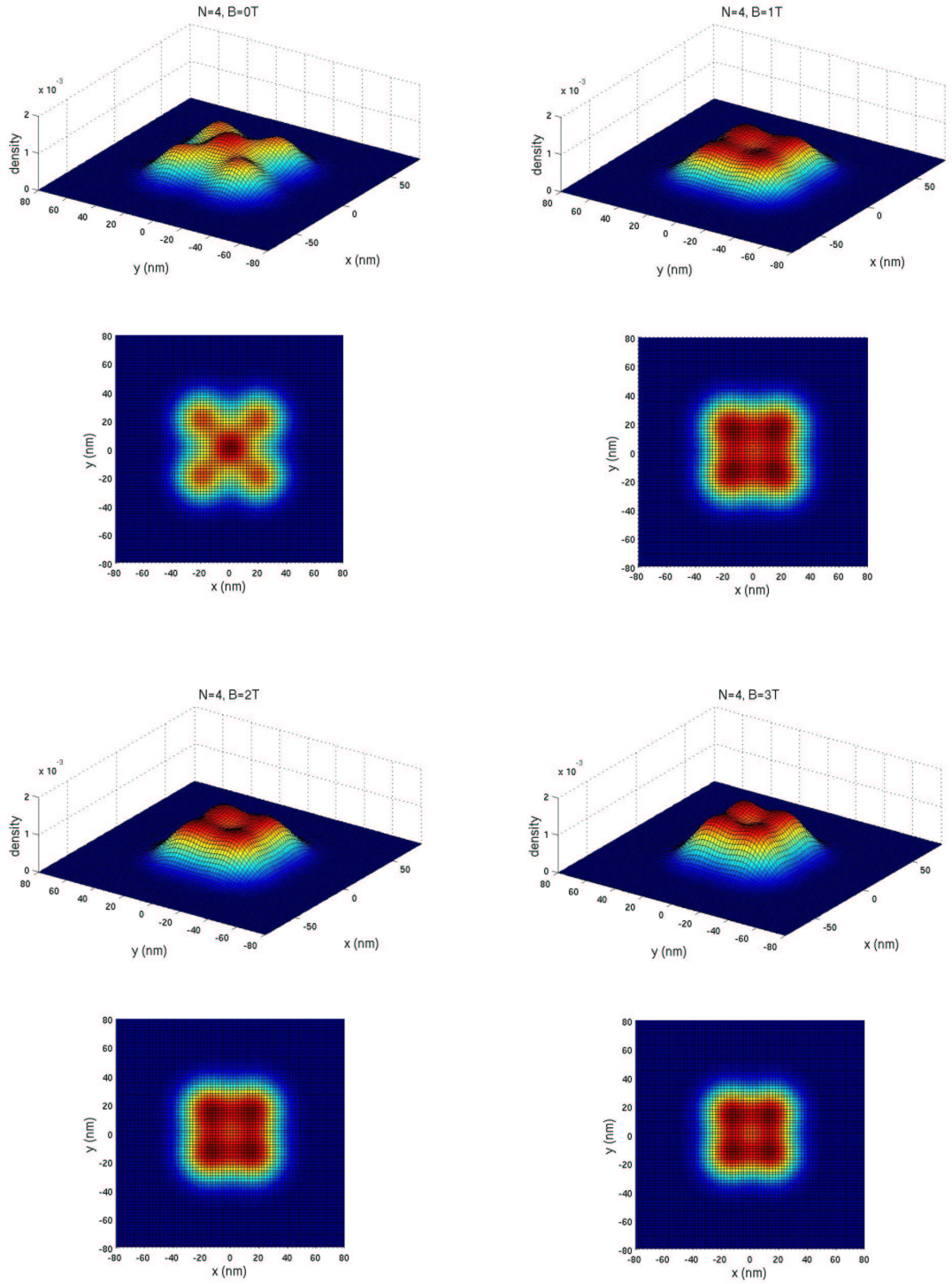

Figure 5.12: The electron densities of a four-electron quantum dot in the case of square symmetric confinement ($\alpha_1 = 0.0,\ \alpha_2 = 0.2$) for unpolarized ($g = -0.44$) interacting electrons at different values of magnetic field $B = 0$ T, $B = 1$ T, $B = 2$ T and $B = 3$ T.

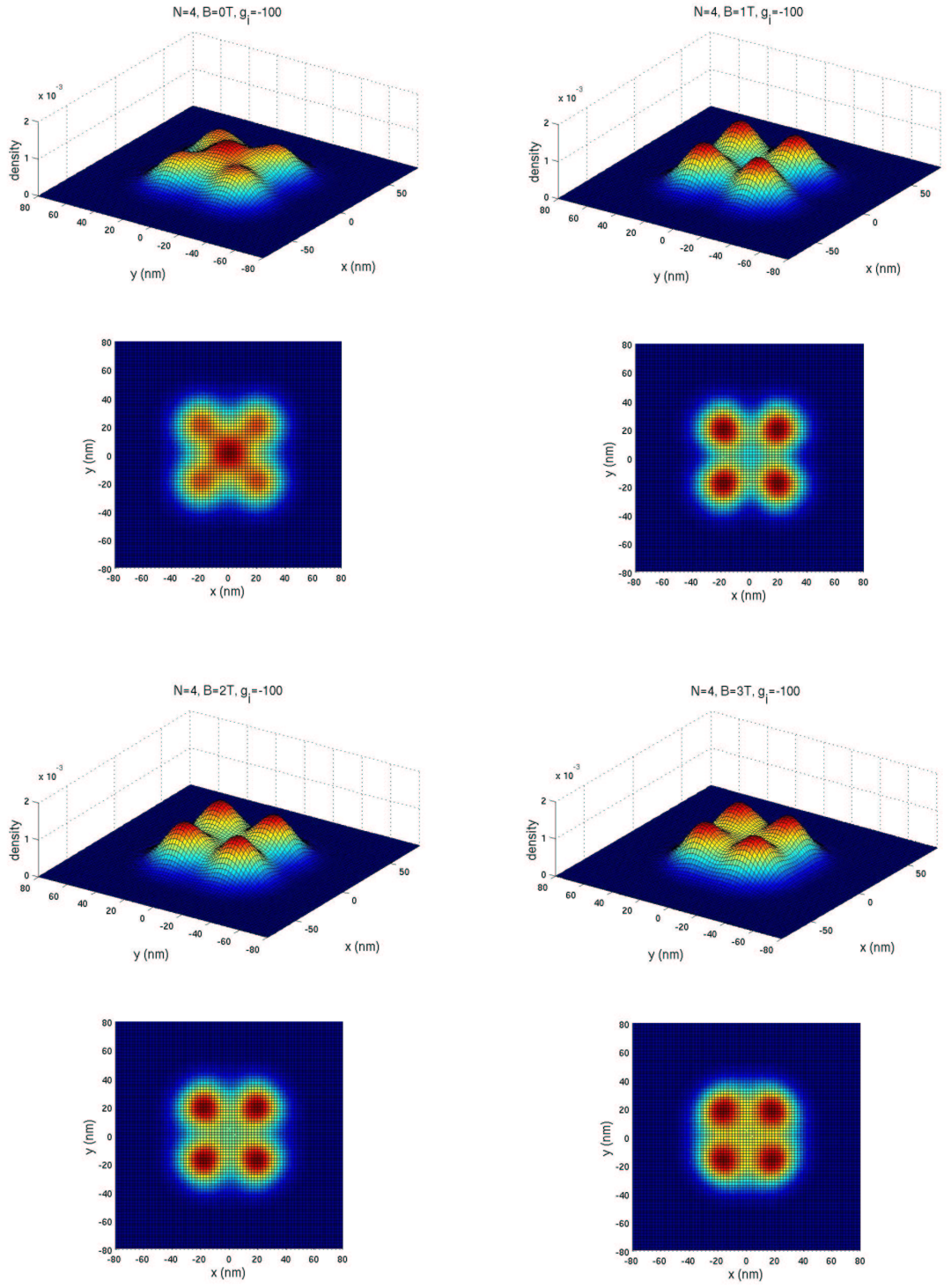

Figure 5.13: The electron densities of a four-electron quantum dot in the case of square symmetric confinement ($\alpha_1 = 0.0,\ \alpha_2 = 0.2$) for polarized ($g_i = -100$) interacting electrons at different values of magnetic field $B = 0$ T, $B = 1$ T, $B = 2$ T and $B = 3$ T.

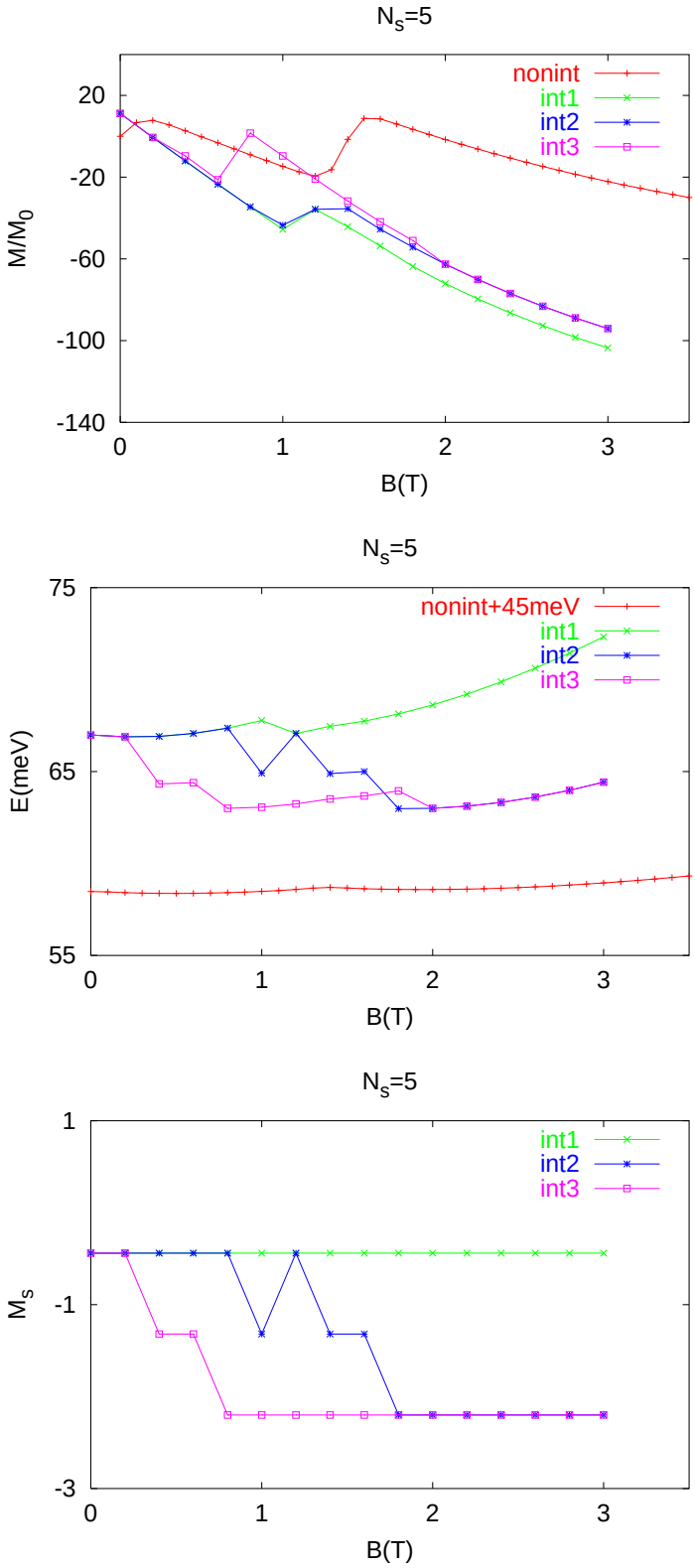

Figure 5.14: The orbital M_o and spin magnetization M_s and the total energy of a five-electron quantum dot in the case of circular confinement ($\alpha_1 = 0.0,\ \alpha_2 = 0.0$) for both noninteracting ("nonint") and interacting electrons ("int1", "int2" and "int3" corresponding to $g = -0.44,\ g_i =$

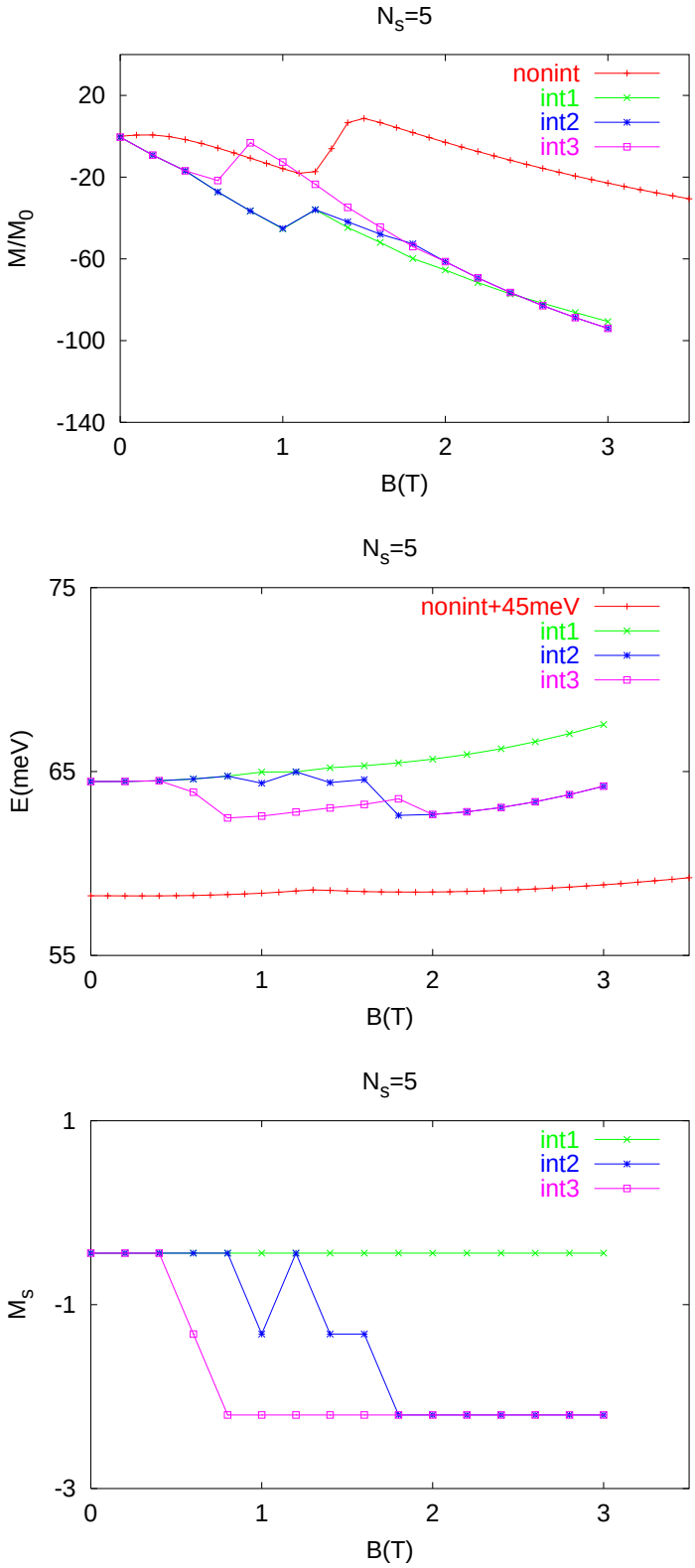

Figure 5.15: The orbital M_o and spin magnetization M_s and the total energy of a five-electron quantum dot in the case of elliptic confinement ($\alpha_1 = 0.1,\ \alpha_2 = 0.0$) for both noninteracting ("nonint") and interacting electrons ("int1", "int2" and "int3" corresponding to $g = -0.44,\ g_i =$

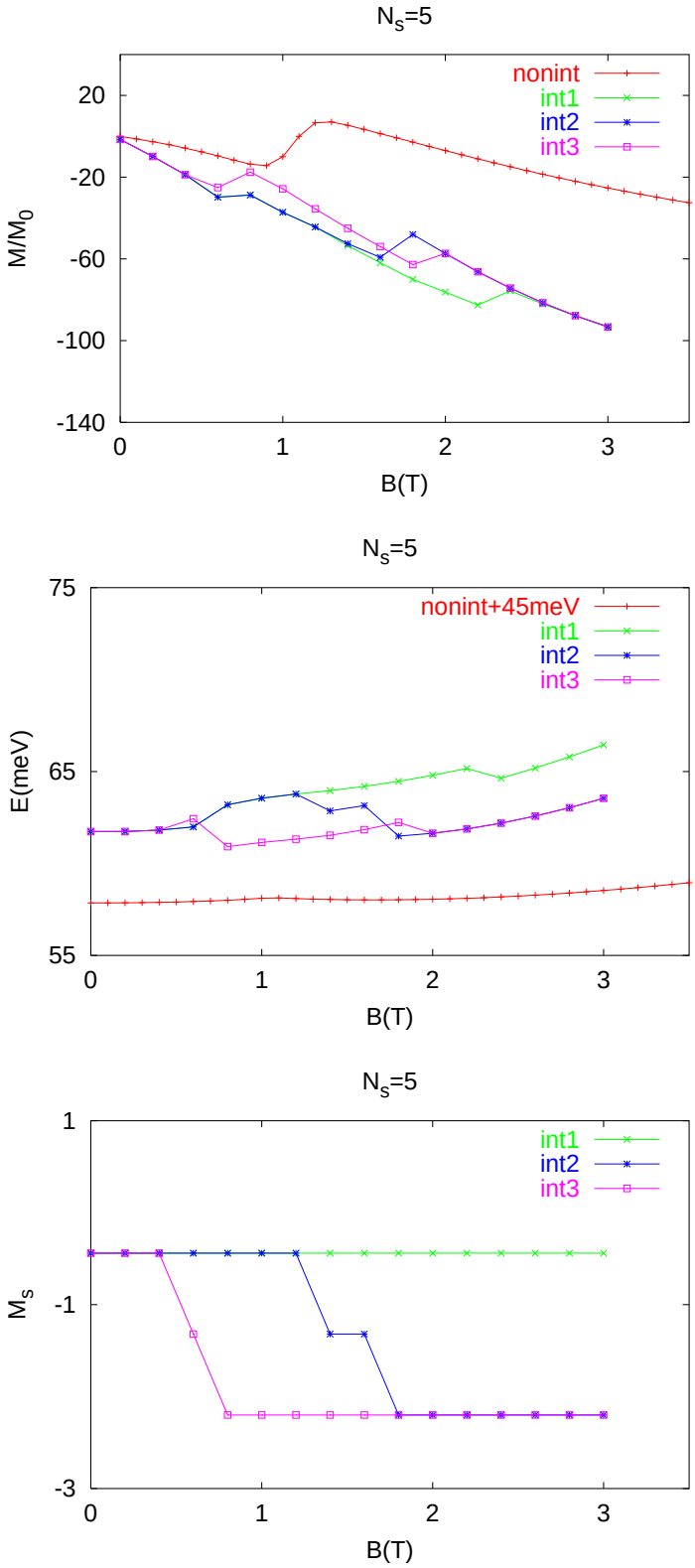

Figure 5.16: The orbital M_o and spin magnetization M_s and the total energy of a five-electron quantum dot in the case of elliptic confinement ($\alpha_1 = 0.2,\ \alpha_2 = 0.0$) for both noninteracting ("nonint") and interacting electrons ("int1", "int2" and "int3" corresponding to $g = -0.44,\ g_i =$

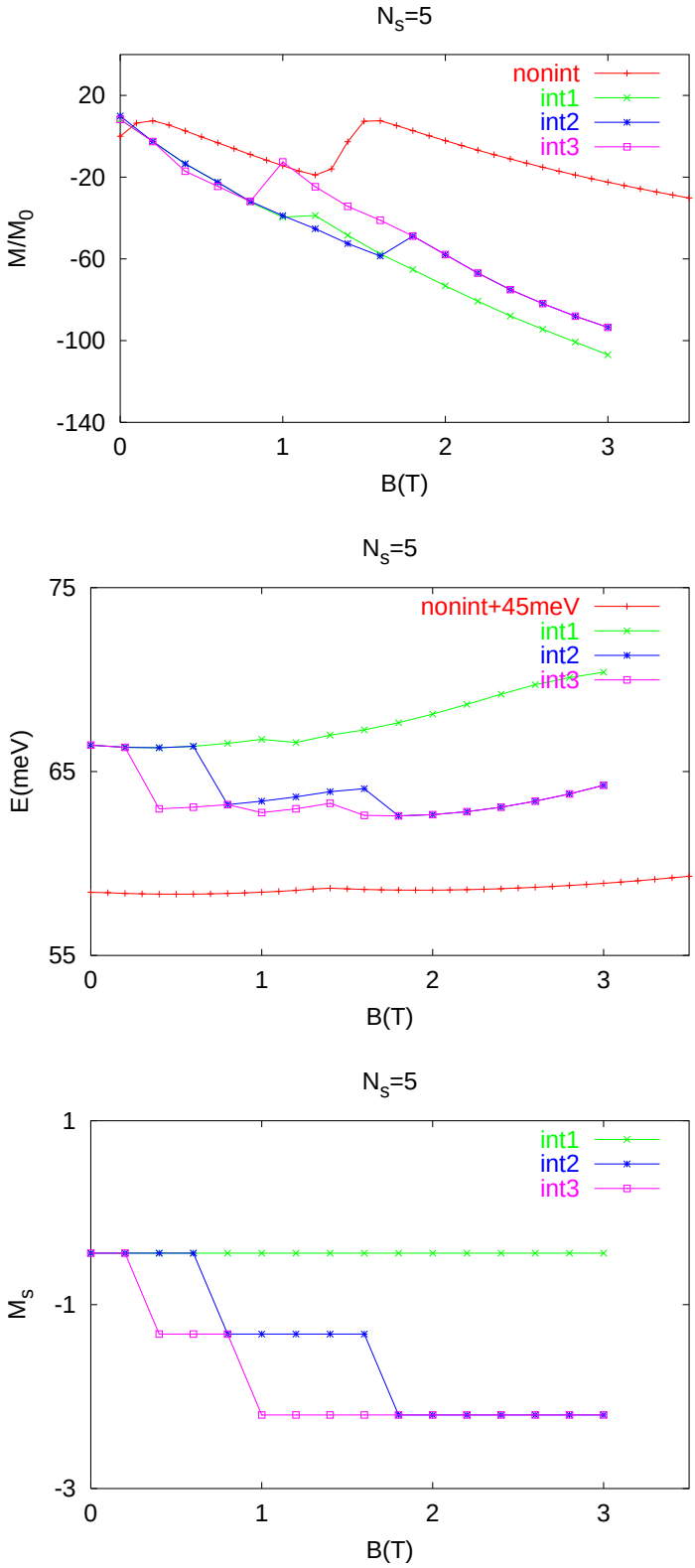

Figure 5.17: The orbital M_o and spin magnetization M_s and the total energy of a five-electron quantum dot in the case of square symmetric confinement ($\alpha_1 = 0.0,\ \alpha_2 = 0.1$) for both noninteracting ("nonint") and interacting electrons ("int1", "int2" and "int3" corresponding to $g = -0.44$,

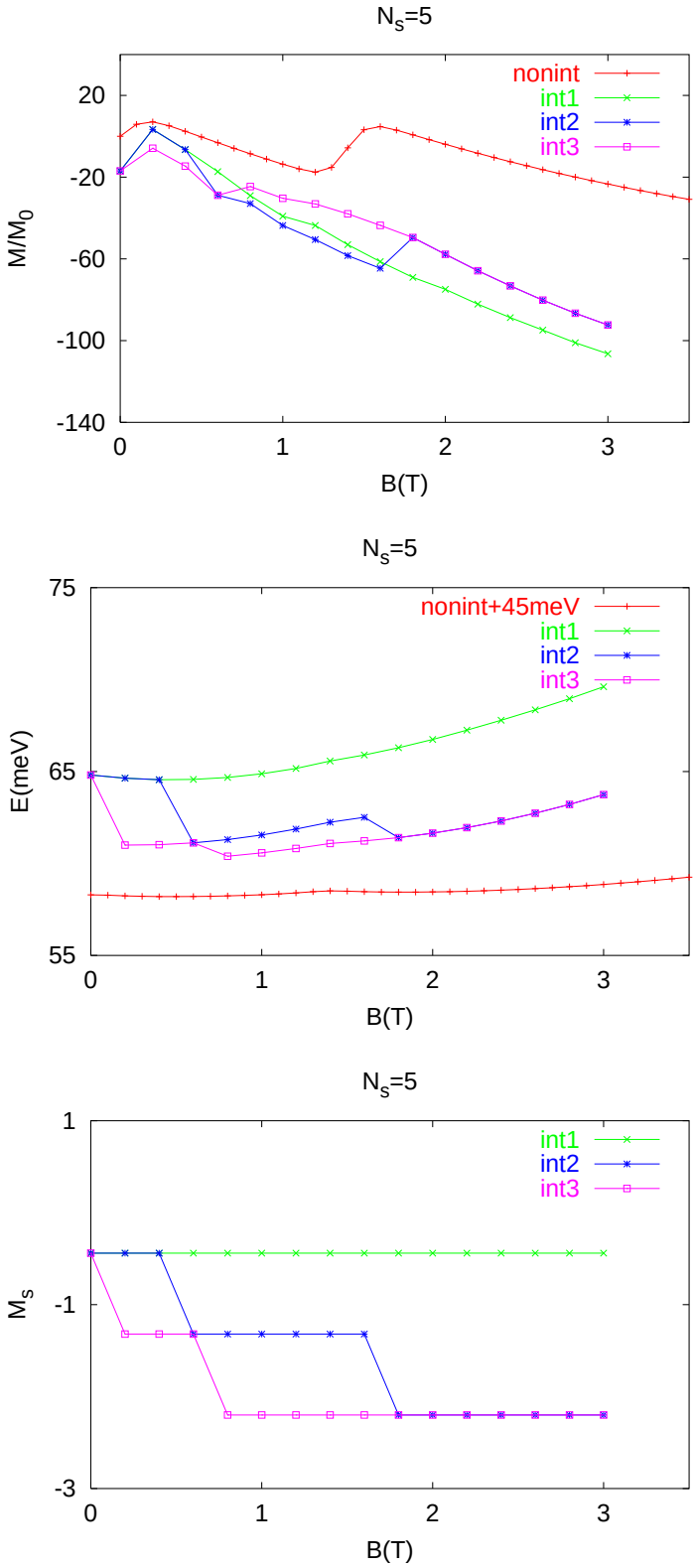

Figure 5.18: The orbital M_o and spin magnetization M_s and the total energy of a five-electron quantum dot in the case of square symmetric confinement ($\alpha_1 = 0.0,\ \alpha_2 = 0.2$) for both noninteracting ("nonint") and interacting electrons ("int1", "int2" and "int3" corresponding to $g = -0.44$,

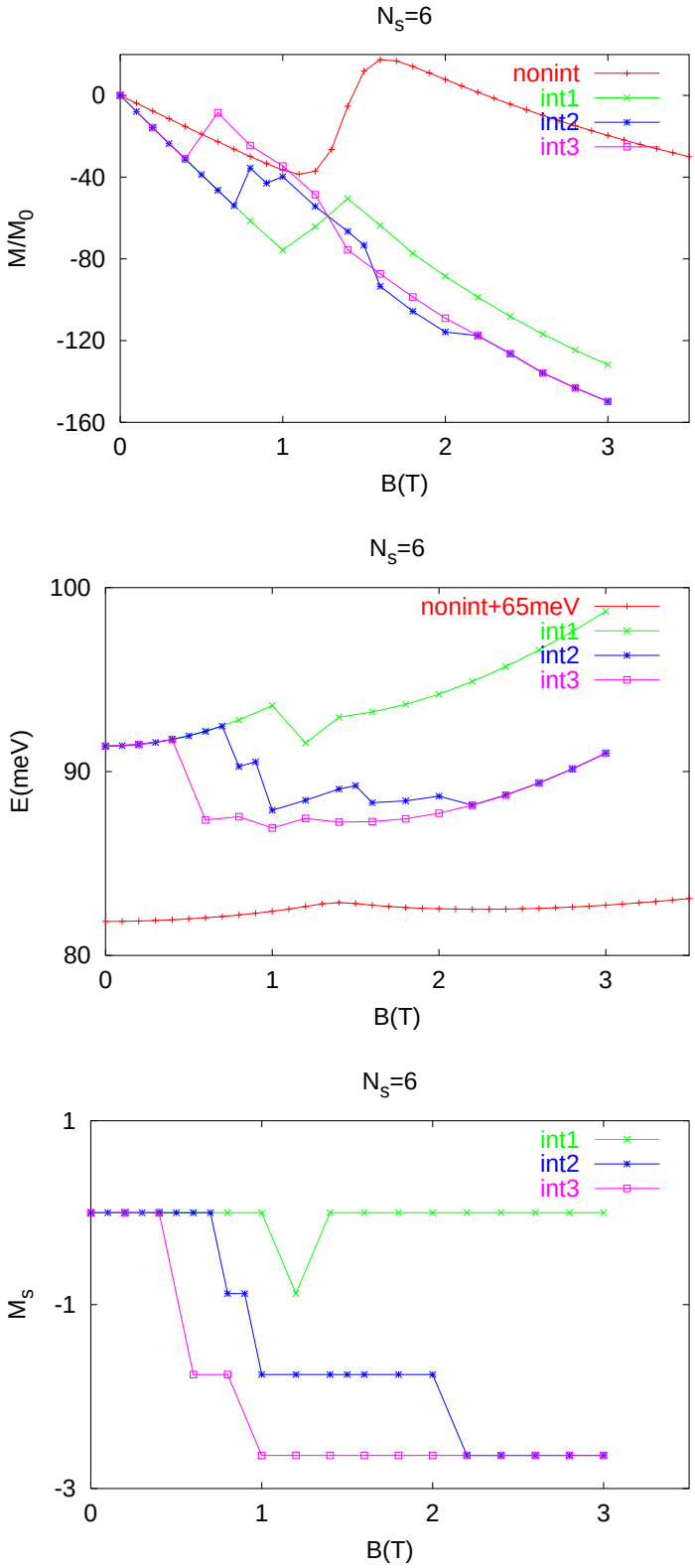

Figure 5.19: The orbital M_o and spin magnetization M_s and the total energy of a six-electron quantum dot in the case of circular confinement ($\alpha_1 = 0.0,\ \alpha_2 = 0.0$) for both noninteracting ("nonint") and interacting electrons ("int1", "int2" and "int3" corresponding to $g = -0.44,\ g_i =$

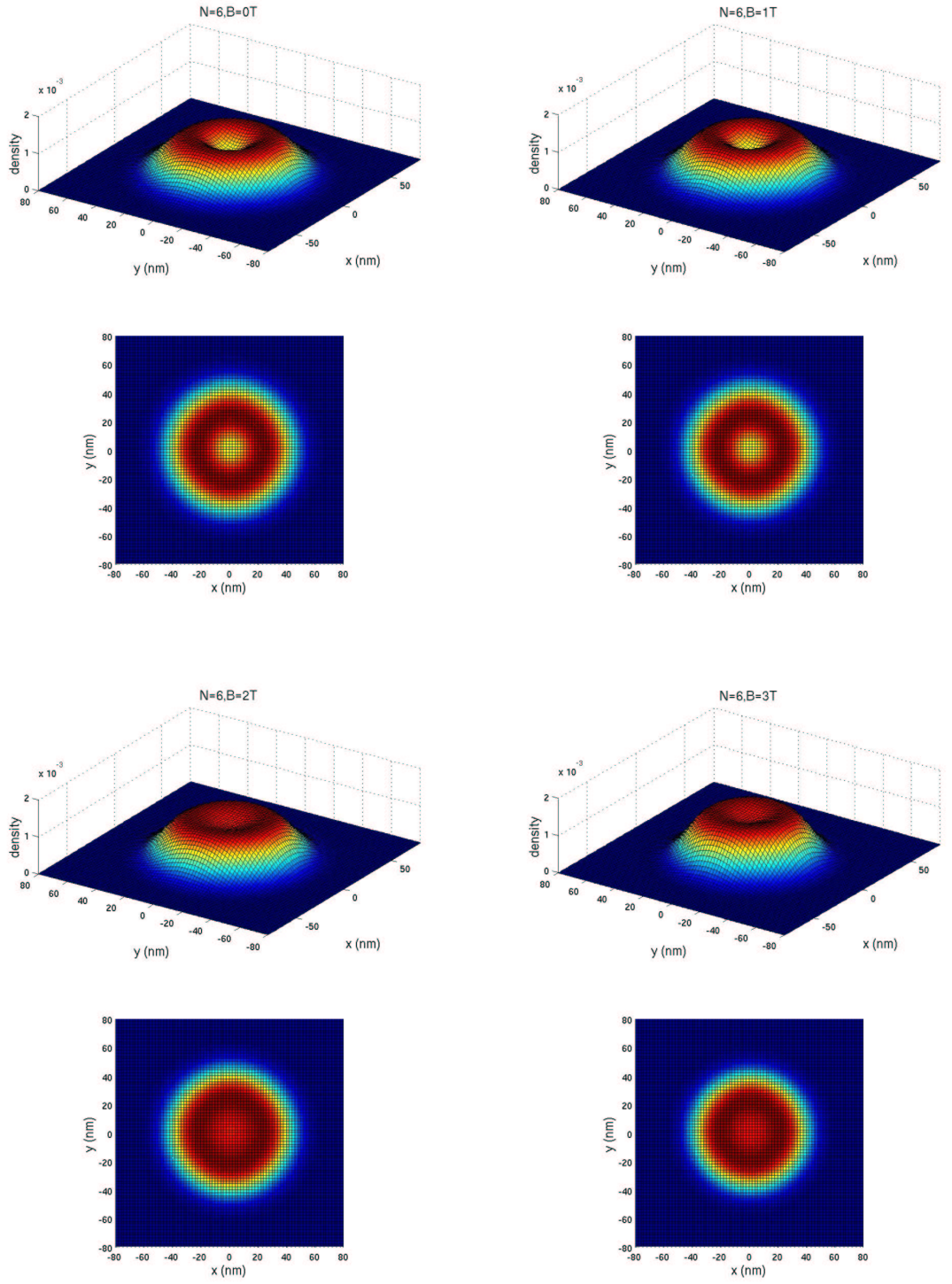

Figure 5.20: The electron densities of a six-electron quantum dot in the case of circular confinement ($\alpha_1 = 0.0,\ \alpha_2 = 0.0$) for unpolarized ($g = -0.44$) interacting electrons at different values of magnetic field $B = 0$ T, $B = 1$ T, $B = 2$ T and $B = 3$ T.

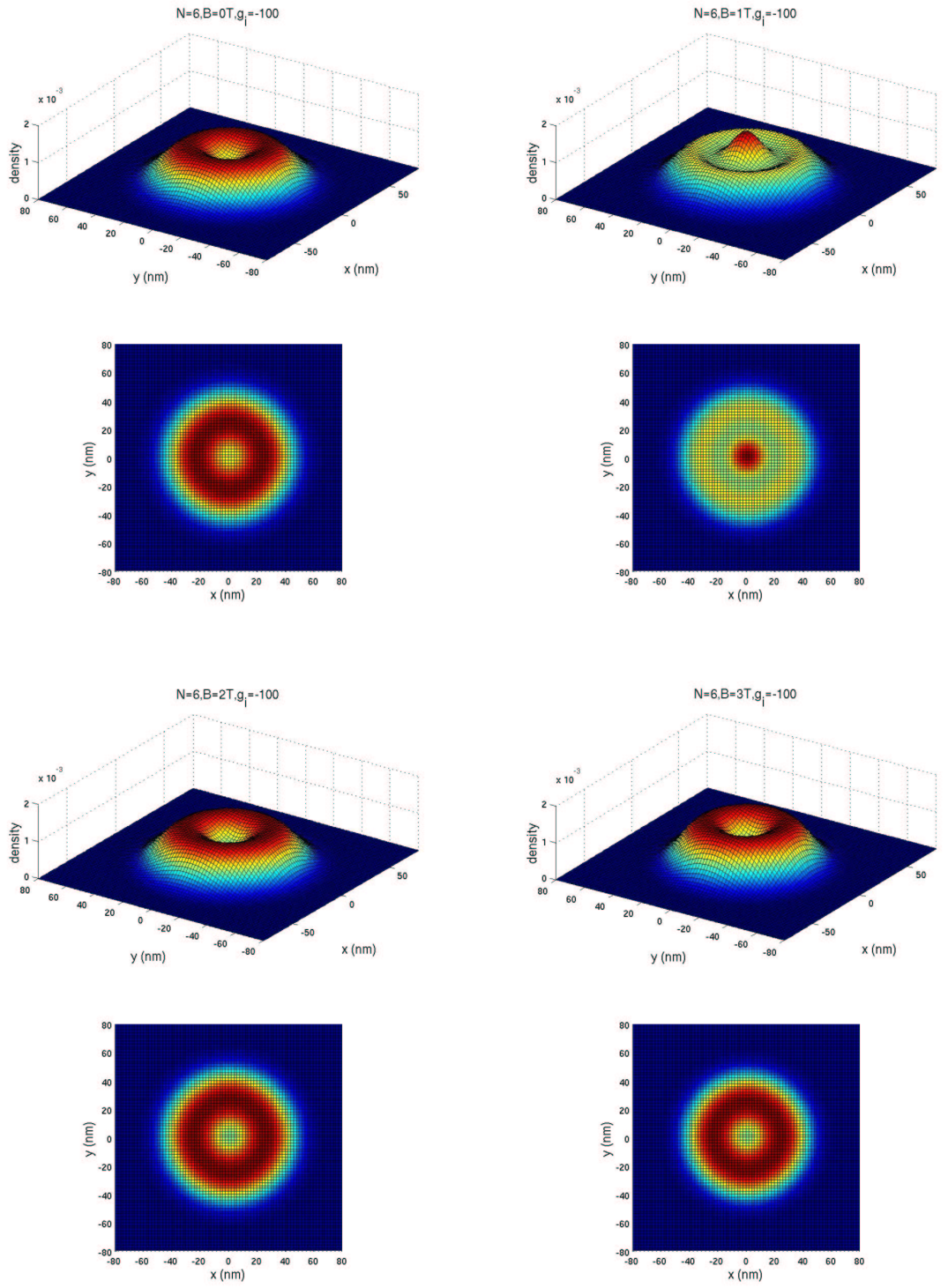

Figure 5.21: The electron densities of a six-electron quantum dot in the case of circular confinement ($\alpha_1 = 0.0,\ \alpha_2 = 0.0$) for polarized ($g_i = -100$) interacting electrons at different values of magnetic field $B = 0$ T, $B = 1$ T, $B = 2$ T and $B = 3$ T.

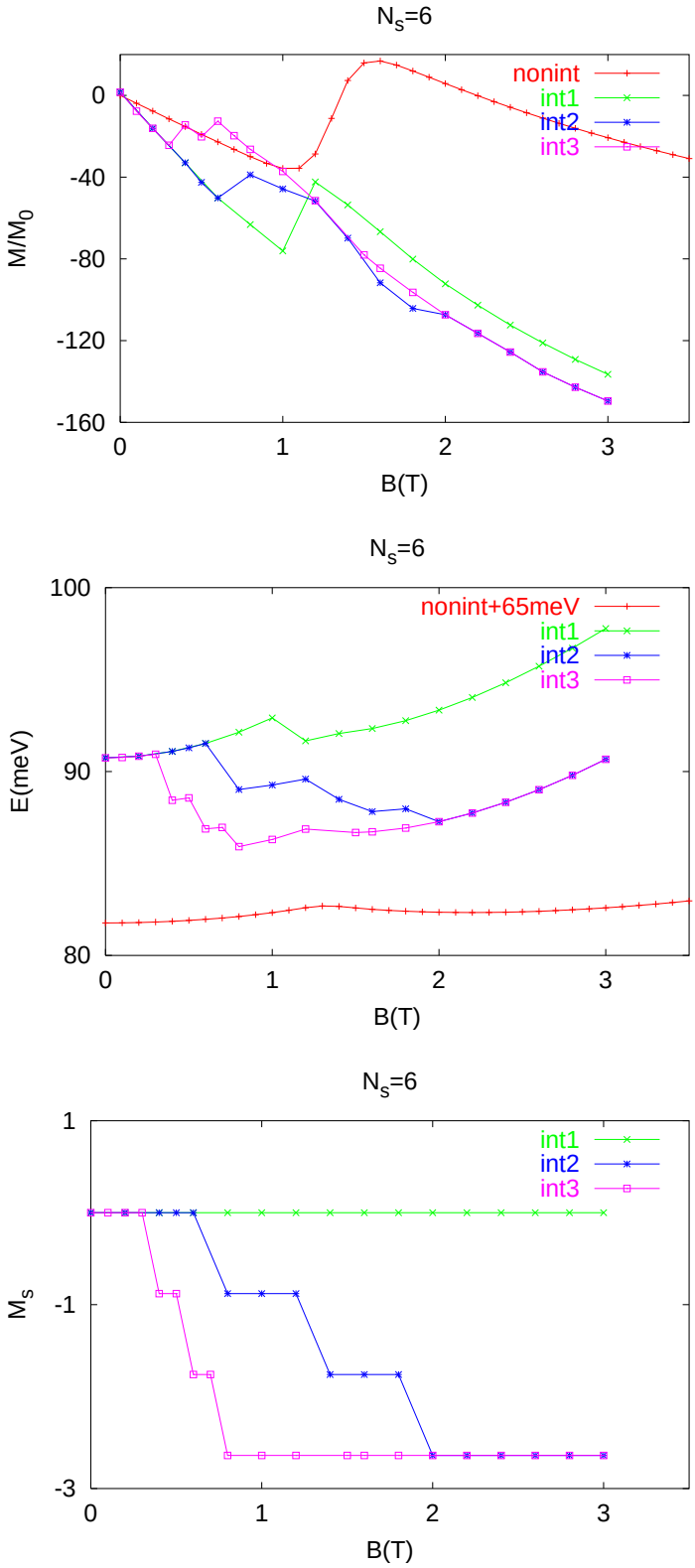

Figure 5.22: The orbital M_o and spin magnetization M_s and the total energy of a six-electron quantum dot in the case of elliptic confinement ($\alpha_1 = 0.1,\ \alpha_2 = 0.0$) for both noninteracting ("nonint") and interacting electrons ("int1", "int2" and "int3" corresponding to $g = -0.44,\ g_i =$

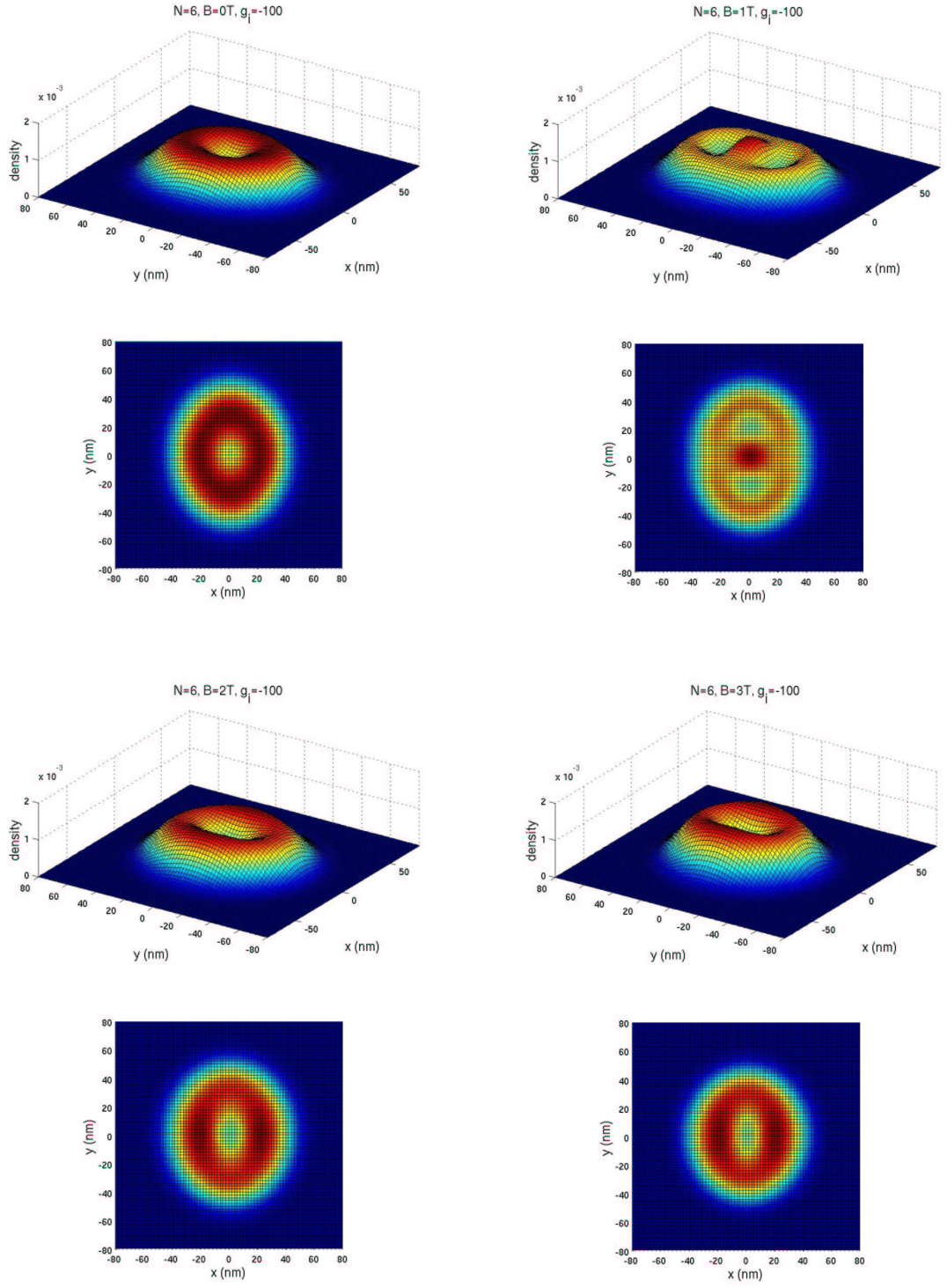

Figure 5.23: The electron densities of a six-electron quantum dot in the case of elliptic confinement ($\alpha_1 = 0.1,\ \alpha_2 = 0.0$) for polarized ($g_i = -100$) interacting electrons at different values of magnetic field $B = 0$ T, $B = 1$ T, $B = 2$ T and $B = 3$ T.

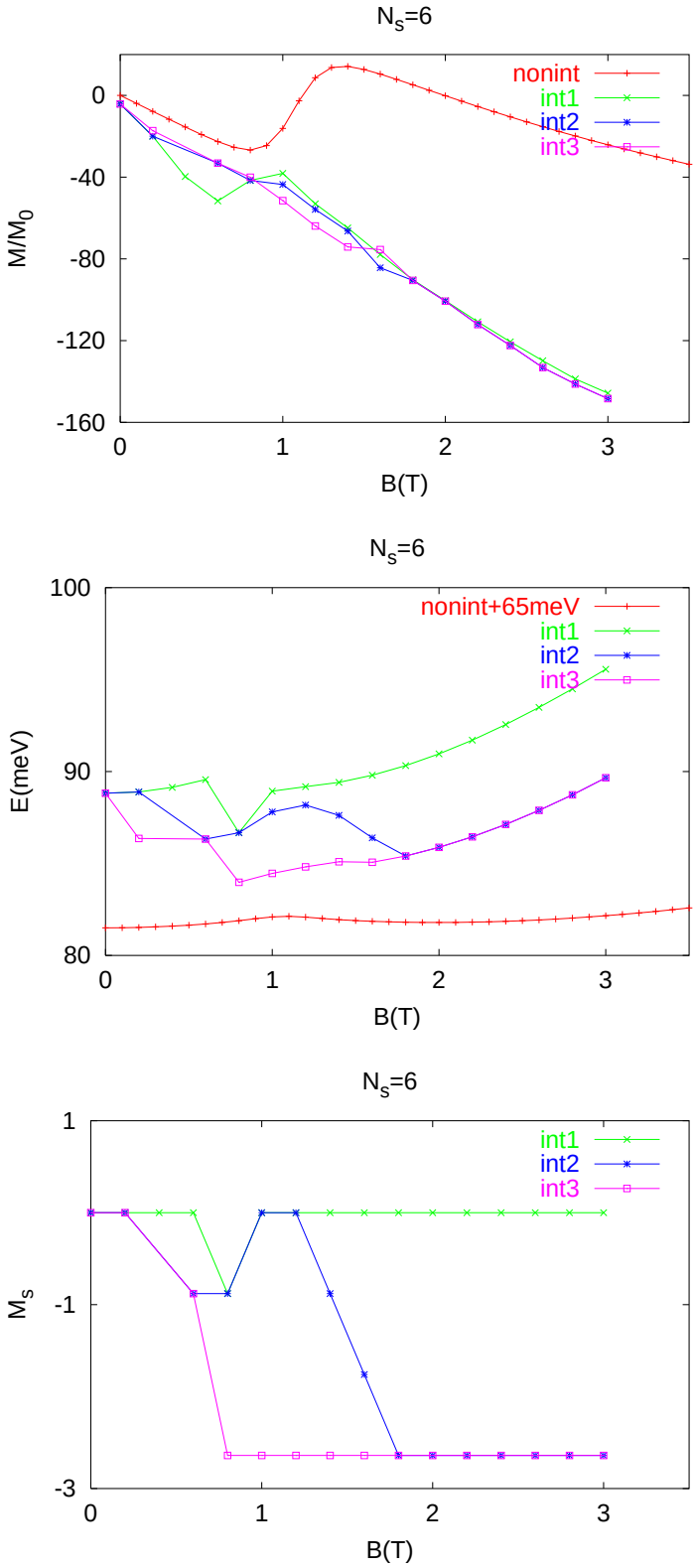

Figure 5.24: The orbital M_o and spin magnetization M_s and the total energy of a six-electron quantum dot in the case of elliptic confinement ($\alpha_1 = 0.2,\ \alpha_2 = 0.0$) for both noninteracting ("nonint") and interacting electrons ("int1", "int2" and "int3" corresponding to $g = -0.44,\ g_i =$

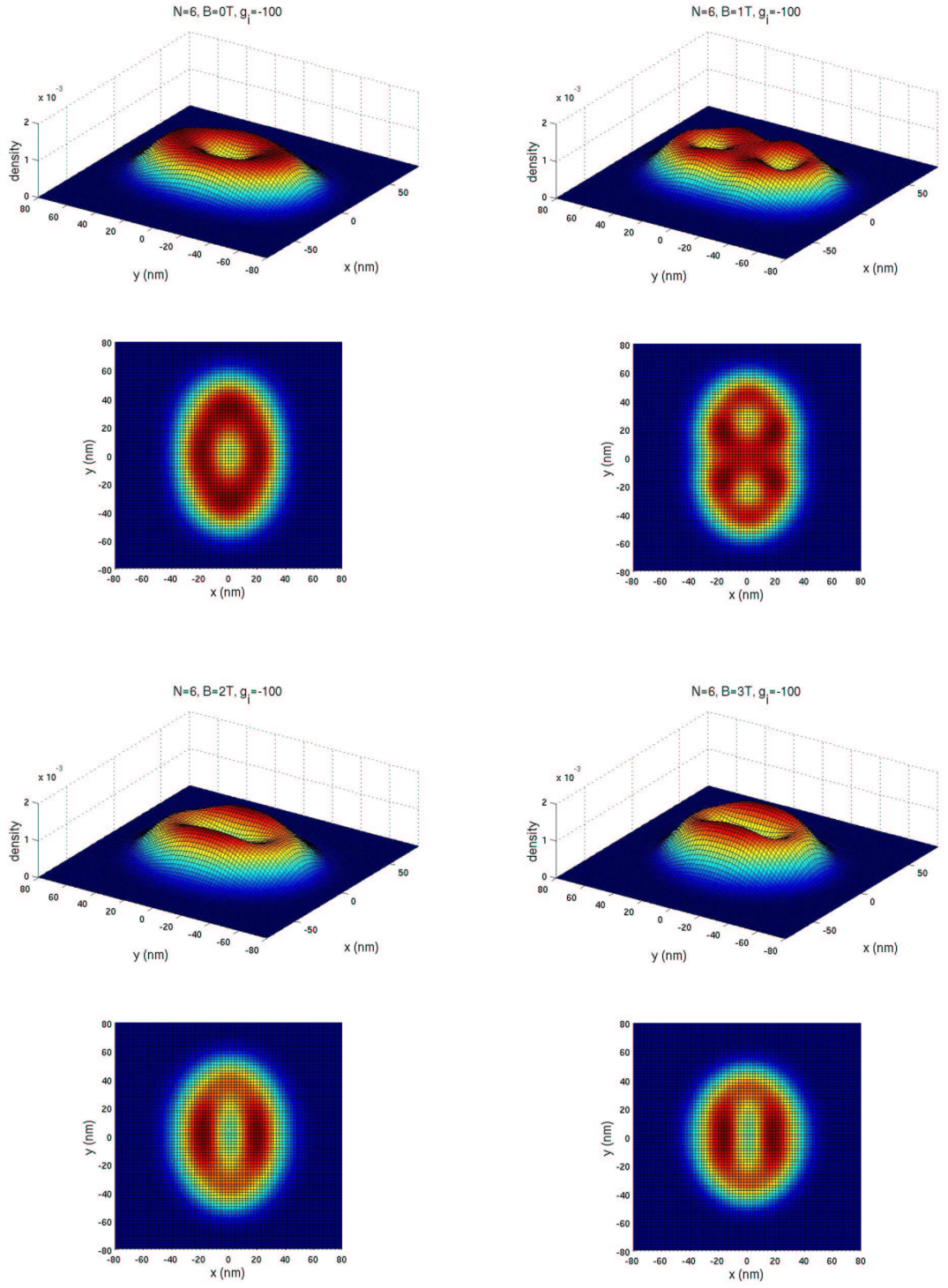

Figure 5.25: The electron densities of a six-electron quantum dot in the case of elliptic confinement ($\alpha_1 = 0.2,\ \alpha_2 = 0.0$) for polarized ($g_i = -100$) interacting electrons at different values of magnetic field $B = 0$ T, $B = 1$ T, $B = 2$ T and $B = 3$ T.

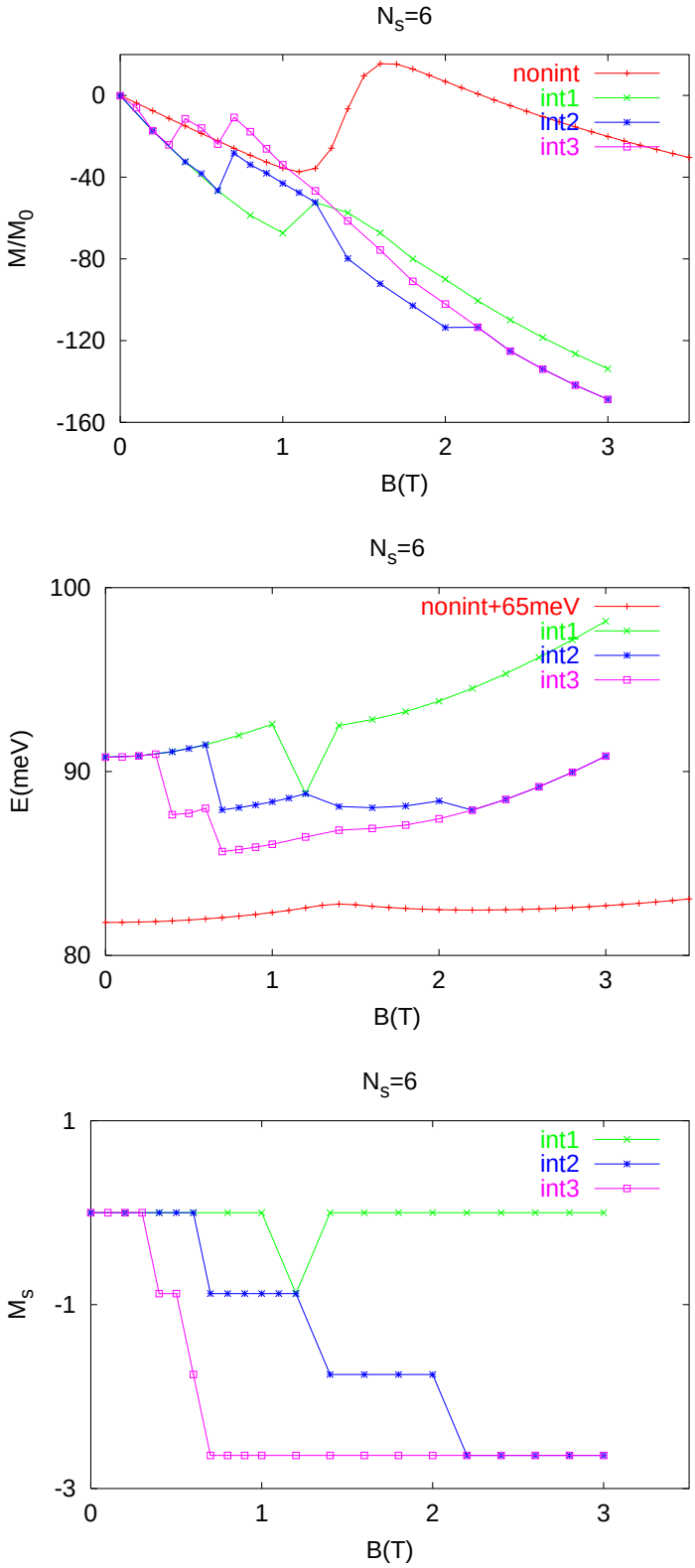

Figure 5.26: The orbital M_o and spin magnetization M_s and the total energy of a six-electron quantum dot in the case of square symmetric confinement ($\alpha_1 = 0.0,\ \alpha_2 = 0.1$) for both noninteracting ("nonint") and interacting electrons ("int1", "int2" and "int3" corresponding to $g = -0.44$,

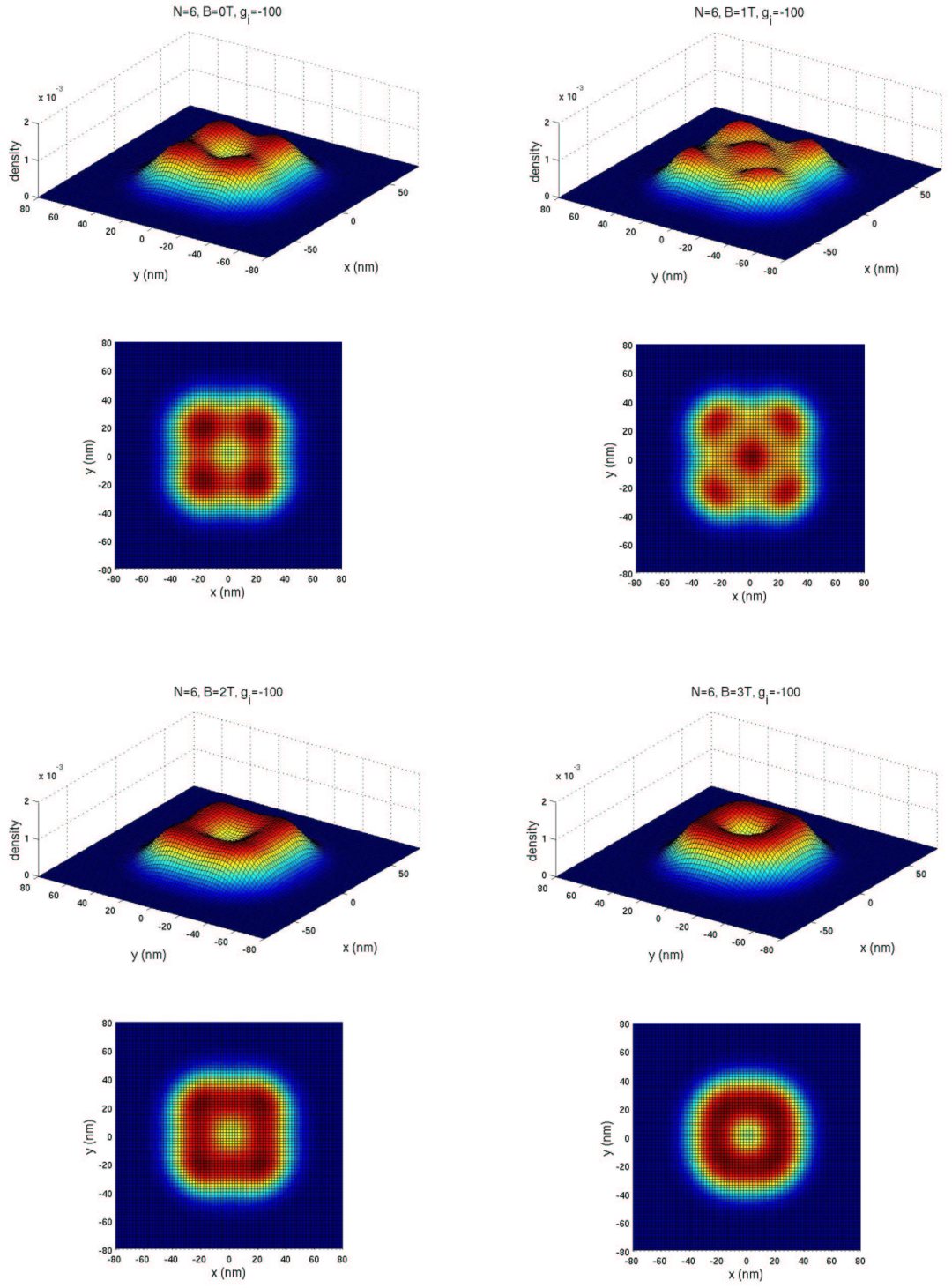

Figure 5.27: The electron densities of a six-electron quantum dot in the case of square symmetric confinement ($\alpha_1 = 0.0,\ \alpha_2 = 0.1$) for polarized ($g_i = -100$) interacting electrons at different values of magnetic field $B = 0$ T, $B = 1$ T, $B = 2$ T and $B = 3$ T.

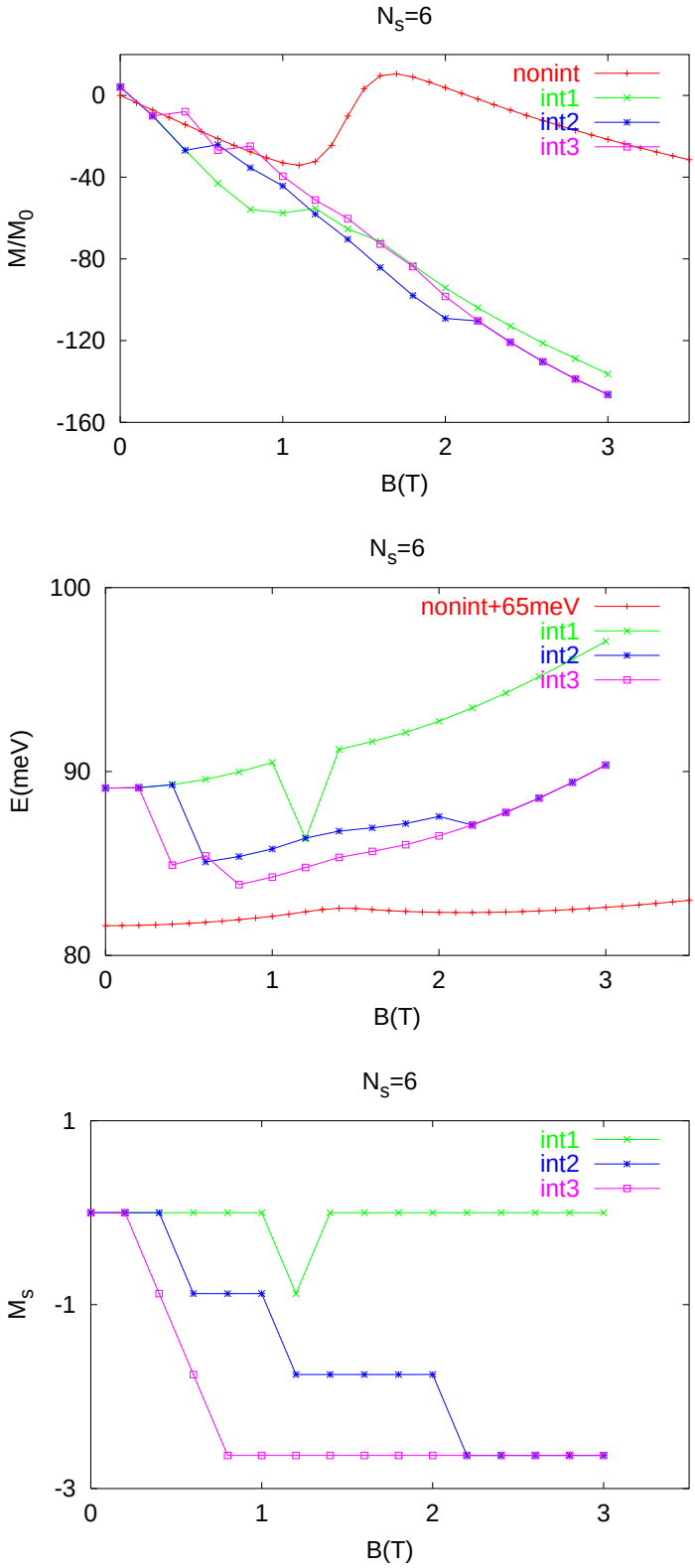

Figure 5.28: The orbital M_o and spin magnetization M_s and the total energy of a six-electron quantum dot in the case of square symmetric confinement ($\alpha_1 = 0.0,\ \alpha_2 = 0.2$) for both noninteracting ("nonint") and interacting electrons ("int1", "int2" and "int3" corresponding to $g = -0.44$,

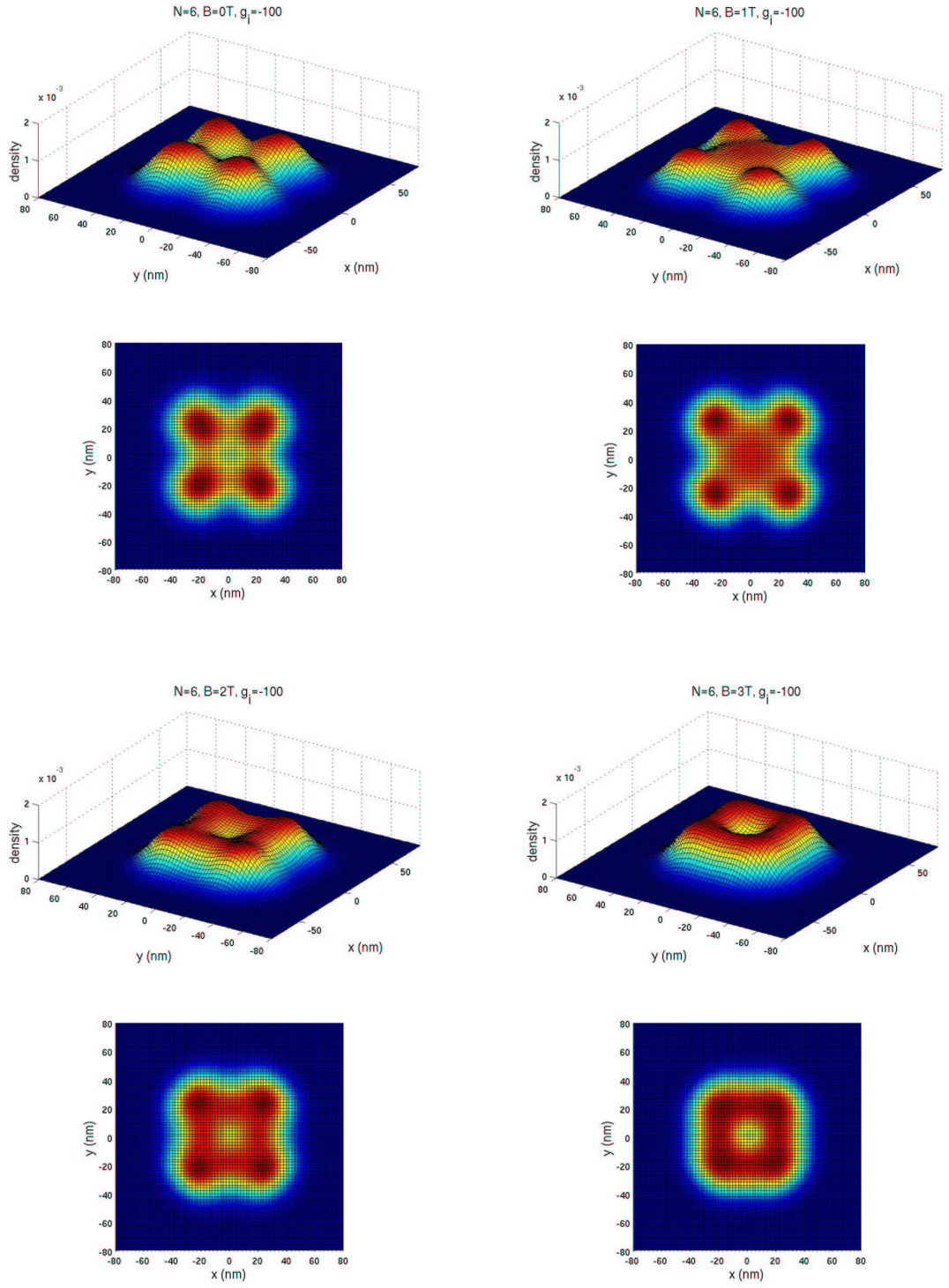

Figure 5.29: The electron densities of a six-electron quantum dot in the case of square symmetric confinement ($\alpha_1 = 0.0,\ \alpha_2 = 0.2$) for polarized ($g_i = -100$) interacting electrons at different values of magnetic field $B = 0$ T, $B = 1$ T, $B = 2$ T and $B = 3$ T.

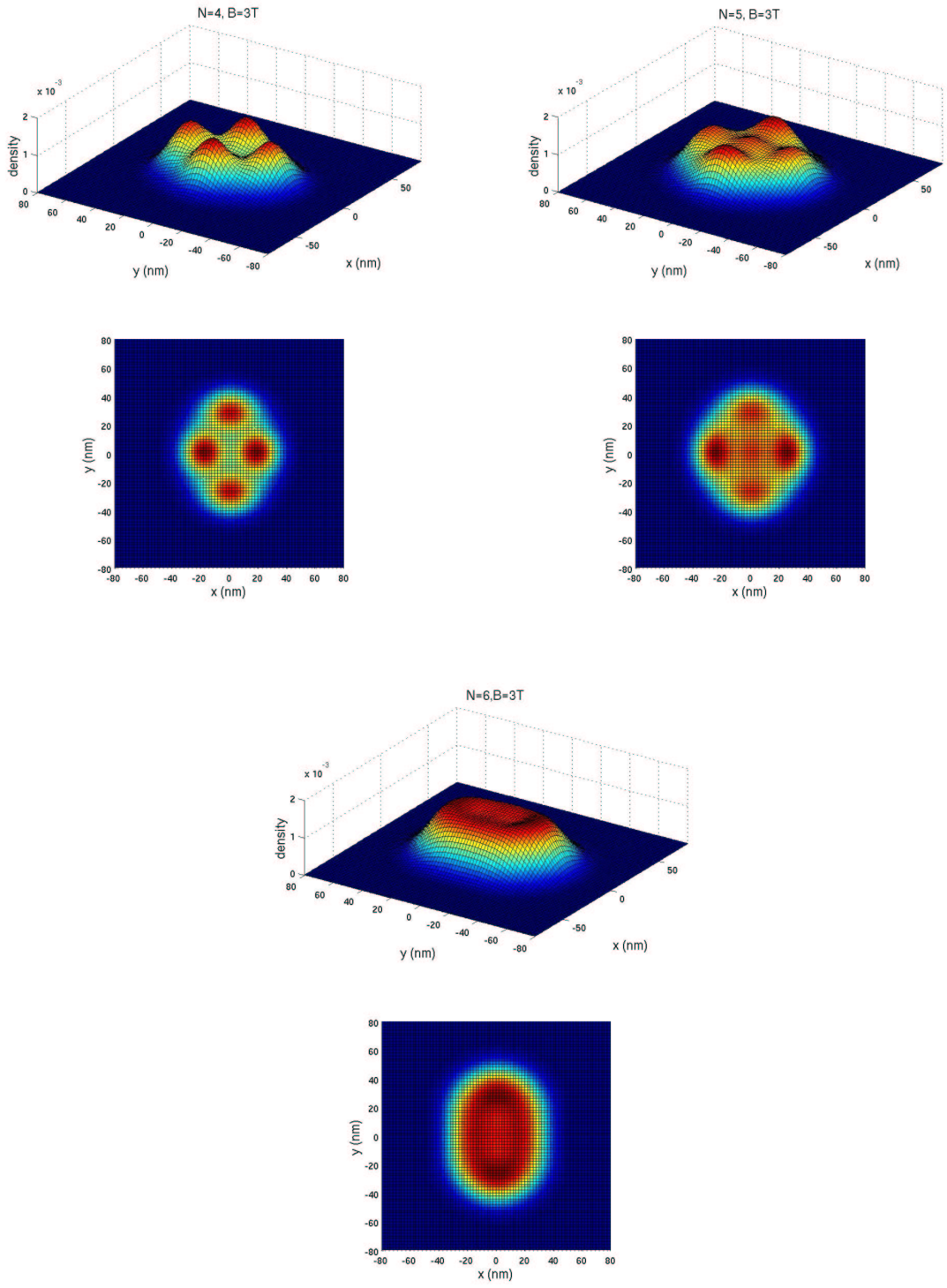

Figure 5.30: Evolution of the electron density at $B = 3$ T for elliptic dots ($\alpha_1 = 0.1, \alpha_2 = 0.0$) with increasing the number of electrons.

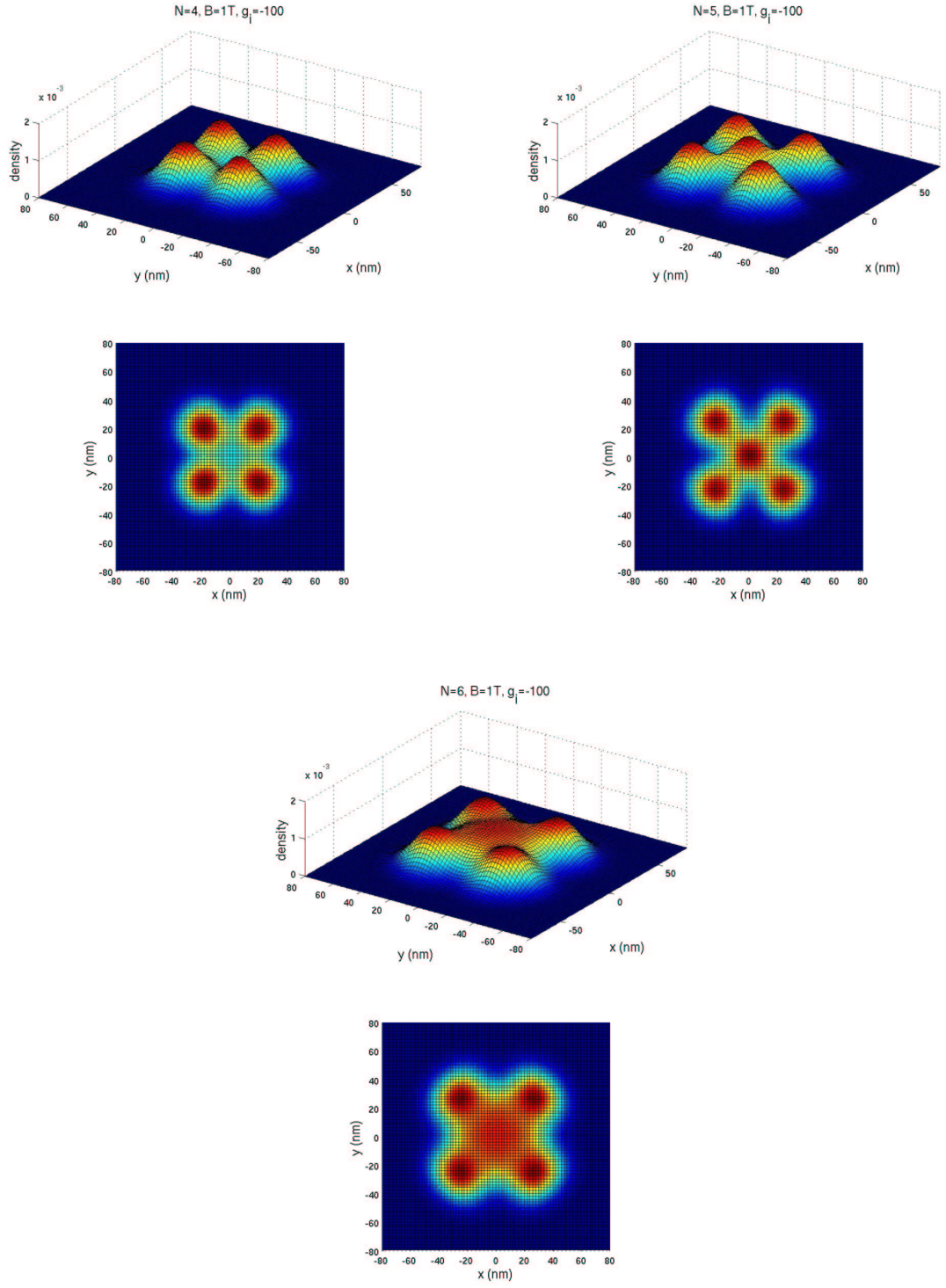

Figure 5.31: Evolution of the electron density at $B = 1$ T for square symmetric dots ($\alpha_1 = 0.0, \alpha_2 = 0.2$) with increasing the number of electrons.

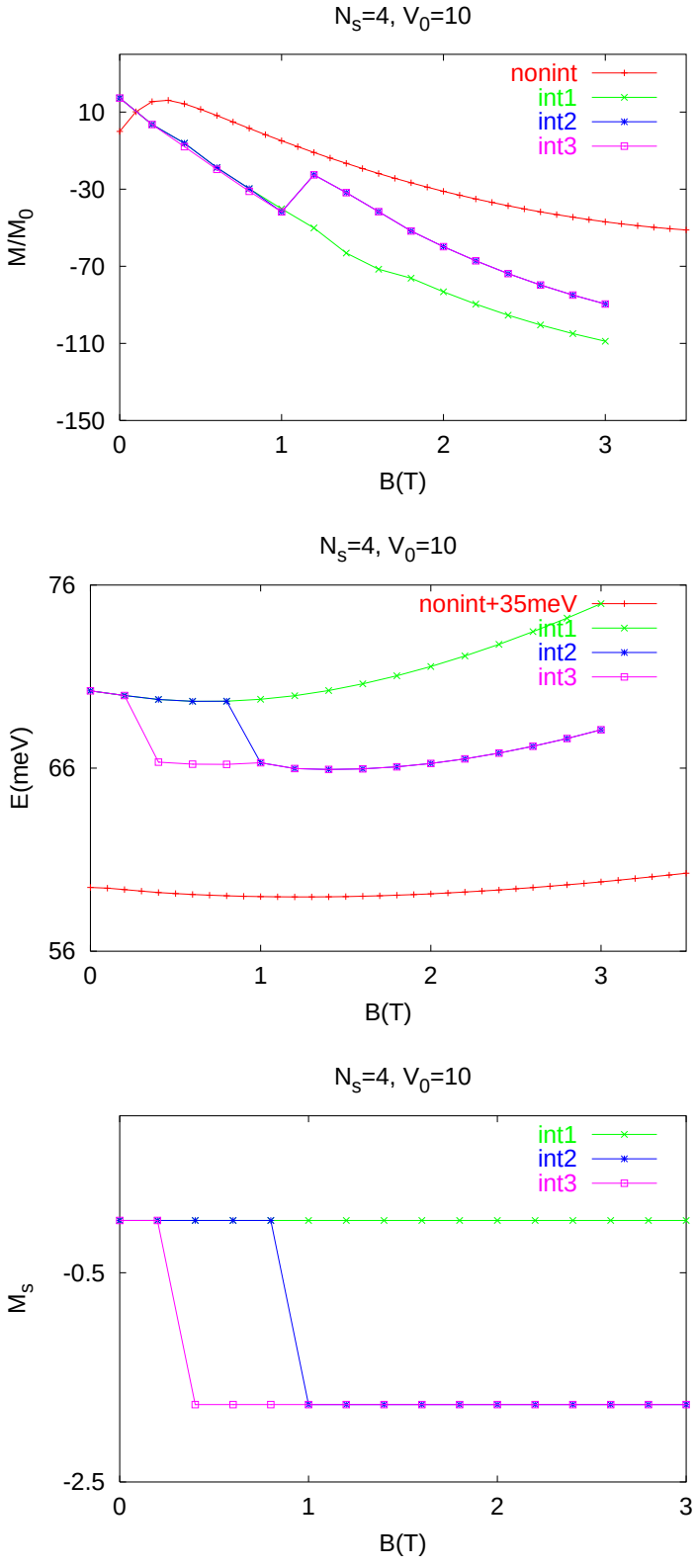

Figure 5.32: The orbital M_o and spin magnetization M_s and the total energy of a four-electron quantum ring in the case of circular confinement ($\alpha_1 = 0.0,\ \alpha_2 = 0.0$) for both noninteracting ("nonint") and interacting electrons ("int1", "int2" and "int3" corresponding to $g = -0.44,\ g_i =$

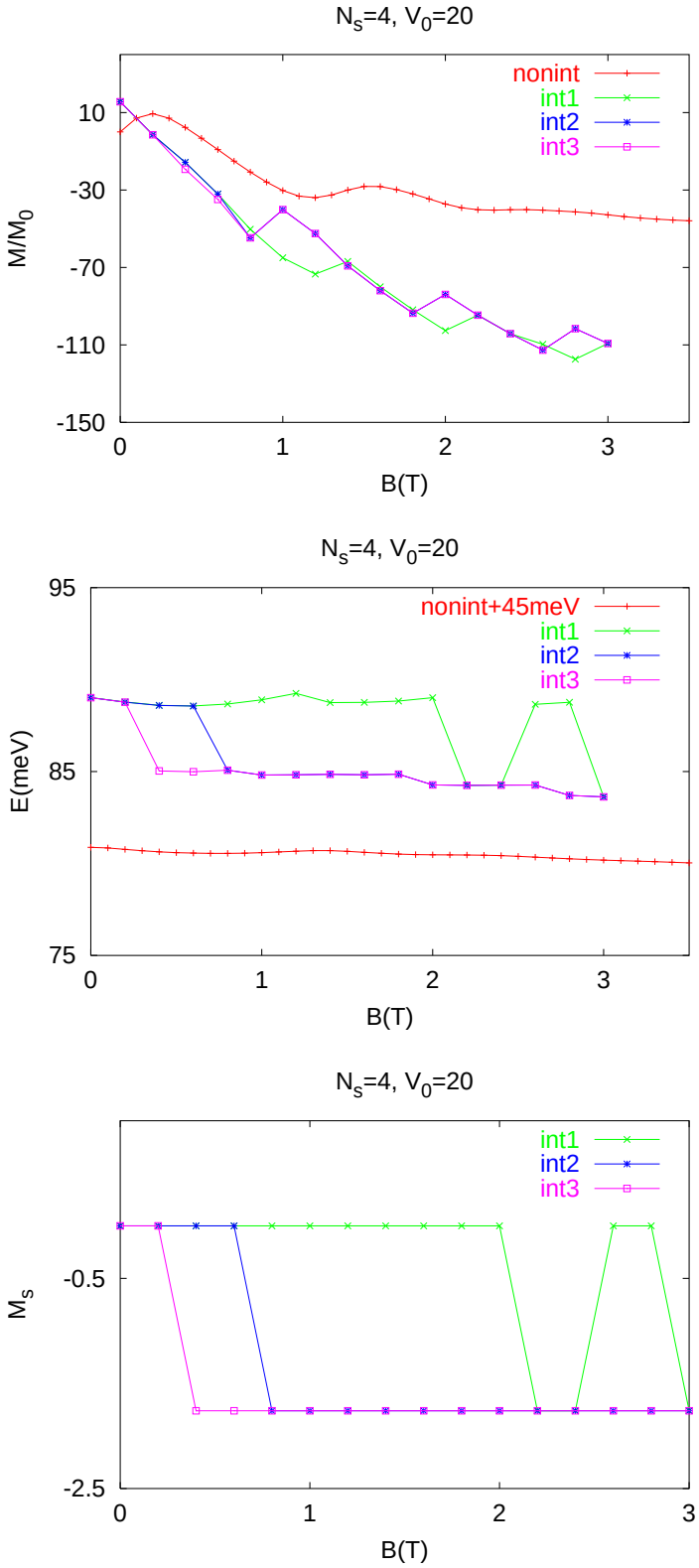

Figure 5.33: The orbital M_o and spin magnetization M_s and the total energy of a four-electron quantum ring in the case of circular confinement ($\alpha_1 = 0.0,\ \alpha_2 = 0.0$) for both noninteracting ("nonint") and interacting electrons ("int1", "int2" and "int3" corresponding to $g = -0.44,\ g_i =$

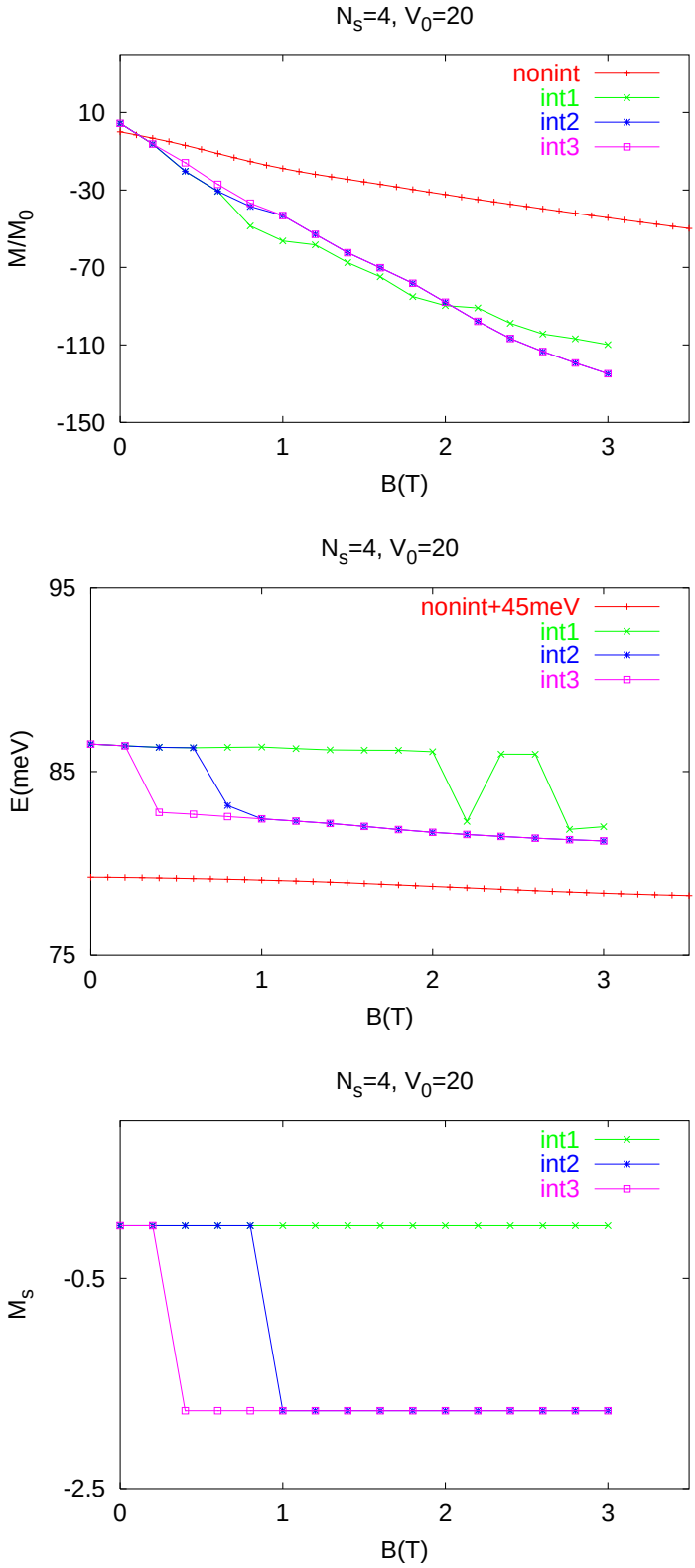

Figure 5.34: The orbital M_o and spin magnetization M_s and the total energy of a four-electron quantum ring in the case of elliptic confinement ($\alpha_1 = 0.1,\ \alpha_2 = 0.0$) for both noninteracting ("nonint") and interacting electrons ("int1", "int2" and "int3" corresponding to $g = -0.44,\ g_i =$

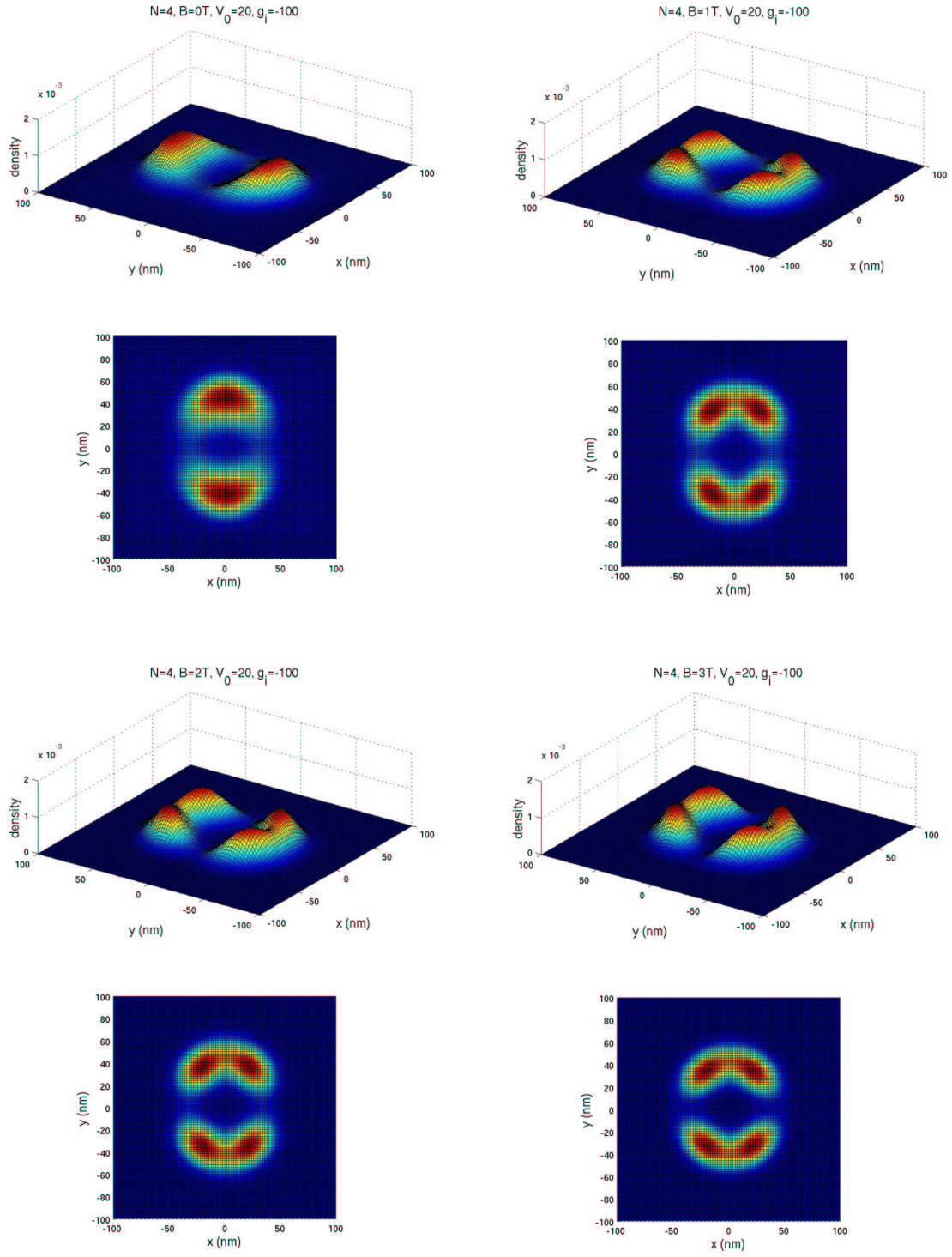

Figure 5.35: The electron densities of a four-electron quantum ring in the case of elliptic confinement ($\alpha_1 = 0.1,\ \alpha_2 = 0.0$) for polarized ($g_i = -100$) interacting electrons at different values of magnetic field $B = 0$ T, $B = 1$ T, $B = 2$ T and $B = 3$ T for $V_0 = 20$.

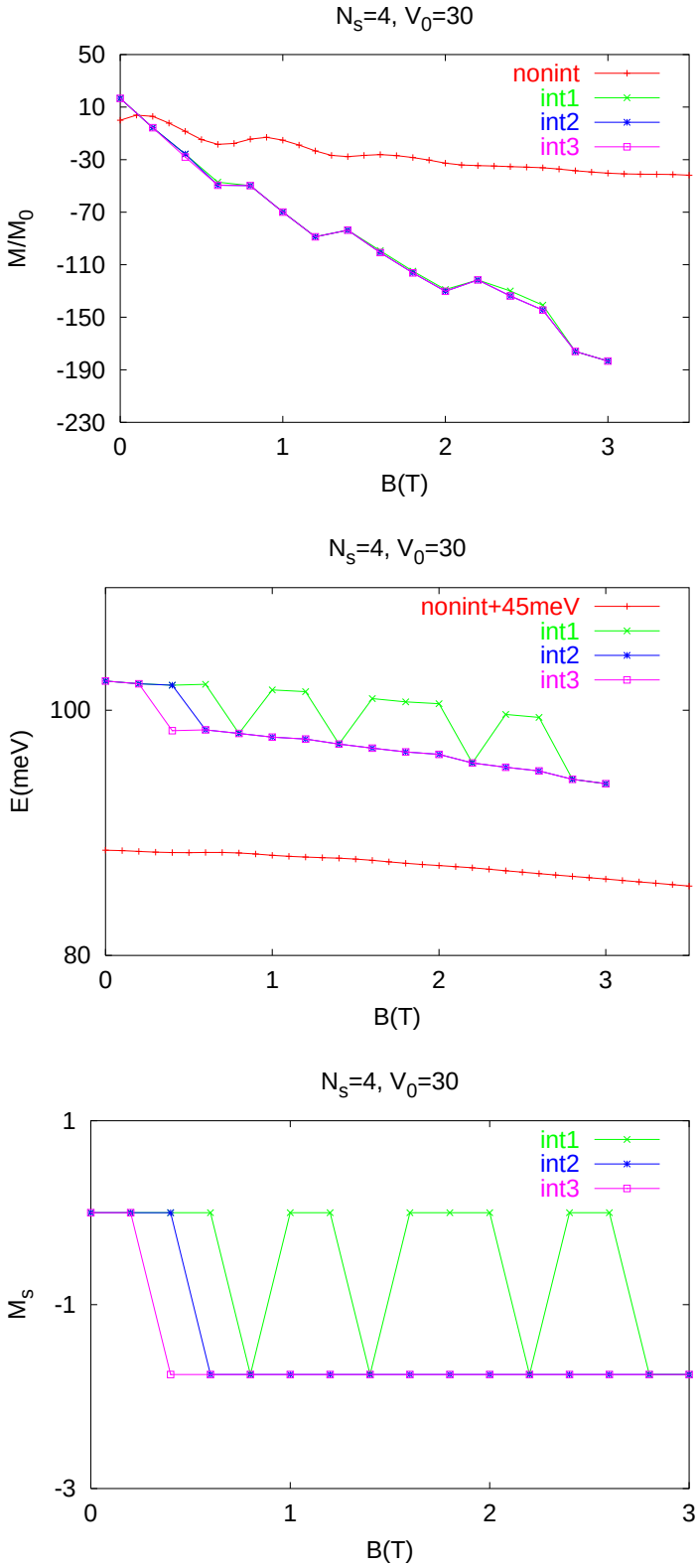

Figure 5.36: The orbital M_o and spin magnetization M_s and the total energy of a four-electron quantum ring in the case of circular confinement ($\alpha_1 = 0.0,\ \alpha_2 = 0.0$) for both noninteracting ("nonint") and interacting electrons ("int1", "int2" and "int3" corresponding to $g = -0.44,\ g_i =$

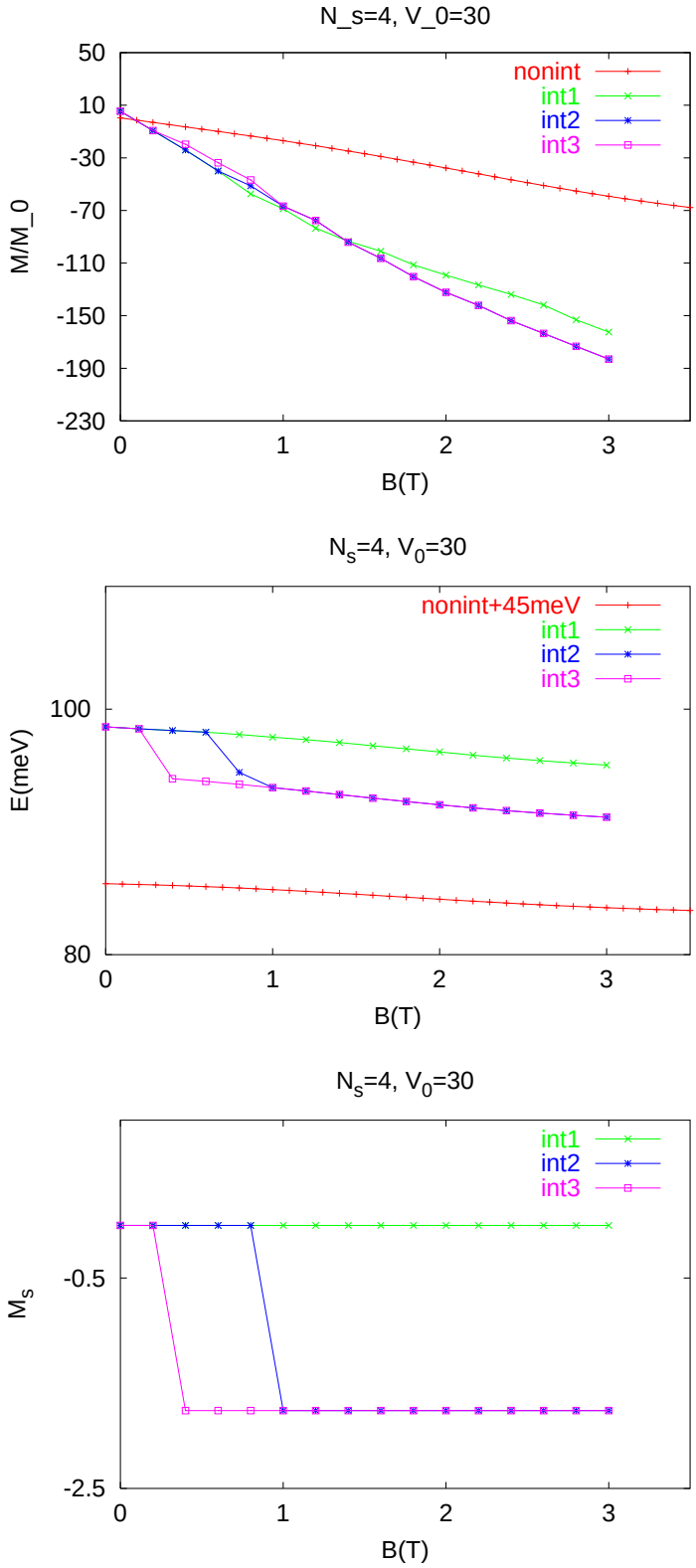

Figure 5.37: The orbital M_o and spin magnetization M_s and the total energy of a four-electron quantum ring in the case of elliptic confinement ($\alpha_1 = 0.1,\ \alpha_2 = 0.0$) for both noninteracting ("nonint") and interacting electrons ("int1", "int2" and "int3" corresponding to $g = -0.44,\ g_i =$

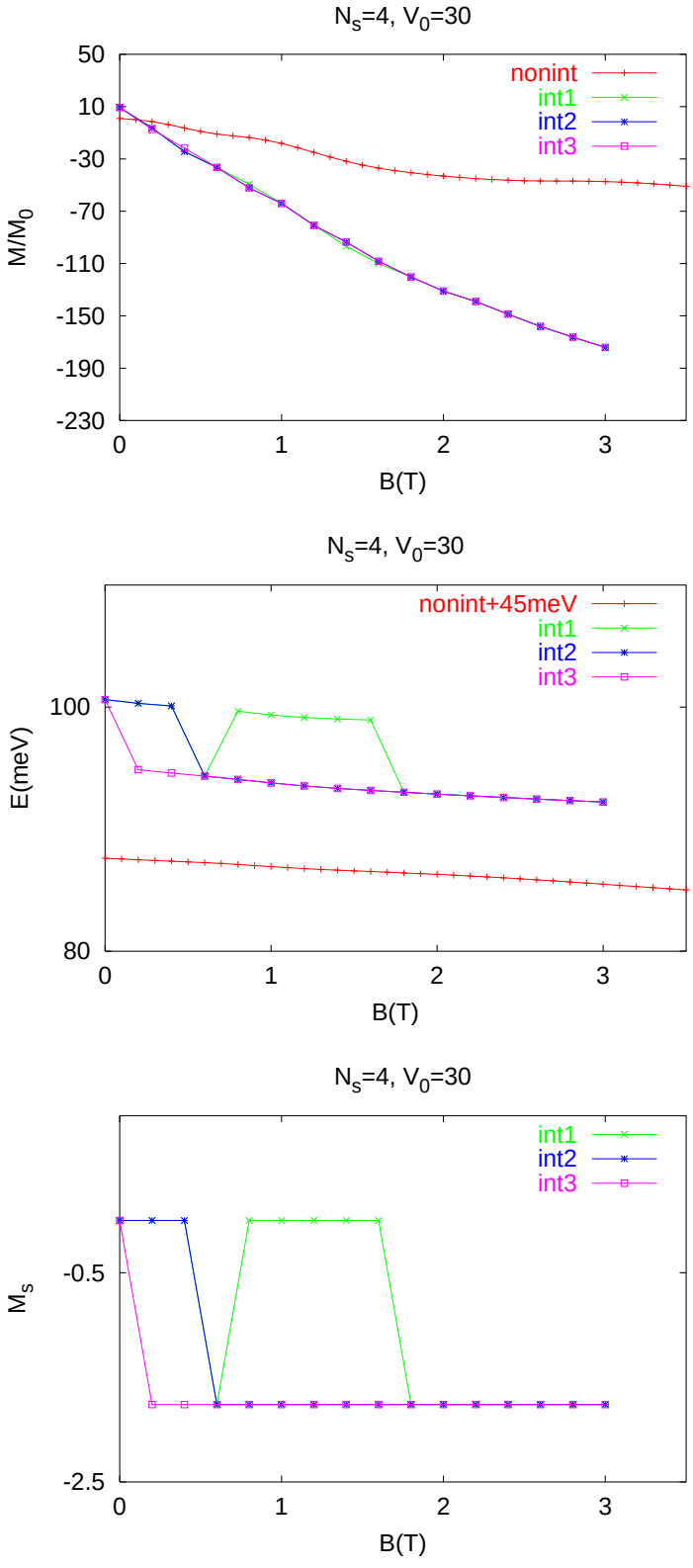

Figure 5.38: The orbital M_o and spin magnetization M_s and the total energy of a four-electron quantum ring in the case of square symmetric confinement ($\alpha_1 = 0.0,\ \alpha_2 = 0.1$) for both noninteracting ("nonint") and interacting electrons ("int1", "int2" and "int3" corresponding to $g = -0.44$,

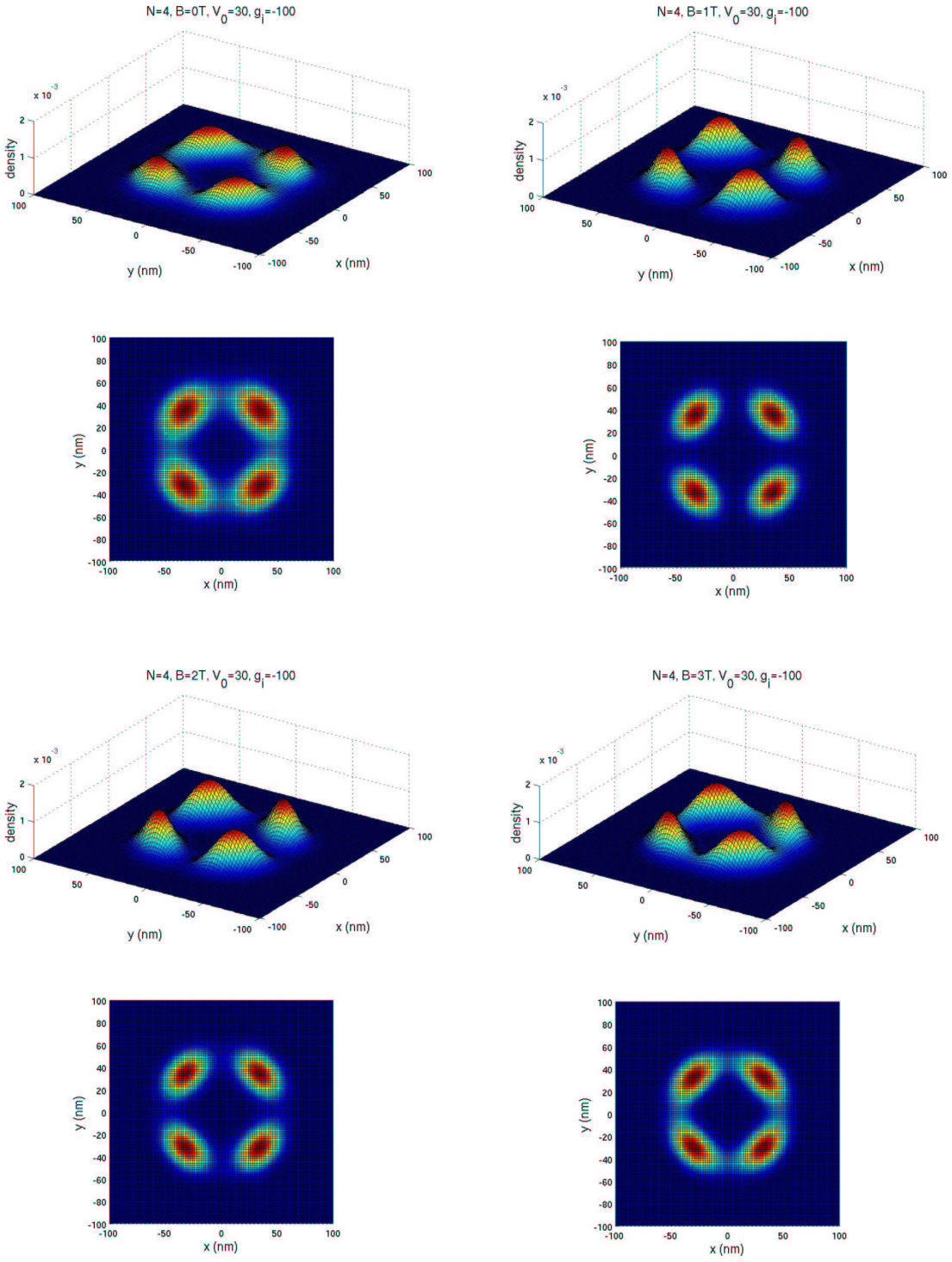

Figure 5.39: The electron densities of a four-electron quantum ring in the case of square symmetric confinement ($\alpha_1 = 0.0,\ \alpha_2 = 0.1$) for polarized ($g_i = -100$) interacting electrons at different values of magnetic field $B = 0$ T, $B = 1$ T, $B = 2$ T and $B = 3$ T for $V_0 = 30$.

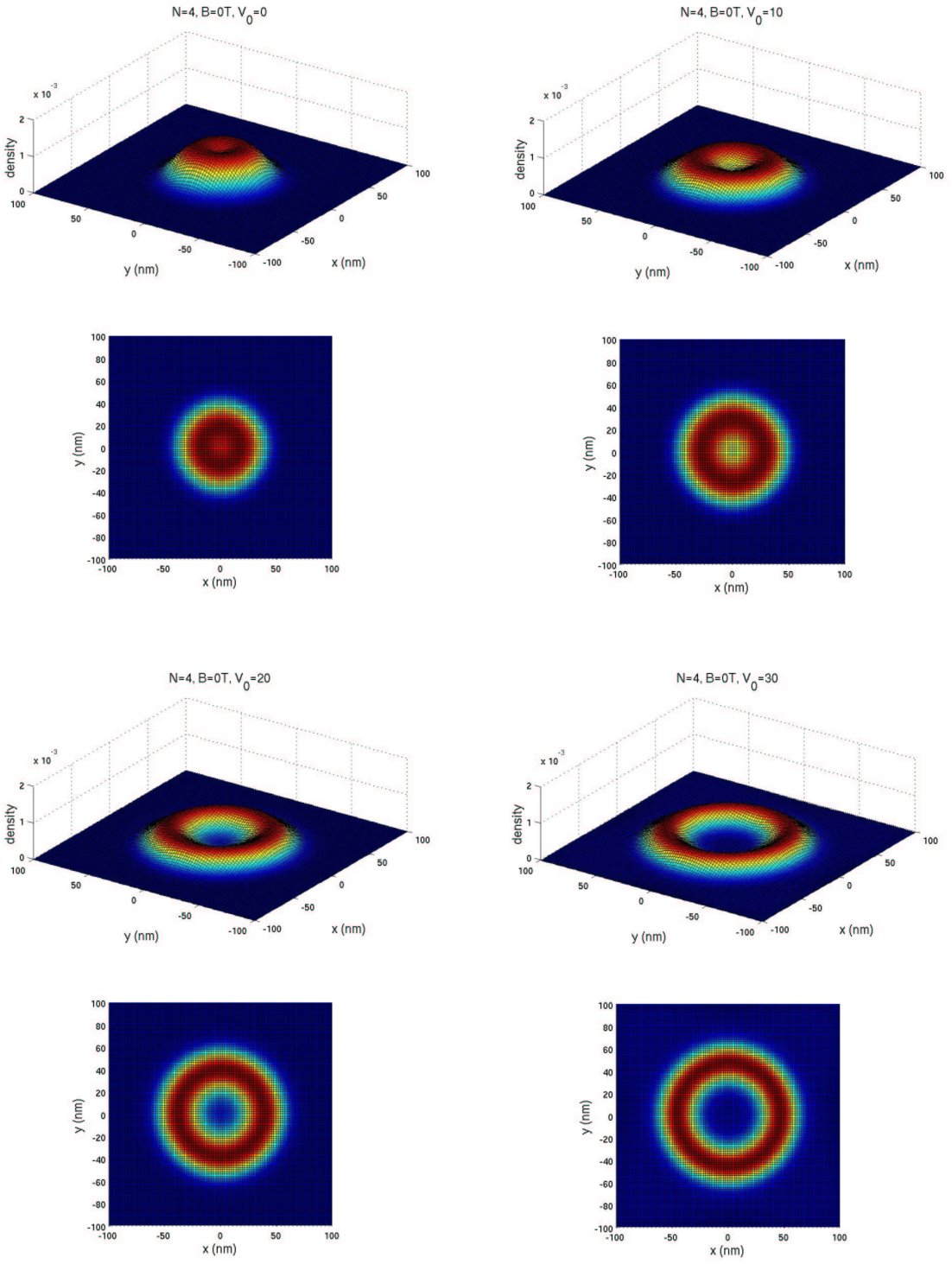

Figure 5.40: Evolution of density at $B = 0$ T with increasing the values of V_0.

Chapter 6

Summary and conclusions

On May 15 2002 the first results on the measurements of the magnetization of the electron system confined in quantum dots were published in Journal of Applied Physics [35], approximately 17 years after the first magnetization measurements where performed on a two-dimensional electron gas in a semiconductor. The measurements are on arrays of dots with few hundreds of electrons in each dot. In anticipation of the experimentalists' intention to measure the magnetization in dots with few electrons, we studied by theoretical models how the magnetization of quantum dots depends on their shape and the number of electrons in them. By a flexible description of the confinement potential we are able to study, circular, elliptic, or square symmetric dots, and we can even add a potential hill in the center and to calculate some properties of these dots as they are tuned to rings.

We have chosen to use the Hartree-Fock approximation for the Coulomb interaction between the electrons and project the resulting nonlocal equation of motion onto the mathematical basis of the eigenfunctions of the noninteracting system, the Fock-Darwin basis. The multipole expansion of the confinement breaks the circular symmetry, meaning that the angular momentum quantum number M is not conserved. The matrix elements of the confinement potential, the Hartree and Fock potentials for the interaction, and the magnetization were evaluated analitycally in order to minimize the program running time and increase its accuracy.

The main conclusion is that the magnetization in the case of few electrons depends strongly on the number of electrons in the system. On the other hand, the magnetization does not strongly depend on the shape of the dots though finer details do correlate with their shape. We have been able to identify the fingerprints of the dot and the ring in the magnetization as we tune the system between these two extremes. Generally, we notice well abrupt changes in the structure of the ground state that happen with increasing magnetic field. This strengthens the hope that measurements of the magnetization will turn out to be an important addition to tools already used to do "spectroscopy" on the many-body ground state of quantum dots. Magnetization has the advantage that it is a

ground state property and should thus give direct information about its structure.

In principle, nothing but CPU-time has limited the number of the electrons considered in each dot in the range 2 - 6. We can expect the model to work well for several tens of electrons, and in that range the Hartree-Fock approximation should even be more appropriate than for few electrons.

Chapter 7

Acknowledgments

I am deeply indebted to my supervisors Viðar Guðmundsson and Andrei Manolescu for their invaluable patience and support to solve the inherent “troubles” in programming and for the opportunity to work in this interesting field and in this amazing country as well. At the same time I would like to thank them and their families for the overall assistance given in anything I did during my stay in Iceland, mainly to Gerlinde Xander and Ileana Manolescu for very instructive conversations about family life and not only.

I would like to mention my gymnasium mathematics teacher Constantin Iliescu and also Prof. Dr. Ebanca and Prof. Dr. Podeanu who helped me to understand mathematics and physics.

I thank my parents and all friends for their support throughout my studies.

Appendix A

Matrix elements

A.1 The matrix elements of the confinement $\langle \Phi_j | V_\varphi | \Phi_i \rangle$

Within this thesis, many calculations were performed analytically to reduce the program running time. In this section we want to evaluate the matrix elements of the confining potential:

$$\langle \Phi_j | V_\varphi | \Phi_i \rangle = \int_{R^2} d\vec{r} \Phi_j^*(\vec{r}) V_\varphi \Phi_i(\vec{r}) \tag{A.1}$$

For solving this integral in a convenient way, the basis functions (3.10) are written as

$$\Phi(r) = \chi(r) e^{-iM\varphi}\,, \tag{A.2}$$

where $r = |\vec{r}|$. By taking into account that $i := (M, n_r)$ and $j := (N, m_r)$ the matrix elements become

$$\langle \Phi_j | V_\varphi | \Phi_i \rangle = \int_0^{2\pi} d\varphi e^{-i\Delta M\varphi} \int_0^{+\infty} dr r \chi_j(r) V_\varphi \chi_i(r)\,, \tag{A.3}$$

where $\Delta M = M - N$. The confinement potential is given by:

$$V_\varphi(r) = \frac{1}{2} m^* \omega_0^2 r^2 \sum_{p=1}^{p_{max}} \alpha_p \cos(2p\varphi)\,, \tag{A.4}$$

such that the angular integration gives

$$\sum_{p=1}^{p_{max}} \alpha_p \int_0^{2\pi} d\varphi e^{-i\Delta M\varphi} \cos(2p\varphi) = \sum_{p=1}^{p_{max}} \alpha_p \pi [\delta_{\Delta M, 2p} + \delta_{\Delta M, -2p}]\,. \tag{A.5}$$

supplying a selection rule which governs these matrix elements

$$\Delta M = \pm 2p\,. \tag{A.6}$$

The matrix elements within a few algebraic steps become

$$\begin{aligned}\langle\Phi_j|V_\varphi|\Phi_i\rangle &= \frac{1}{2}m^*\omega_0^2\left[\frac{n_r!}{(|M|+n_r)!}\cdot\frac{m_r!}{(|N|+m_r)!}\right]^{1/2}\times\sum_{p=1}^{p_{max}}\alpha_p[\delta_{\Delta M,2p}+\delta_{\Delta M,-2p}]\\ &\times \int_0^{+\infty}drr\left(\frac{r^2}{2a^2}\right)^{\frac{|M|+|N|}{2}+1}e^{\frac{-r^2}{2a^2}}L_{n_r}^{|M|}\left(\frac{r^2}{2a^2}\right)L_{m_r}^{|N|}\left(\frac{r^2}{2a^2}\right),\end{aligned}$$

By changing the variables in the integral,

$$x=\frac{r^2}{2a^2},\quad dx=\frac{r}{a^2}dr,\quad dr=\frac{a^2}{r}dx,$$

it transforms into:

$$I=\int_0^{+\infty}dxx^{\frac{|M|+|N|}{2}+1}e^{-x}L_{n_r}^{|M|}(x)L_{m_r}^{|N|}(x)\,.$$

We have thus the matrix elements:

$$\langle\Phi_j|V_\varphi|\Phi_i\rangle=\frac{1}{2}m^*\omega_0^2\left[\frac{n_r!}{(|M|+n_r)!}\cdot\frac{m_r!}{(|N|+m_r)!}\right]^{1/2}\times\sum_{p=1}^{p_{max}}\alpha_p[\delta_{\Delta M,2p}+\delta_{\Delta M,-2p}]\times I\,.$$

To evaluate the integral I we have a relation, see [19]

$$\sum_{n_r=0}^{+\infty}L_n^\alpha(x)=(1-z)^{-\alpha-1}e^{\frac{xz}{z-1}},$$

with $|z|<1$. Therefore we have further:

$$\begin{aligned}\sum_{n_r=0}^{+\infty}I\cdot z^{n_r} &= \sum_{n_r=0}^{+\infty}z^{n_r}\int_0^{+\infty}dxx^{\frac{|M|+|N|}{2}+1}e^{-x}L_{m_r}^{|N|}(x)L_{n_r}^{|M|}(x)\\ &= \frac{1}{(1-z)^{|M|+1}}\int_0^{+\infty}dxe^{-\frac{x}{1-z}}x^{\frac{|M|+|N|}{2}+1}L_{m_r}^{|N|}(x)\end{aligned}$$

Using the relation [19]

$$\int_0^{+\infty}e^{-st}t^\beta L_n^\alpha(t)dt=\frac{\Gamma(\beta+1)\Gamma(\alpha+n+1)}{n!\Gamma(\alpha+1)}s^{-\beta-1}F\left(-n,\beta+1;\alpha+1;\frac{1}{s}\right),\quad\text{(A.7)}$$

where: $Re\,(\beta)>-1$, $Re\,(s)>0$, Γ is the *Gamma function* defined as $\Gamma(n)=(n-1)\,!$, and F is *the hypergeometric series*, defined in [19]:

$$F(\alpha,\beta;\gamma;z)=1+\frac{\alpha\cdot\beta}{\gamma\cdot1}\cdot z+\frac{\alpha(\alpha+1)\beta(\beta+1)}{\gamma(\gamma+1)\cdot1\cdot2}\cdot z^2+\frac{\alpha(\alpha+1)(\alpha+2)\beta(\beta+1)(\beta+2)}{\gamma(\gamma+1)(\gamma+2)\cdot1\cdot2\cdot3}\cdot z^3+\cdots.\quad\text{(A.8)}$$

After a few algebraic steps the left hand side of relation (A.7) becomes:

$$\sum_{n_r=0}^{+\infty} I\cdot z^{n_r} = (1-z)^{\frac{|N|-|M|}{2}+1}\cdot\frac{\left(\frac{|N|+|M|}{2}+1\right)!(|N|+m_r)!}{m_r!(|N|)!} \times F\left(-m_r,\frac{|N|+|M|}{2}+2;|N|+1;1-z\right). \quad (A.9)$$

The hypergeometric series is a polynomial of the order m_r in $(1-z)$ and the right hand side of equation (A.9) is therefore a polynomial of the order $m_r+\frac{|N|-|M|}{2}+1$ in $(1-z)$. By introducing the relation (A.8) in the right hand side of relation (A.9) and after a few algebraic steps we get a new selection rule:

$$n_r \le m_r+\frac{|N|-|M|}{2}+1. \quad (A.10)$$

Since, physically, $n_r\ge 0$, it is obvious that $\frac{|N|-|M|}{2}+1\ge 0$ is only true in the case $|N|\ge|M|$ (a stronger condition than necessary). As the integral I is independent of this choice (the interchange $(M,n_r)\longleftrightarrow(N,m_r)$ yields the same integral), to evaluate the integral over r for $|M|>|N|$ we simply interchange (M,n_r) and (N,m_r). By writing the expression (A.9) as a polynomial in t, we obtain:

$$\sum_{n_r=0}^{+\infty} I\cdot z^{n_r}=\sum_{k=0}^{m_r}(1-z)^{l+k}\cdot(-1)^k\cdot\frac{\left(\frac{|M|+|N|}{2}+k+1\right)!(|N|+m_r)!}{k!(m_r-k)!(|N|+k)!},$$

and taking into account another formula [19]

$$(a+x)^n=\sum_{k=0}^{n}\left(\begin{array}{c} n\\ k\end{array}\right)x^k a^{n-k},$$

with

$$\left(\begin{array}{c} n\\ k\end{array}\right)=\frac{n(n-1)(n-2)\ldots(n-k+1)}{1\cdot 2\cdot\ldots\cdot k}=\frac{n!}{k!(n-k)!}.$$

and

$$l=\frac{|N|-|M|}{2}+1,$$

we obtain:

$$\sum_{n_r=0}^{+\infty} I\cdot z^{n_r}=\sum_{n_r=0}^{m_r+l}\sum_{k=0}^{m_r}(-1)^{k+n_r}\cdot\frac{\left(\frac{|M|+|N|}{2}+k+1\right)!(|N|+m_r)!}{k!(m_r-k)!(|N|+k)!}\left(\begin{array}{c} k+l\\ n_r\end{array}\right)z^{n_r}. \quad (A.11)$$

By identifying the coefficients in (A.11), we get for the integral

$$I=\sum_{k=0}^{m_r}(-1)^{k+n_r}\frac{\left(\frac{|M|+|N|}{2}+k+1\right)!(|N|+m_r)!}{k!(m_r-k)!(|N|+k)!}\frac{\left(\frac{|N|-|M|}{2}+k+1\right)!}{n_r!\left(\frac{|N|-|M|}{2}+k+1-n_r\right)!}. \quad (A.12)$$

Therefore, the matrix elements of the confinement potential becomes [21]:

$$\begin{aligned}\langle\Phi_j|V_\varphi|\Phi_i\rangle &= \frac{1}{2}m^*\omega_0^2a^2\left[\frac{m_r!(|N|+m_r)!}{n_r!(|M|+n_r)!}\right]^{1/2}\times\sum_{p=1}^{p_{max}}\alpha_p[\delta_{\Delta M,2p}+\delta_{\Delta M,-2p}] \\ &\times \sum_{k=0}^{m_r}(-1)^{k+n_r}\frac{\left(\frac{|M|+|N|}{2}+k+1\right)!}{k!(m_r-k)!(|N|+k)!}\cdot\frac{\left(\frac{|N|-|M|}{2}+k+1\right)!}{\left(\frac{|N|-|M|}{2}+k+1-n_r\right)!}.\end{aligned} \tag{A.13}$$

Here we consider $\frac{1}{(-n)!}=0$, $n=1,2,\ldots$

A.2 The Hartree matrix elements $\langle\Phi_k|V_H|\Phi_l\rangle$

The Hartree matrix elements are given by

$$\langle\Phi_k|V_H|\Phi_l\rangle=\int_{R^2}d\vec{r}\,\Phi_k^*(\vec{r})V_H\Phi_l(\vec{r})=\frac{e^2}{4\pi\varepsilon_0\varepsilon_r}\int_{R^2}d\vec{r}\,\Phi_k^*(\vec{r})\left[\int_{R^2}d\vec{r}\,'\frac{n_s(\vec{r}\,')}{|\vec{r}-\vec{r}\,'|}\right]\Phi_l(\vec{r}), \tag{A.14}$$

where V_H is the Hartree potential and according to [36] $\frac{1}{|\vec{r}-\vec{r}\,'|}$ can be written as:

$$\frac{1}{|\vec{r}-\vec{r}\,'|}=\sum_{m=-\infty}^{+\infty}e^{im(\varphi-\varphi')}\int_0^{+\infty}dkJ_m(k\vec{r})J_m(k\vec{r}\,'), \tag{A.15}$$

where J_m is a Bessel-function of order m. Then the matrix elements become:

$$\begin{aligned}\langle\Phi_k|V_H|\Phi_l\rangle &= \frac{e^2}{4\pi\varepsilon_0\varepsilon_r}\int_{R^2}d\vec{r}\,\Phi_k^*(\vec{r}) \\ &\times \left[\int_{R^2}d\vec{r}\,'\sum_{m=-\infty}^{+\infty}e^{im(\varphi-\varphi')}\int_0^{+\infty}dkJ_m(k\vec{r})J_m(k\vec{r}\,')n_s(\vec{r}\,')\right]\Phi_l(\vec{r}).\end{aligned}$$

We write the basis functions (3.10) as (A.2) and within a few algebraic steps we get for the integration over φ that:

$$\int_0^{2\pi}d\varphi e^{i(m+K-L)\varphi}=\int_0^{2\pi}d\varphi e^{i[m-(L-K)]\varphi}=2\pi\delta_{m,L-K}$$

Therefore for a given L and K, only one term in the sum over m is non-zero, that is $m=L-K$, all the others are zero. To solve the integral over φ', the electron density must be written in terms of the basis functions:

$$n_s(\vec{r}\,')=\sum_\alpha f(\varepsilon_\alpha)|\Psi_\alpha(\vec{r}\,')|^2=\sum_\alpha f(\varepsilon_\alpha)\sum_{p,q}C_{\alpha p}^*C_{\alpha q}\Phi_p^*(\vec{r}\,')\Phi_q(\vec{r}\,'),$$

where $p := (M, n_r)$ and $q := (N, m_r)$. By using again the relation (A.2), the electron density is

$$n_s(\vec{r}\,') = \sum_\alpha f(\varepsilon_\alpha) \sum_{p,q} C_{\alpha p} C_{\alpha q} \chi_p(\vec{r}\,') \chi_q(\vec{r}\,') e^{i(M-N)\varphi'} . \tag{A.16}$$

The integration over φ' leads to:

$$\int_0^{2\pi} d\varphi e^{i(M-N-m)\varphi'} = \int_0^{2\pi} d\varphi e^{i[(M-N)-(L-K)]\varphi'} = 2\pi\delta_{M-N,L-K} . \tag{A.17}$$

From relation (A.17) emerges the selection rule which tells us that for given L, K, M and N only one term in the sum is non-zero, namely for $L-K = M-N$, all the other terms being zero. Therefore the Hartree matrix elements become:

$$\begin{aligned} \langle \Phi_k | V_H | \Phi_l \rangle &= (2\pi)^2 \frac{e^2}{4\pi\varepsilon_0\varepsilon_r} \sum_\alpha f(\varepsilon_\alpha) \sum_{p,q} C_{\alpha p} C_{\alpha q} \\ &\times \int_0^{+\infty} dk \left[\int_0^{+\infty} dr r \chi_k(r) J_{L-K}(kr) \chi_l(r) \right] \\ &\times \left[\int_0^{+\infty} dr' r' \chi_p(r') J_{M-N}(kr') \chi_q(r') \right] \delta_{M-N,L-K} . \end{aligned}$$

To simplify the writing of the Hartree matrix elements I'll use a few notations for the wavefunctions:

$$\chi_k(r) = \beta_k \left(\frac{r}{a}\right)^{|K|} e^{-\frac{r^2}{4a^2}} L_{k_r}^{|K|} \left(\frac{r^2}{2a^2}\right) \tag{A.18}$$

with

$$\beta_k = \frac{1}{2^{\frac{|K|+1}{2}} a} \cdot \left(\frac{k_r!}{\pi(|K|+k_r)!} \right)^{1/2} \tag{A.19}$$

This gives:

$$\begin{aligned} \langle \Phi_k | V_H | \Phi_l \rangle &= (2\pi)^2 \frac{e^2}{4\pi\varepsilon_0\varepsilon_r} \beta_k \beta_l \sum_\alpha f(\varepsilon_\alpha) \sum_{p,q} C_{\alpha p} C_{\alpha q} \beta_p \beta_q \delta_{M-N,L-K} \\ &\times \int_0^{+\infty} dk \left[\int_0^{+\infty} dr r \left(\frac{r}{a}\right)^{|K|+|L|} e^{-\frac{r^2}{2a^2}} L_{k_r}^{|K|} \left(\frac{r^2}{2a^2}\right) L_{l_r}^{|L|} \left(\frac{r^2}{2a^2}\right) J_{L-K}(kr) \right] \\ &\times \left[\int_0^{+\infty} dr' r' \left(\frac{r'}{a}\right)^{|M|+|N|} e^{-\frac{r^2}{2a^2}} L_{n_r}^{|M|} \left(\frac{r'^2}{2a^2}\right) L_{m_r}^{|N|} \left(\frac{r'^2}{2a^2}\right) J_{M-N}(kr') \right] . \end{aligned}$$

The Laguerre polynomials are [19]

$$L_{k_r}^{|K|} \left(\frac{r^2}{2a^2}\right) = \sum_{\nu=0}^{n_r} \frac{(-1)^\nu}{2^\nu \cdot \nu!} \begin{pmatrix} n_r + |M| \\ n_r - \nu \end{pmatrix} \left(\frac{r}{a}\right)^{2\nu} , \tag{A.20}$$

and then the Hartree matrix elements transform into:

$$\begin{aligned}\langle\Phi_k|V_H|\Phi_l\rangle &= (2\pi)^2\frac{e^2}{4\pi\varepsilon_0\varepsilon_r}\beta_k\beta_l\sum_\alpha f(\varepsilon_\alpha)\sum_{p,q}C_{\alpha p}C_{\alpha q}\beta_p\beta_q\sum_{\kappa=0}^{k_r}\sum_{\lambda=0}^{l_r}\sum_{\nu=0}^{n_r}\sum_{\mu=0}^{m_r}\frac{(-1)^{\kappa+\lambda+\nu+\mu}}{\kappa!\lambda!\nu!\mu!}\\ &\times\begin{pmatrix}k_r+|K|\\ k_r-\kappa\end{pmatrix}\begin{pmatrix}l_r+|L|\\ l_r-\lambda\end{pmatrix}\begin{pmatrix}n_r+|M|\\ n_r-\nu\end{pmatrix}\begin{pmatrix}m_r+|N|\\ m_r-\mu\end{pmatrix}\\ &\times\int_0^{+\infty}dk\frac{1}{2^{\kappa+\lambda}}\left[\int_0^{+\infty}drr\left(\frac{r}{a}\right)^{|K|+|L|+2(\kappa+\lambda)}e^{-\frac{r^2}{2a^2}}J_{L-K}(kr)\right]\\ &\times\frac{1}{2^{\nu+\mu}}\left[\int_0^{+\infty}dr'r'\left(\frac{r'}{a}\right)^{|M|+|N|+2(\nu+\mu)}e^{-\frac{r'^2}{2a^2}}J_{M-N}(kr')\right].\end{aligned}$$

The integrals, over r and r', can be calculated using the relation [19]

$$\int_0^{+\infty}dxx^\mu e^{-\alpha x^2}J_\nu(\beta x)=\frac{\beta^\nu\Gamma\left(\frac{\nu+\mu+1}{2}\right)}{2^{\nu+1}\alpha^{\frac{1}{2}(\nu+\mu+1)}\Gamma(\nu+1)}\,{}_1F_1\left(\frac{\nu+\mu+1}{2};\nu+1;-\frac{\beta^2}{4\alpha}\right) \tag{A.21}$$

where ${}_1F_1(\alpha;\gamma;z)$ is the *confluent hypergeometric function* [19]. Therefore, the integral over r is:

$$\begin{aligned}\int_0^{+\infty}drr\left(\frac{r}{a}\right)^{|K|+|L|+2(\kappa+\lambda)}e^{-\frac{r^2}{2a^2}}J_{L-K}(kr) &= 2^{\frac{|K|+|L|+K-L}{2}}+(ka)^{L-K}a^2\frac{\left(\frac{L-K+|K|+|L|}{2}+\kappa+\lambda\right)!}{(L-K)!}\\ &\times{}_1F_1\left(\frac{L-K+|K|+|L|}{2}+\kappa+\lambda+1;L-K+1;-\frac{k^2a^2}{2}\right).\end{aligned}$$

The integral over r' is of the same kind. With the redefinition

$$\gamma_k=(2\pi)^{1/2}2^{\frac{|K|}{2}}a\beta_k=\left[\frac{k_r!}{(|K|+k_r)!}\right]^{1/2}$$

and by taking into account the selection rule $L-K=M-N$, the Hartree matrix elements are:

$$\begin{aligned}
\langle k|V_H|l\rangle &= \frac{e^2}{4\pi\varepsilon_0\varepsilon_r}\gamma_k\gamma_l\sum_\alpha f(\varepsilon_\alpha)\sum_{p,q}C_{\alpha p}C_{\alpha q}\gamma_p\gamma_q\sum_{\kappa=0}^{k_r}\sum_{\lambda=0}^{l_r}\sum_{\nu=0}^{n_r}\sum_{\mu=0}^{m_r}\frac{(-1)^{\kappa+\lambda+\nu+\mu}}{\kappa!\lambda!\nu!\mu!}\\
&\times \begin{pmatrix} k_r+|K| \\ k_r-\kappa \end{pmatrix}\begin{pmatrix} l_r+|L| \\ l_r-\lambda \end{pmatrix}\begin{pmatrix} n_r+|M| \\ n_r-\nu \end{pmatrix}\begin{pmatrix} m_r+|N| \\ m_r-\mu \end{pmatrix}\\
&\times \frac{\left(\frac{L-K+|K|+|L|}{2}+\kappa+\lambda\right)!}{(L-K)!}\cdot\frac{\left(\frac{M-N+|M|+|N|}{2}+\nu+\mu\right)!}{(M-N)!}\\
&\times \int_0^{+\infty}dk\left(\frac{k^2a^2}{2}\right)^{L-K}{}_1F_1\left(\frac{L-K+|K|+|L|}{2}+\kappa+\lambda+1;L-K+1;-\frac{k^2a^2}{2}\right)\\
&\times {}_1F_1\left(\frac{M-N+|M|+|N|}{2}+\nu+\mu+1;M-N+1;-\frac{k^2a^2}{2}\right).
\end{aligned}$$

Using the transformation [19]

$${}_1F_1(\alpha;\gamma;x)=e^x\,{}_1F_1(\gamma-\alpha;\gamma;-x) \tag{A.22}$$

the Hartree matrix elements become [21]:

$$\begin{aligned}
\langle k|V_H|l\rangle &= \frac{e^2}{4\pi\varepsilon_0\varepsilon_r}\left[\frac{k_r!}{(|K|+k_r)!}\cdot\frac{l_r!}{(|L|+l_r)!}\right]^{1/2}\sum_\alpha f(\varepsilon_\alpha)\sum_{p,q}C_{\alpha p}C_{\alpha q}\\
&\times \left[\frac{n_r!}{(|M|+n_r)!}\cdot\frac{m_r!}{(|N|+m_r)!}\right]^{1/2}\sum_{\kappa=0}^{k_r}\frac{(-1)^\kappa}{\kappa!}\cdot\frac{(k_r+|K|)!}{(k_r-\kappa)!(\kappa+|K|)!}\\
&\times \sum_{\lambda=0}^{l_r}\frac{(-1)^\lambda}{\lambda!}\cdot\frac{(l_r+|L|)!}{(l_r-\lambda)!(\lambda+|L|)!}\cdot\frac{\left(\frac{L-K+|L|+|K|}{2}+\kappa+\lambda\right)!}{(L-K)!}\\
&\times \sum_{\nu=0}^{n_r}\frac{(-1)^\nu}{\nu!}\cdot\frac{(n_r+|M|)!}{(n_r-\nu)!(\nu+|M|)!}\\
&\times \sum_{\mu=0}^{m_r}\frac{(-1)^\mu}{\mu!}\cdot\frac{(m_r+|N|)!}{(m_r-\mu)!(\mu+|N|)!}\cdot\frac{\left(\frac{M-N+|M|+|N|}{2}+\nu+\mu\right)!}{(M-N)!}\\
&\times \int_0^{+\infty}dk\left(\frac{k^2a^2}{2}\right)^{L-K}e^{-k^2a^2}\,{}_1F_1\left(\frac{L-K-|K|-|L|}{2}-\kappa-\lambda;L-K+1;\frac{k^2a^2}{2}\right)\\
&\times {}_1F_1\left(\frac{M-N-|M|-|N|}{2}-\nu-\mu;M-N+1;\frac{k^2a^2}{2}\right).
\end{aligned}$$

A.3 The Fock matrix elements $\langle\Phi_k|V_F|\Phi_l\rangle$

The Fock matrix elements are given by

$$\langle\Phi_k|V_F|\Phi_l\rangle = -\int_{R^2} d\vec{r}\,d\vec{r}\,'\Delta(\vec{r},\vec{r}\,')\Phi_k^*(\vec{r})\Phi_l(\vec{r}\,')\,, \tag{A.23}$$

where

$$\Delta(\vec{r},\vec{r}\,') = \frac{e^2}{4\pi\varepsilon_0\varepsilon_r}\sum_\alpha f(\varepsilon_\alpha)\frac{\Psi_\alpha^*(\vec{r}\,')\cdot\Psi_\alpha(\vec{r})}{|\vec{r}-\vec{r}\,'|}$$

and by using relation (A.15) the Fock matrix elements become:

$$\begin{aligned}\langle\Phi_k|V_F|\Phi_l\rangle &= -\frac{e^2}{4\pi\varepsilon_0\varepsilon_r}\sum_\alpha f(\varepsilon_\alpha)\sum_{m=-\infty}^{+\infty} e^{im(\varphi-\varphi')} \\ &\times \int_0^{+\infty} dk\left[\int_{R^2} d\vec{r}\,\Phi_k^*(\vec{r})J_m(k\vec{r})\Psi_\alpha(\vec{r})\right]\times\left[\int_{R^2} d\vec{r}\,'\Phi_l(\vec{r}\,')J_m(k\vec{r}\,')\Psi_\alpha^*(\vec{r}\,')\right]\end{aligned}$$

But:

$$\Psi_\alpha(\vec{r}) = \sum_q C_{\alpha q}\Phi_q(\vec{r})\,,$$

$$\Psi_\alpha^*(\vec{r}\,') = \sum_q C_{\alpha p}\Phi_p^*(\vec{r})\,,$$

where: $p := (M,n_r)$, $q := (N,m_r)$, $l := (L,l_r)$ and $k := (K,k_r)$. We have dropped the asterisk on $C_{\alpha p}$ since it is a real quantity. With all these changes and help of relation (A.2), the Fock matrix elements transform into:

$$\begin{aligned}\langle\Phi_k|V_F|\Phi_l\rangle &= -\frac{e^2}{4\pi\varepsilon_0\varepsilon_r}\sum_\alpha f(\varepsilon_\alpha)\sum_{p,q} C_{\alpha p}C_{\alpha q} \\ &\times \int_0^{+\infty} dk\left[\int_0^{+\infty} dr r\chi_k(r)J_m(kr)\chi_q(r)\int_0^{2\pi} d\varphi e^{i[m-(N-K)]\varphi}\right] \\ &\times \left[\int_0^{+\infty} dr' r'\chi_l(r')J_m(kr')\chi_p(r')\int_0^{2\pi} d\varphi' e^{i[(M-L)-m]\varphi'}\right].\end{aligned}$$

By solving the integral over φ and φ' we get:

$$\int_0^{2\pi} d\varphi\cdot e^{i[m-(N-K)]\varphi} = 2\pi\delta_{m,N-K} \tag{A.24}$$

For given N and K, relation (A.24) means that only one term of the sum over m is non-zero, that is $m = N-K$; and

$$\int_0^{2\pi} d\varphi'\cdot e^{i[(M-L)-(N-K)]\varphi'} = 2\pi\delta_{M-L,N-K} \tag{A.25}$$

Relation (A.25) defines the selection rule, which implies that, for given L, K, M and N only one term in the sum is non-zero, namely for $M-L=N-K$, all the others being zero. By following the same way as used for Hartree matrix elements and using the relations (A.18), (A.19), (A.20), (A.21) and (A.22) the Fock matrix elements become:

$$\begin{aligned}
\langle k|V_F|l\rangle &= -\frac{e^2}{4\pi\varepsilon_0\varepsilon_r}\sum_{\alpha} f(\varepsilon_\alpha)\sum_{p,q} C_{\alpha p}C_{\alpha q}\left[\frac{k_r!}{(|K|+k_r)!}\cdot\frac{l_r!}{(|L|+l_r)!}\right]^{1/2} \\
&\times \left[\frac{n_r!}{(|M|+n_r)!}\cdot\frac{m_r!}{(|N|+m_r)!}\right]^{1/2}\sum_{\kappa=0}^{k_r}\frac{(-1)^\kappa}{\kappa!}\cdot\frac{(k_r+|K|)!}{(k_r-\kappa)!(\kappa+|K|)!} \\
&\times \sum_{\mu=0}^{m_r}\frac{(-1)^\mu}{\mu!}\cdot\frac{(m_r+|N|)!}{(m_r-\mu)!(\mu+|N|)!}\cdot\frac{\left(\frac{N-K+|N|+|K|}{2}+\kappa+\mu\right)!}{(N-K)!} \\
&\times \sum_{\lambda=0}^{l_r}\frac{(-1)^\lambda}{\lambda!}\cdot\frac{(l_r+|L|)!}{(l_r-\lambda)!(\lambda+|L|)!} \\
&\times \sum_{\nu=0}^{n_r}\frac{(-1)^\nu}{\nu!}\cdot\frac{(n_r+|M|)!}{(n_r-\nu)!(\nu+|M|)!}\cdot\frac{\left(\frac{M-L+|M|+|L|}{2}+\lambda+\nu\right)!}{(M-L)!} \\
&\times \int_0^{+\infty} dk\left(\frac{k^2a^2}{2}\right)^{N-K} e^{-k^2a^2}\,{}_1F_1\left(\frac{N-K-|N|-|L|}{2}-\kappa-\mu;N-K+1;\frac{k^2a^2}{2}\right) \\
&\times {}_1F_1\left(\frac{M-L-|M|-|L|}{2}-\lambda-\nu;M-L+1;\frac{k^2a^2}{2}\right).
\end{aligned}$$

A.4 The matrix elements of the confinement potential for a ring

In the case of quantum rings the confinement potential is:

$$V_{\text{conf}}(r,\varphi)=\frac{1}{2}m^*\omega_0^2r^2\left[1+\sum_{p=1}^{p_{max}}\alpha_p\cos(2p\varphi)\right]+V_0exp(-\gamma r^2)\,, \tag{A.26}$$

where the last term creates a potential hill in the middle of the quantum dot. The corresponding matrix elements are:

$$\langle\Phi_j|V_{\varphi'}|\Phi_i\rangle=\int_{R^2}d\vec{r}\,\Phi_j^*(\vec{r})V_{\varphi'}\Phi_i(\vec{r})\,, \tag{A.27}$$

where

$$V_{\varphi'}=V_0e^{-\gamma r^2}\,. \tag{A.28}$$

For calculating this integral the basis functions (3.10) are written according to (A.2) and by taking into account that $i := (M, n_r)$ and $j := (N, m_r)$ the matrix elements become

$$\langle \Phi_j | V_{\varphi'} | \Phi_i \rangle = \int_0^{2\pi} d\varphi e^{-i\Delta M\varphi} \int_0^{+\infty} dr r \chi_j(r) V_{\varphi'} \chi_i(r)\,, \tag{A.29}$$

where $\Delta M = M - N$. The angular integration gives:

$$\int_0^{2\pi} d\varphi e^{-i\Delta M\varphi} = 2\pi\delta_{M,N}\,. \tag{A.30}$$

The equation (A.30) creates the selection rule:

$$\Delta M = 0\,.$$

The matrix elements become:

$$\langle \Phi_j | V_{\varphi'} | \Phi_i \rangle = 2\pi V_0 \cdot \delta_{M,N} \times I\,, \tag{A.31}$$

where

$$\begin{aligned} I &= \int_0^{+\infty} dr r e^{-\gamma r^2} \chi_j(r)\chi_i(r) = \frac{1}{2^{\frac{|M|+|N|}{2}+1} a^2 \pi} \left[\frac{n_r!}{(|M|+n_r)!}\cdot\frac{m_r!}{(|N|+m_r)!}\right]^{1/2} \\ &\times \int_0^{+\infty} dr \left(\frac{r}{a}\right)^{|M|+|N|} e^{-(1+2a^2\gamma)\cdot\frac{r^2}{2a^2}} L_{n_r}^{|M|}\left(\frac{r^2}{2a^2}\right) L_{m_r}^{|N|}\left(\frac{r^2}{2a^2}\right). \end{aligned} \tag{A.32}$$

By changing the variables in the integral,

$$x = \frac{r^2}{2a^2}, \quad dx = \frac{r}{a^2}dr, \quad dr = \frac{a^2}{r}dx,$$

within a few algebraic steps the integral I becomes:

$$I = \frac{1}{2\pi}\left[\frac{n_r!}{(|M|+n_r)!}\cdot\frac{m_r!}{(|N|+m_r)!}\right]^{1/2} \int_0^{+\infty} dx x^{\frac{|M|+|N|}{2}} e^{-(1+2a^2\gamma)x} L_{n_r}^{|M|}(x) L_{m_r}^{|N|}(x)$$

The Laguerre functions can be expanded as polynomials, see [37]

$$L_n^{\alpha}(x) = \sum_{k=0}^{n} \frac{\Gamma(n+\alpha+1)}{\Gamma(k+\alpha+1)}\cdot\frac{(-x)^k}{k!(n-k)!}\,, \tag{A.33}$$

and by using the relations (A.33), (A.7) and (A.8), within a few algebraic steps the integral take the form:

$$\begin{aligned} I &= \frac{1}{2\pi}\left[\frac{n_r!}{(|M|+n_r)!}\cdot\frac{m_r!}{(|N|+m_r)!}\right]^{1/2} \sum_{k'=0}^{m_r}\sum_{k=0}^{n_r} (-1)^{k+k'} \frac{1}{(1+2a^2\gamma)^{\frac{|M|+|N|}{2}+k+k'+1}} \\ &\times \frac{(|M|+n_r)!}{k!(n_r-k)!(|M|+k)!}\cdot\frac{(|N|+m_r)!\left(\frac{|M|+|N|}{2}+k+k'\right)!}{k'!(m_r-k')!(|N|+k')!} \end{aligned} \tag{A.34}$$

and therefore relation (A.31) transform into:

$$\begin{aligned}\langle\Phi_j|V_{\varphi'}|\Phi_i\rangle &= V_0\cdot\delta_{M,N}\cdot\frac{1}{(1+2a^2\gamma)^{\frac{|M|+|N|}{2}+1}}\times\left[\frac{n_r!}{(|M|+n_r)!}\cdot\frac{m_r!}{(|N|+m_r)!}\right]^{1/2}\\ &\times\sum_{k'=0}^{m_r}(-1)^{k'}\cdot\frac{1}{(1+2a^2\gamma)^{k'}}\cdot\frac{1}{k'!(m_r-k')!}\cdot\frac{(|N|+m_r)!}{(|N|+k')!}\\ &\times\sum_{k=0}^{n_r}(-1)^{k}\cdot\frac{1}{(1+2a^2\gamma)^{k}}\cdot\frac{\left(\frac{|M|+|N|}{2}+k+k'\right)!}{k!(n_r-k)!}\cdot\frac{(|M|+n_r)!}{(|M|+k)!}\,.\end{aligned}$$

A.5 The matrix elements of position x, $\langle\Phi_j|x|\Phi_i\rangle$

The position matrix elements are given by

$$\langle\Phi_j|x|\Phi_i\rangle=\int_{R^2}d\vec{r}\,\Phi_j^*(\vec{r})\,x\,\Phi_i(\vec{r})=\int_{R^2}d\vec{r}\,\Phi_j^*(\vec{r})\,r\cos\varphi\,\Phi_i(\vec{r})\,, \tag{A.35}$$

By expanding the basis functions (3.10) as (A.2) the matrix elements transform into

$$\langle\Phi_j|x|\Phi_i\rangle=\int_0^{+\infty}drr^2\chi_j(r)\chi_i(r)\int_0^{2\pi}d\varphi\cos\varphi e^{-i\Delta M\varphi}\,,$$

where $i:=(M,n_r)$, $j:=(N,m_r)$, $\Delta M=M-N$. By solving the integral over φ we get the selection rule:

$$\int_0^{2\pi}d\varphi\cos\varphi e^{-i\Delta M\varphi}=\pi(\delta_{\Delta M,1}+\delta_{\Delta M,-1})\,,$$

therefore for given M and N, the selection rule $\Delta M=\pm1$ tells that only for these values of ΔM, the integrals over φ are non-zero, all the others being zero. Under these conditions the matrix elements become:

$$\langle\Phi_j|x|\Phi_i\rangle=\pi(\delta_{\Delta M,1}+\delta_{\Delta M,-1})\cdot\int_0^{+\infty}drr^2\chi_j(r)\chi_i(r)\,.$$

According to (3.10) and (A.2) the integral over r becomes:

$$\begin{aligned}I &= \int_0^{+\infty}drr^2\chi_j(r)\chi_i(r)=\frac{1}{2^{\frac{|M|+|N|}{2}+1}a^2\pi}\left[\frac{n_r!}{(|M|+n_r)!}\cdot\frac{m_r!}{(|N|+m_r)!}\right]^{1/2}\\ &\times\int_0^{+\infty}drr^2\left(\frac{r}{a}\right)^{|M|+|N|}e^{-\frac{r^2}{2a^2}}L_{n_r}^{|M|}\left(\frac{r^2}{2a^2}\right)L_{m_r}^{|N|}\left(\frac{r^2}{2a^2}\right)\end{aligned}$$

By using the expansion of Laguerre functions as polynomials (A.20), the integral I becomes:

$$\begin{aligned} I &= \frac{1}{2^{\frac{|M|+|N|}{2}+1}a^2\pi}\left[\frac{n_r!}{(|M|+n_r)!}\cdot\frac{m_r!}{(|N|+m_r)!}\right]^{1/2} \\ &\times \sum_{\nu=0}^{n_r}\sum_{\mu=0}^{m_r}\frac{(-1)^{\nu+\mu}}{2^{\nu+\mu}\cdot\nu!\cdot\mu!}\cdot\frac{(n_r+|M|)!}{(n_r-\nu)!(\nu+|M|)!}\cdot\frac{(m_r+|N|)!}{(m_r-\mu)!(\mu+|N|)!} \\ &\times \int_0^{+\infty} dr r^2\left(\frac{r}{a}\right)^{|M|+|N|+2(\nu+\mu)} e^{-\frac{r^2}{2a^2}} \end{aligned}$$

The last integral can be solved by taking into account relation [19]:

$$\int_0^{+\infty} dx x^{2n+1}e^{-px^2} = \frac{n!}{2p^{n+1}}\,, \tag{A.36}$$

where $p>0$. This integral leads to:

$$\int_0^{+\infty} dr r^2\left(\frac{r}{a}\right)^{|M|+|N|+2(\nu+\mu)} e^{-\frac{r^2}{2a^2}} = 2^{\frac{|M|+|N|+1}{2}+\nu+\mu}a^3\left(\frac{|M|+|N|+1}{2}+\nu+\mu\right)!\,,$$

so, the integral I becomes:

$$\begin{aligned} I &= \frac{1}{2\pi}\sqrt{2}a\left[\frac{n_r!}{(|M|+n_r)!}\cdot\frac{m_r!}{(|N|+m_r)!}\right]^{1/2}\sum_{\nu=0}^{n_r}\sum_{\mu=0}^{m_r}\frac{(-1)^{\nu+\mu}}{2^{\nu+\mu}\nu!\cdot\mu!} \\ &\times \frac{(n_r+|M|)!}{(n_r-\nu)!(\nu+|M|)!}\cdot\frac{(m_r+|N|)!}{(m_r-\mu)!(\mu+|N|)!}\cdot\left(\frac{|M|+|N|+1}{2}+\nu+\mu\right)!\,, \end{aligned}$$

therefore the position matrix elements become:

$$\begin{aligned} \langle\Phi_j|x|\Phi_i\rangle &= (\delta_{\Delta M,1}+\delta_{\Delta M,-1})\cdot\frac{1}{2}\sqrt{2}a\left[\frac{n_r!}{(|M|+n_r)!}\cdot\frac{m_r!}{(|N|+m_r)!}\right]^{1/2} \\ &\times \sum_{\nu=0}^{n_r}\frac{(-1)^{\nu}}{\nu!}\cdot\frac{(n_r+|M|)!}{(n_r-\nu)!(\nu+|M|)!} \\ &\times \sum_{\mu=0}^{m_r}\frac{(-1)^{\mu}}{\mu!}\cdot\frac{(m_r+|N|)!}{(m_r-\mu)!(\mu+|N|)!}\cdot\left(\frac{|M|+|N|+1}{2}+\nu+\mu\right)! \end{aligned}$$

where $(\delta_{\Delta M,1}+\delta_{\Delta M,-1})=1$ because of selection rule $(\Delta M=\pm 1)$.

A.6 The matrix elements of position y, $\langle\Phi_j|y|\Phi_i\rangle$

The position matrix elements are given by

$$\langle\Phi_j|y|\Phi_i\rangle = \int_{R^2} d\vec{r}\,\Phi_j^*(\vec{r})\,y\,\Phi_i(\vec{r}) = \int_{R^2} d\vec{r}\,\Phi_j^*(\vec{r})\,r\sin\varphi\,\Phi_i(\vec{r})\,, \tag{A.37}$$

By expanding the basis functions (3.10) as (A.2) the matrix elements transform into

$$\langle \Phi_j | y | \Phi_i \rangle = \int_0^{+\infty} dr r^2 \chi_j(r) \chi_i(r) \int_0^{2\pi} d\varphi \sin\varphi e^{-i\Delta M \varphi}$$

where $i := (M, n_r)$, $j := (N, m_r)$, $\Delta M = M - N$. By solving the integral over φ we get the selection rule:

$$\int_0^{2\pi} d\varphi \sin\varphi e^{-i\Delta M \varphi} = \frac{\pi}{i}(\delta_{\Delta M,1} - \delta_{\Delta M,-1}) \,,$$

therefore for given M and N, the selection rule $\Delta M = \pm 1$ tells that only for these values of ΔM, the integrals over φ are non-zero, all the others being zero. Under these conditions the matrix elements become:

$$\langle \Phi_j | y | \Phi_i \rangle = \frac{\pi}{i}(\delta_{\Delta M,1} - \delta_{\Delta M,-1}) \cdot \int_0^{+\infty} dr r^2 \chi_j(r) \chi_i(r) \,.$$

By following the same way as used for matrix elements of position x and using the relations (3.10), (A.2) and (A.36), within a few algebraic steps the position matrix elements become:

$$\begin{aligned}
\langle \Phi_j | y | \Phi_i \rangle &= \frac{1}{i}(\delta_{\Delta M,1} - \delta_{\Delta M,-1}) \cdot \frac{1}{2}\sqrt{2}a \left[\frac{n_r!}{(|M| + n_r)!} \cdot \frac{m_r!}{(|N| + m_r)!} \right]^{1/2} \\
&\times \sum_{\nu=0}^{n_r} \frac{(-1)^\nu}{\nu!} \cdot \frac{(n_r + |M|)!}{(n_r - \nu)!(\nu + |M|)!} \\
&\times \sum_{\mu=0}^{m_r} \frac{(-1)^\mu}{\mu!} \cdot \frac{(m_r + |N|)!}{(m_r - \mu)!(\mu + |N|)!} \cdot \left(\frac{|M| + |N| + 1}{2} + \nu + \mu \right)!
\end{aligned}$$

where $(\delta_{\Delta M,1} - \delta_{\Delta M,-1}) = \Delta M = M - N$ because of selection rule $(\Delta M = \pm 1)$.

Appendix B

Magnetization

B.1 The orbital magnetization $\mathscr{M}_o$

The general formula of the local probability current density carried by an electron located in the α state is defined as:

$$j_\alpha(\vec{r}) = \frac{\hbar}{m^*}\mathbf{Re}[\Psi^*_\alpha(\vec{r})\cdot D\cdot\Psi_\alpha(\vec{r})], \tag{B.1}$$

where

$$D = \frac{\vec{\nabla}}{i} - \frac{e\vec{A}}{\hbar}. \tag{B.2}$$

Therefore the total probability current density is defined by:

$$j(\vec{r}) = \sum_\alpha f(\varepsilon_\alpha) j_\alpha(\vec{r}), \tag{B.3}$$

and within a few algebraic steps becomes:

$$j(\vec{r}) = \frac{\hbar}{m^*}\sum_\alpha f(\varepsilon_\alpha)\mathbf{Re}\left[\frac{1}{i}\Psi^*_\alpha(\vec{r})\nabla\Psi_\alpha(\vec{r}) - \frac{e\vec{A}}{\hbar}\Psi^*_\alpha(\vec{r})\Psi_\alpha(\vec{r})\right]. \tag{B.4}$$

The electrical current density is defined as:

$$J(\vec{r}) = -e\cdot j(\vec{r}). \tag{B.5}$$

The orbital magnetization $\mathscr{M}_o$ is defined as:

$$\mathscr{M}_o = \frac{1}{2c}\cdot\frac{1}{\mathscr{A}}\cdot\int_{R^2} d\vec{r}\cdot\vec{r}\times\langle\vec{J}(\vec{r})\rangle = \frac{1}{2c}\cdot\frac{1}{\mathscr{A}}\left[\int_{R^2} d\vec{r}\cdot\vec{r}\times\vec{J}_r(\vec{r}) + \int_{R^2} d\vec{r}\cdot\vec{r}\times\vec{J}_\varphi(\vec{r})\right] \tag{B.6}$$

where c is the speed of light (only used in cgs-units), $\mathscr{A}$ is the area of dot and by taking into account that $\vec{r} \times \vec{J}_r(\vec{r}) = 0$, the orbital magnetization transforms into:

$$\begin{aligned}
\mathscr{M}_o &= \frac{1}{2c} \cdot \frac{1}{\mathscr{A}} \int_{R^2} d\vec{r} \cdot \vec{r} \times \vec{J}_\varphi(\vec{r}) \\
&= -\frac{1}{\mathscr{A}} \cdot \frac{e\hbar}{2m^* c} \sum_\alpha f(\varepsilon_\alpha) \int_{R^2} d\vec{r} \cdot \vec{r} \times \mathbf{Re} \left[\frac{1}{i} \Psi_\alpha^*(\vec{r}) \nabla_\alpha \Psi_\alpha(\vec{r}) - \frac{e\vec{A}}{\hbar} \Psi_\alpha^*(\vec{r}) \Psi_\alpha(\vec{r}) \right] \\
&= -\frac{1}{\mathscr{A}} \cdot \mu_B \sum_\alpha f(\varepsilon_\alpha) \left[\int_{R^2} d\vec{r} r \cdot \mathbf{Re} \left(\frac{1}{i} \Psi_\alpha^* \nabla_\alpha \Psi_\alpha \right) - \frac{e}{\hbar} \int_{R^2} d\vec{r} \, (\vec{r} \times \vec{A}) \Psi_\alpha^* \Psi_\alpha \right],
\end{aligned}$$

where μ_B is the Bohr magneton given by

$$\mu_B = \frac{e\hbar}{2m^* c}.$$

But we have

$$\Psi_\alpha = \sum_p C_{\alpha p} \Phi_p = \sum_p C_{\alpha p} \chi_p e^{-iM\varphi}$$

and with help of relation (3.10):

$$\nabla_\alpha \Psi_\alpha = \frac{1}{r} \cdot \frac{\partial \Psi_\alpha}{d\varphi} = -i \cdot \frac{M}{r} \Psi_\alpha \Longrightarrow \Psi_\alpha^* \nabla_\alpha \Psi_\alpha = -i \cdot \frac{M}{r} \Psi_\alpha^* \Psi_\alpha$$

$$\vec{r} \times \vec{A} = \vec{r} \times \frac{1}{2} (\vec{r} \times \vec{B}) = -\frac{1}{2} B r^2$$

With this the orbital magnetization transforms into:

$$\mathscr{M}_o = -\frac{1}{\mathscr{A}} \cdot \mu_B \sum_\alpha f(\varepsilon_\alpha) \left[-M \int_{R^2} d\vec{r} \Psi_\alpha^*(\vec{r}) \Psi_\alpha(\vec{r}) + \frac{eB}{2\hbar} \int_{R^2} d\vec{r} \, r^2 \Psi_\alpha^*(\vec{r}) \Psi_\alpha(\vec{r}) \right]$$

We know that the characteristic magnetic length a, (3.12), is a function of the magnetic length l, defined in (3.3), the parabolic confinement frequency ω_0, and the cyclotron frequency ω_c, (3.4) so

$$\frac{eB}{2\hbar} = \frac{1}{2l^2} = \frac{1}{2a^2} \cdot \frac{\omega_c}{\Omega}.$$

We also know that:

$$\Psi_\alpha(\vec{r}) = \sum_p C_{\alpha p} \Phi_p(\vec{r}) = \sum_p C_{\alpha p} \chi_p(\vec{r}) e^{-iM\varphi},$$

$$\Psi_\alpha^*(\vec{r}) = \sum_q C_{\alpha q} \Phi_q(\vec{r}) = \sum_q C_{\alpha q} \chi_q(\vec{r}) e^{iN\varphi},$$

$$\Psi_\alpha^*(\vec{r}) \Psi_\alpha(\vec{r}) = \sum_{p,q} C_{\alpha p} C_{\alpha q} \chi_p(\vec{r}) \chi_q(\vec{r}) e^{-i\Delta M\varphi},$$

where $\Delta M = M - N$. Then the orbital magnetization becomes:

$$\begin{aligned}\frac{\mathscr{M}_o \cdot \mathscr{A}}{\mu_B} &= \sum_\alpha f(\varepsilon_\alpha) \sum_{p,q} C_{\alpha p} C_{\alpha q} \left[M \int_0^{+\infty} dr r \chi_p(r) \chi_q(r) \int_0^{2\pi} d\varphi e^{-i\Delta M \varphi} \right] \\ &- \sum_\alpha f(\varepsilon_\alpha) \sum_{p,q} C_{\alpha p} C_{\alpha q} \left[\frac{1}{2a^2} \cdot \frac{\omega_c}{\Omega} \int_0^{+\infty} dr r^3 \chi_p(r) \chi_q(r) \int_0^{2\pi} d\varphi e^{-i\Delta M \varphi} \right].\end{aligned}$$

The integral over φ leads to:

$$\int_0^{2\pi} d\varphi e^{-i\Delta M \varphi} = \int_0^{2\pi} d\varphi e^{i(N-M)\varphi} = 2\pi \delta_{N,M},$$

and therefore, the orbital magnetization is:

$$\frac{\mathscr{M}_o \cdot \mathscr{A}}{\mu_B} = 2\pi \delta_{N,M} \sum_\alpha f(\varepsilon_\alpha) \sum_{p,q} C_{\alpha p} C_{\alpha q} \left[M \int_0^{+\infty} dr r \chi_p(r) \chi_q(r) - \frac{1}{2a^2} \cdot \frac{\omega_c}{\Omega} \int_0^{+\infty} dr r^3 \chi_p(r) \chi_q(r) \right]$$

We consider

$$\begin{aligned} I &= \int_0^{+\infty} dr r \chi_p(r) \chi_q(r) = \frac{1}{2^{\frac{|M|+|N|}{2}+1} a^2 \pi} \cdot \left[\frac{m_r!}{(|N|+m_r)!} \cdot \frac{n_r!}{(|M|+n_r)!} \right]^{1/2} \\ &\times \int_0^{+\infty} dr r \left(\frac{r}{a} \right)^{|M|+|N|} e^{-\frac{r^2}{2a^2}} L_{m_r}^{|N|} \left(\frac{r^2}{2a^2} \right) L_{n_r}^{|M|} \left(\frac{r^2}{2a^2} \right), \end{aligned} \tag{B.7}$$

and

$$\begin{aligned} I' &= \int_0^{+\infty} dr r^3 \chi_p(r) \chi_q(r) = \frac{1}{2^{\frac{|M|+|N|}{2}+1} a^2 \pi} \cdot \left[\frac{m_r!}{(|N|+m_r)!} \cdot \frac{n_r!}{(|M|+n_r)!} \right]^{1/2} \\ &\times \int_0^{+\infty} dr r^3 \left(\frac{r}{a} \right)^{|M|+|N|} e^{-\frac{r^2}{2a^2}} L_{m_r}^{|N|} \left(\frac{r^2}{2a^2} \right) L_{n_r}^{|M|} \left(\frac{r^2}{2a^2} \right). \end{aligned} \tag{B.8}$$

By using relations (A.20) and (A.36) within a few algebraic steps the integrals I and I' are:

$$\begin{aligned} I &= \frac{1}{2\pi} \cdot \left[\frac{m_r!}{(|N|+m_r)!} \cdot \frac{n_r!}{(|M|+n_r)!} \right]^{1/2} \sum_{\mu=0}^{m_r} \sum_{\nu=0}^{n_r} \frac{(-1)^{\mu+\nu}}{\nu! \mu!} \\ &\times \frac{(|N|+m_r)!}{(m_r-\mu)!(|N|+\mu)!} \cdot \frac{(|M|+n_r)!}{(n_r-\nu)!(|M|+\nu)!} \cdot \left(\frac{|M|+|N|}{2} + \mu + \nu \right)!, \end{aligned} \tag{B.9}$$

and

$$\begin{aligned} I' &= \frac{a^2}{\pi} \cdot \left[\frac{n_r!}{(|M|+n_r)!} \cdot \frac{m_r!}{(|N|+m_r)!} \right]^{1/2} \sum_{\mu=0}^{m_r} \sum_{\nu=0}^{n_r} \frac{(-1)^{\mu+\nu}}{\nu! \mu!} \\ &\times \frac{(|N|+m_r)!}{(m_r-\mu)!(|N|+\mu)!} \cdot \frac{(|M|+n_r)!}{(n_r-\nu)!(|M|+\nu)!} \cdot \left(\frac{|M|+|N|}{2} + \mu + \nu + 1 \right)!. \end{aligned} \tag{B.10}$$

Having the values of these integrals we can evaluate the orbital magnetization being:

$$\begin{aligned}\frac{\mathscr{M}_o\cdot\mathscr{A}}{\mu_B} &= \delta_{N,M}\sum_\alpha f(\varepsilon_\alpha)\sum_{p,q}C_{\alpha p}C_{\alpha q}\left[\frac{n_r!}{(|M|+n_r)!}\cdot\frac{m_r!}{(|N|+m_r)!}\right]^{1/2}\\ &\times \sum_{\mu=0}^{m_r}\sum_{\nu=0}^{n_r}\frac{(-1)^{\mu+\nu}}{\nu!\mu!}\frac{(|N|+m_r)!}{(m_r-\mu)!(|N|+\mu)!}\cdot\frac{(|M|+n_r)!}{(n_r-\nu)!(|M|+\nu)!} \qquad \text{(B.11)}\\ &\times \left[M\left(\frac{|M|+|N|}{2}+\mu+\nu\right)!-\frac{\hbar\omega_c}{\hbar\Omega}\left(\frac{|M|+|N|}{2}+\mu+\nu+1\right)!\right].\end{aligned}$$

B.2 The Hartree-Fock orbital magnetization $\mathscr{M}_o$

In the case of the Hartree-Fock approximation the current density is nonlocal and we proceed in a different manner. The magnetization for one electron is the standard orbital magnetic moment:

$$\vec{\mathscr{M}} = \vec{r}\times\vec{J}\xrightarrow{2D}(xj_y-yj_x)\vec{k}, \qquad \text{(B.12)}$$

where

$$\vec{J} = -e\dot{\vec{r}} = \frac{ie}{\hbar}[\hat{H},\hat{r}], \qquad \text{(B.13)}$$

and therefore

$$j_x = \frac{ie}{\hbar}[\hat{H},\hat{x}]. \qquad \text{(B.14)}$$

The orbital magnetization for a single Hartree-Fock state is:

$$\begin{aligned}\mathscr{M}_\alpha &= (\alpha|\mathscr{M}|\alpha) = [(\alpha|xj_y|\alpha)-(\alpha|yj_x|\alpha)]\\ &= \sum_\beta[(\alpha|x|\beta\rangle\cdot\langle\beta|j_y|\alpha)-(\alpha|y|\beta\rangle\cdot\langle\beta|j_x|\alpha)]. \qquad \text{(B.15)}\end{aligned}$$

where we denote by ordinary parenthesis (or) the interacting states and by $\langle$ or $\rangle$ the noninteracting states. Generally, we have for:

$$\begin{aligned}\langle\alpha|j_x|\beta\rangle &= \frac{ie}{\hbar}\langle\alpha|[\hat{H},\hat{x}]|\beta\rangle = \frac{ie}{\hbar}[\langle\alpha|\hat{H}\hat{x}|\beta\rangle-\langle\alpha|\hat{x}\hat{H}|\beta\rangle]\\ &= \frac{ie}{\hbar}\sum_\gamma[\langle\alpha|\hat{H}|\gamma\rangle\cdot\langle\gamma|\hat{x}|\beta\rangle-\langle\alpha|\hat{x}|\gamma\rangle\cdot\langle\gamma|\hat{H}|\beta\rangle]. \qquad \text{(B.16)}\end{aligned}$$

Therefore for the orbital magnetization we have:

$$\begin{aligned}\mathscr{M}_\alpha &= \frac{ie}{\hbar}\sum_{\beta,\gamma}(\alpha|x|\beta\rangle\cdot[\langle\beta|H|\gamma\rangle\cdot\langle\gamma|y|\alpha)-\langle\beta|y|\gamma\rangle\cdot\langle\gamma|H|\alpha)]\\ &- \frac{ie}{\hbar}\sum_{\beta,\gamma}(\alpha|y|\beta\rangle\cdot[\langle\beta|H|\gamma\rangle\cdot\langle\gamma|x|\alpha)-\langle\beta|x|\gamma\rangle\cdot\langle\gamma|H|\alpha)], \qquad \text{(B.17)}\end{aligned}$$

where:

$$|\alpha) = \sum_{\tau} C_{\tau\alpha} |\tau\rangle = \sum_{\tau} |\tau\rangle\langle\tau|\alpha\rangle\,, \tag{B.18}$$

and

$$(\alpha| = \sum_{\delta} C_{\delta\alpha} \langle\delta| = \sum_{\delta} \langle\alpha|\delta\rangle\langle\delta|\,. \tag{B.19}$$

The orbital magnetization for one state, α is then:

$$\begin{aligned} \mathscr{M}_\alpha &= \frac{ie}{\hbar} \sum_{\beta,\gamma,\delta,\tau} C_{\delta\alpha} \cdot C_{\tau\alpha} \langle\delta|x|\beta\rangle \cdot [\langle\beta|H|\gamma\rangle \cdot \langle\gamma|y|\tau\rangle - \langle\beta|y|\gamma\rangle \cdot \langle\gamma|H|\tau\rangle] \\ &- \frac{ie}{\hbar} \sum_{\beta,\gamma,\delta,\tau} C_{\delta\alpha} \cdot C_{\tau\alpha} \langle\delta|y|\beta\rangle \cdot [\langle\beta|H|\gamma\rangle \cdot \langle\gamma|x|\tau\rangle - \langle\beta|x|\gamma\rangle \cdot \langle\gamma|H|\tau\rangle]\,, \end{aligned} \tag{B.20}$$

and the total magnetization for all the states is:

$$\mathscr{M}_o = \sum_{\alpha} f(\varepsilon_\alpha) \cdot \mathscr{M}_\alpha\,. \tag{B.21}$$

Bibliography

[1] T. Demel, D. Heitman, P. Grambow, and K. Ploog, Phys. Rev. Lett. **64**, 788 (1990).

[2] T. Demel, D. Heitmann, P. Grambow, and K. Ploog, Phys. Rev. B **38**, 12732 (1988).

[3] V. Gudmundsson, A. Brataas, P. Grambow, T. Kurth, and D. Heitmann, Phys. Rev. B **51**, 17744 (1995).

[4] P. A. Maksym and T. Chakraborty, Phys. Rev. Lett **65**, 108 (1990).

[5] D. A. Broido, K. Kempa, and P. Bakshi, Phys. Rev. B **42**(17), 11400 (1990).

[6] V. Gudmundsson and R. Gerhardts, Phys. Rev. B **43**(14), 12098 (1991).

[7] D. Pfannkuche and R. Gerhardts, Phys. Rev. B **44**(23), 13132 (1991).

[8] D. Pfannkuche, V. Gudmundsson, P. Hawrylak, and R. Gerhardts, Solid-State Electronics **37**(4-6), 1221 (1994).

[9] D. Pfannkuche, V. Gudmundsson, and P. Maksym, Phys. Rev. B **47**, 2244 (1993).

[10] D. Pfannkuche and S. E. Ulloa, Phys. Rev. Lett. **74**, 1194 (1995).

[11] R. C. Ashoori, H. L. Stormer, L. J. S. Weiner, S. Pearton, K. Baldwin, and K. West, Phys. Rev. Lett. **68**(20), 3088 (1992).

[12] W. Sheng and H. Xu, Physica B **256-258**, 152 (1998).

[13] I. Magnúsdóttir and V. Gudmundsson, Phys. Rev. B **61**, 10229 (2000).

[14] T. Ando, A. Fowler, and F. Stern, Rev. Mod. Phys. **54**, 437 (1982).

[15] M. Hatzakis, Nanolithography pp. 13–23 (1994).

[16] R. Krahne, *Far-Infrared Spectroscopy on Quantum Dots and Density-Modulated Two-Dimensional Electron Systems*, Ph.D. thesis, University of Hamburg (2000).

[17] V. Fock, Z. Phys. **47**, 446 (1928).

[18] C. G. Darwin, Proc. Camb. Phil. Soc **27**, 86 (1930).

[19] I. S. Gradshteyn and L. M. Ryzhik, *Tables of Integrals, Series and Products* (Academic Press, Florida, 1982).

[20] I. Magnúsdóttir and V. Gudmundsson, Eðlisfræði á Íslandi **IX** (1999).

[21] I. Magnúsdóttir, *Effects of shape on the far-infrared absorption of quantum dots*, Master's thesis, Háskóli Íslands (1999).

[22] A. Lorke, R. J. Luyken, A. O. Govorov, J. P. Kotthaus, J. M. Garcia, and P. M. Petroff, Phys. Rev. Lett. **84**, 2223 (2000).

[23] G. Vasile and V. Gudmundsson, Eðlisfræði á Íslandi **X** (2001).

[24] Y. Chen and V. Gudmundsson, Eðlisfræði á Íslandi **IX** (1999).

[25] E. K. U. Gross, E. Runge, and O. Heinonen, *Many-Particle Theory* (Adam Hilger, Bristol, 1991).

[26] A. L. Fetter and J. D. Walecka, *Quantum Theory of Many-Particle systems* (McGraw-Hill Book Company, 1971).

[27] D. Grundler, I. Meinel, F. S. Bargsteadt, and D. Heitmann, Physica B **249-251**, 693 (1998).

[28] I. Meinel, T. Hengstmann, D. Grundler, and D. Heitmann, Phys. Rev. Lett. **82**(4), 819 (1999).

[29] S. A. J. Wiegers, M. Specht, L. P. Levy, M. Y. Simmons, D. A. Ritchie, A. Cavanna, E. B, G. Martinez, and P. Wyder, Phys. Rev. Lett. **79**(17), 3238 (1997).

[30] V. Gudmundsson and G. Pálsson, Physica Scripta T **54**, 92 (1994).

[31] M. Koskinen, M. Manninen, and S. M. Reimann, Phys. Rev. Lett. **79**, 1389 (1997).

[32] M. Büttiker, Y. Imry, and R. Landauer, Phys. Rev. Lett. **96A**, 365 (1983).

[33] W. C. Tan and J. C. Inkson, Phys. Rev. B **60**(8), 5626 (1999).

[34] A. Aldea, V. Moldoveanu, M. Nita, A. Manolescu, V. Gudmundsson, and B. Tanatar, Condensed Matter **preprint cond-mat/0207307** (2002).

[35] M. P. Schwarz, G. Grundler, M. Wilde, C. Heyn, and D. Heitmann, J. Appl. Phys. **91**, 6875 (2002).

[36] J. D. Jackson, *Classical Electrodynamics* (John Wiley and Sons, Inc, USA, 1975), 2nd ed.

[37] N. N. Lebedev, *Special Functions and Their Applications* (Dover Publications, INC., New York, 1972).